THESIS

PLATE FRAME AND BAR PLATE EVAPORATOR MODEL VALIDATION AND VOLUME MINIMIZATION

Submitted by

John Robert Simon III

Department of Mechanical Engineering

In partial fulfillment of the requirements

For the degree of Master of Science

Colorado State University

Fort Collins, Colorado

Fall 2019

Master's Committee:

Advisor: Todd M. Bandhauer

Jason Quinn
Ellison Carter

ABSTRACT

PLATE FRAME AND BAR PLATE EVAPORATOR MODEL VALIDATION AND VOLUME MINIMIZATION

Vapor compression chillers are the primary cooling technology for large building applications. Chillers have a large up front capital cost, with the heat exchangers accounting for the majority of the cost. Heat exchanger cost is a function of size, and therefore, a reduction in heat exchanger size can be correlated to a reduction in chiller capital cost. Few investigations focus on the reduction in heat exchanger size for vapor compression systems. Therefore, this investigation aims to decrease the size of chillers by predicting the minimum evaporator volume for a fixed performance. Only the evaporator was minimized because it was assumed that a similar process could be performed for the condenser in a future study. The study focused on a simple vapor compression cycle, and implemented high fidelity heat exchanger models for two compact heat exchanger types: brazed bar plate and gasketed plate and frame. These models accounted for variable fluid properties, phase change, and complex geometries within the evaporator core. The models used in this investigation were developed based on liquid-coupled evaporators in an experimental vapor compression system, and validated using collected data. The bar plate model was validated based on sizing and pressure drop to mean absolute errors of 14.2% and 14.0%, respectively. The plate frame model was validated for sizing to mean absolute errors equal to 7.9%; however, due to measurement uncertainty, pressure drop was not validated. The heat exchanger models were integrated into a simple vapor compression cycle model to determine the minimum required evaporator volume. Both heat exchanger types, in parallel and counter flow arrangements

were minimized in this study. The minimum volume was achieved by varying the ratio between core length and number of channels. It was found that for both heat exchanger types, the parallel flow arrangement resulted in a smaller volume than the counter flow arrangement. Furthermore, the bar plate heat exchanger resulted in an optimum volume 91% smaller than the plate frame counterpart.

ACKNOWLEDGEMENTS

Many involved in my life have supported my way to submitting this thesis, however Dr. Todd Bandhauer has been the key contributor. Dr. Bandhauer saw potential in me as far back as my sophomore year in undergraduate thermodynamics, to the extent to offer me a position in his lab. He has supported my progression as a student, going from a technician constructing the TCCS, to an undergraduate student in 498, to a Masters student working on heat exchanger modeling. I truly appreciate the tough love that has challenge me and caused me to become a better engineer.

The Interdisciplinary Thermal Science (ITS) Lab has offered immense amounts of support on my way as well. The lab truly has a community culture where everyone helps everyone. I would like to first thank Alex Grauberger as my friend who has stood next to me on my way through the lab, working with me in building the TCCS and though 498. Shane Garland and Derek Young have also been in a pivotal role in my graduate career due to their contribution to this project. They helped edit my work and solve technical problems as they arose. The rest of the lab deserves great thanks as well for their moral and emotional support over the last three years.

I would like to thank Barber-Nichols, Inc. for their financial support through the Barber-Nichols, Inc. Fellowship. It was a great honor to be recognized for my work by industry.

Finally I would like to thank my friends and family for their support outside of the lab. This journey has been a trying one and their confidence in me has allowed me to keep moving forward. Special thanks is in order for my parents and my wife. Thank you Mom and Dad for giving me the opportunity to get to graduate school and words of wisdom which inevitably became a key argument for me to work toward a Master's degree. And thank you Kristina for creating a loving home with me and joining me on a journey through graduate school.

TABLE OF CONTENTS

LIST OF TABLES

LIST OF FIGURES

NOMENCLATURE

Symbol	Description	Units
A	Area	m^2
Bo	Boiling number	-
Bn	Bond number	-
C_{min}	Minimum heat capacity rate	kW K^{-1}
Cr	Heat capacity rate ratio	-
C	Constant	
Co	Confinement number	-
COP	Coefficient of performance	-
Cp	Heat capacity	kW kg^{-1}
CV	Control volume	-
d	Diameter	m
Dh	Hydraulic Diameter	m
Error	Error	-
f	Friction factor	-
F	Enhancement factor	-
FH	Fin height	m
FP	Fin pitch	m
Fr	Huang et al geometric factor	-
FT	Fin thickness	m

g	Gravitational constant	m s^{-2}
G	Mass Flux	kg m^{-2} s^{-1}
Ge	Han et al. geometric factor	-
h	Heat transfer coefficient	kW m^{-2} K^{-1}
i	Enthalpy	kW kg^{-1}
j	Vertical coordinate	-
K	Minor loss coefficient	-
k	Thermal conductivity	kW m^{-1} K^{-1}
L	Length	m
$LMTD$	Log mean temperature difference	K
$\dot{M}$	Mass flow rate	kg s^{-1}
MAE	Mean absolute error	-
MW	Molecular weight	kg $kmol^{-1}$
N	Wilson plot coefficient	-
NTU	Number of transfer units	-
Nu	Nusselt number	-
P	Pressure	kPa
P_{co}	Corrugation pitch	M
Pr	Prandtl number	-
q	Heat transfer rate	kW
q''	Heat flux	kW m^{-2}
R	Thermal resistance	K kW^{-1}
Re	Reynolds number	-

S	Suppression factor	-
S_x	Uncertainty variable used in calculation	-
S_y	Uncertainty variable of interest	-
T	Temperature	°C
UA	Over all Conductance	kW K^{-1}
$\bar{V}$	Velocity	m s^{-1}
W	Width	m
X	Vapor quality	-
Y	Correction factor	-
z	Horizontal coordinate	-
α	Thermal diffusivity	m s^{-2}
β	Chevron angle	Deg
δ	Thickness	m
Del x	Uncertainty of the parameter used in calculation	-
Del y	Uncertainty of the parameter of interest	-
Δ	Change	-
ε	Heat exchanger effectiveness	-
Γ	Gas to liquid pressure loss ratio	-
η	Efficiency	-
μ	Viscosity	kg m^{-1} s^{-1}
θ	Bubble contact angle	Deg
ρ	Density	kg m^{-3}
σ	Surface tension	N m^{-1}

SUBSCRIPTS

Symbol	Description	Units
accel	Acceleration	
b	Base	
c	Channel	
com	Compressor	
con	Condenser	
conv	Convection	
cross	Cross sectional	
eq	Equivilant	
Evap	Evaporator	
f	Fin	
fg	Saturated liquid to saturated vapor	
fric	Frictional	
g	Water-glycol	
grav	Gravitational	
ht	Heat transfer	
HX	Heat exchanger	
in	In	
l	Liquid	
m	Mean	

manifold	Manifold	
max	Maximum	
min	Minimum	
n	Total control volumes	
nb	Nucleate Boiling	
o	Bubble	
out	Out	
ov	Over all	
plate	Plate	
r	Refrigerant	
red	Reduced	
sat	Saturation	
sh	Superheated region	
sl	Saturated liquid	
sp	Single phase	
sv	Saturated vapor	
T	“T” junction	
total	Total	
tp	Two Phase	
v	Vapor	
wall	Wall	
weighted	Weighted	

Chapter 1. Introduction

1.1. Background

The air conditioning market has grown dramatically in the past few years, particularly in developing markets. In China, the demand for air conditioning has dramatically increased, 15% per year for the last ten years. This increased demand has caused air conditioning to be the highest electrical consumer in large cities during the summer. For instance, in Shanghai, air conditioning accounts for up to 40% of the total electricity consumed [1]. This is a common issue across other nations, such as Middle Eastern countries and India. During summer months, some areas of these countries can reach dangerously high temperatures and are not cooling to safe levels at night [2]. In Quriyat, Oman, the highest night time low temperature ever recorded was 42.6 °C in the summer of 2018. As these temperatures continue rising due to climactic changes, the need for cooling is becoming more than just a luxury for first world countries, but a necessity for all people. Increased amounts of research into practical cooling is required to increase system efficiency while also considering a reduction in cost and size. Due to the growing populations in developing countries a reduction in overall size and cost is required for effective large scale implementation.

The vapor compressions cycle (VCC) is one of the most common cycles used for building cooling. The cycle utilizes the infinitely high heat capacity of a phase change refrigerant to transfer heat from a cold reservoir to a hot reservoir, the opposite direction of natural heat flow, while consuming a small amount of energy. Four components make up the simple cycle, the evaporator, compressor, condenser, and expansion device [3]. The evaporator, between state points 1 and 2 in Figure 1-1, couples the vapor compression cycle to the cold reservoir. In the ideal cycle operation, the heat from the cold reservoir enters the heat exchanger and is used to vaporize the two phase

refrigerant to a saturated vapor at constant pressure. The refrigerant is then compressed isentropically from state points 2 to 3, which increases the pressure and subsequently the saturation temperature above the hot reservoir temperature. The refrigerant then passes through the condenser, state points 3 and 4, where it is cooled at constant pressure from a super-heated vapor to a saturated liquid by rejecting heat to the hot reservoir. Finally, the refrigerant passes through an expansion device, state points 4 to 1, to drop the saturation pressure temperature below the cold reservoir by isenthalpic expansion. The coefficient of performance (COP) is a metric used to express the efficiency of a VCC and is defined by the cooling duty of the evaporator divided by the energy consumed by the compressor. The cycle described above is representative of a simple, ideal cycle. Components can be added to construct a more complicated cycle to improve cycle efficiency, and component efficiencies can be included to account for real world irreversibilities.

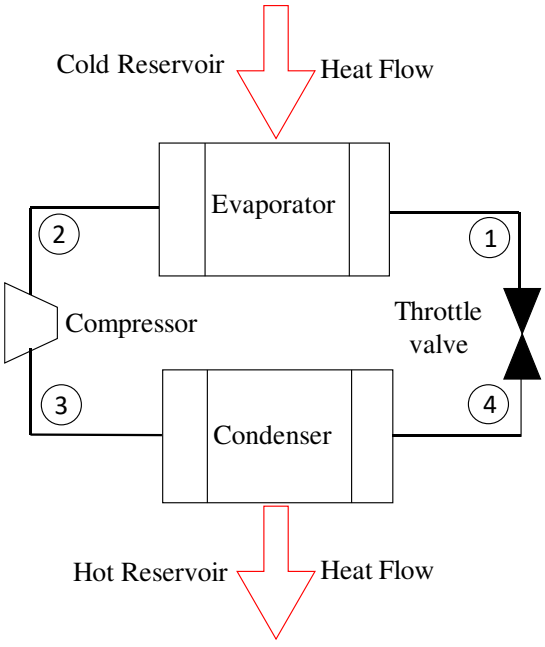

Figure 1-1. Schematic of a simple vapor compression cycle.

One method of cycle improvement is to add an additional heat exchanger between the evaporator and compressor on the low pressure side and between the compressor and the expander

and shown in Figure 1-2. This added heat exchanger recuperates heat in the cycle, further superheating the vapor entering the compressor and sub-cooling the liquid entering the expansion device, increasing cycle thermodynamic efficiency.

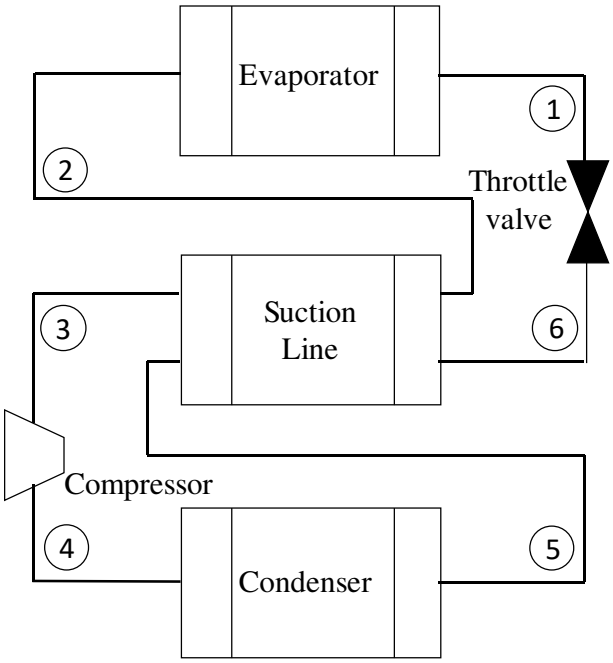

Figure 1-2. Schematic of a suction line vapor compression cycle.

The compressor is a prime example of a component with an associated efficiency. In the ideal cycle the compressor is assumed to be isentropic, where no entropy is generated through compression. However, in reality, some entropy will be generated which is accounted for by the compressor efficiency. Depending on the application and the desire to increase the isentropic efficiency, there are a variety of compressor types available. In residential scale VCCs, the compressor is commonly a reciprocating piston compressor, see Figure 1-3, while for more efficient systems, scroll and screw compressors are used. In large building scale VCC systems which want high efficiencies, oil free centrifugal compressors are used, see Figure 1-4.

Figure 1-3. Reciprocating compressor. [104]

Figure 1-4. Danfoss Turbocor centrifugal compressor. [105]

The heat exchangers in the ideal cycle are assumed to have no pressure losses, while in reality, pressure losses exist that can have an impact on performance. These losses can be included in analysis to account for the performance loss associated with the increased compression ratio required to overcome the pressure loss. Furthermore, the refrigerant often leaves the evaporator super-heated, which can diminish evaporator performance. Similarly in the condenser, the refrigerant can exit as a sub cooled liquid, diminishing condenser effectiveness. However, a sub

cooled condenser can decreasing evaporator inlet quality, even causing subcooled referent to enter the evaporator.

When considering the evaporator and condenser, either heat exchanger can be air or liquid coupled. In small home units, it is common for both heat exchangers to be air coupled, directly transferring heat between the hot and cold reservoirs with the inside air and outside air, respectively. It is common for these heat exchangers to be a tube and fin design. Refrigerant is passed through a long serpentine tube attached to plate fins as shown in Figure 1-5.

Figure 1-5. Tube and fin condenser. [106]

The plate fins act as extended surfaces to increase air side heat transfer area. For more compact air coupled applications aluminum brazed heat exchangers are used, see Figure 1-6. In these heat exchangers the refrigerant is distributed to oblong tubes via a header and collected at the end of the pass. Air is passed over the tubes and through fins.

Figure 1-6. Aluminum brazed air coupled heat exchanger.

In large building scale applications, the condenser and evaporator are often liquid coupled and used to create distributed cooling. In these cases shell and tube heat exchangers are common [4]. Shell and tube heat exchangers typically have coolant flow through tube banks that are immersed in a shell of flowing refrigerant, see Figure 1-7.

Figure 1-7. Shell and tube evaporator. [107]

This type of heat exchanger has a low surface area to volume ratio, on the order of 100 m^2/m^3. There are several other heat exchanger types which have significantly higher ratios. Plate frame heat exchangers, for instance, have surface area to volume ratios of 400 m^2/m^3. These heat exchangers pass fluids between corrugated plates alternating between fluids, see Figure 1-8.

Figure 1-8. Plate and Frame evaporator. [108]

Another option for liquid coupled systems are compact bar plate heat exchangers which can achieve surface area to volume ratios on the order of 1000 m^2/m^3 [5]. Compact heat exchangers are constructed by stacking plates separated by fins to form fluid channels that are metallurgically bonded using a brazing process, see Figure 1-9. Neither plate frame nor bar plate heat exchangers are commonly used in industry and present an opportunity for a more volume efficient system while maintaining performance by utilizing heat exchangers with a higher surface area to volume ratio.

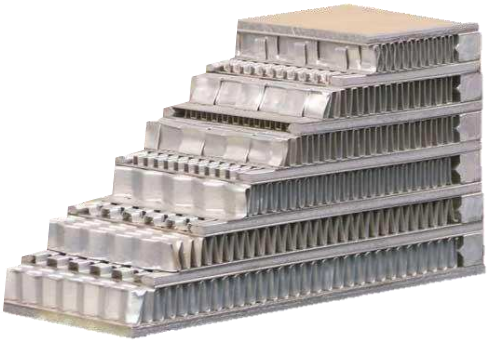

Figure 1-9. Cut away of a bar plate heat exchanger. [109]

1.2. Research Objectives

Though there are a considerable number of studies into vapor compression cycle optimization, none focus on the minimization of the evaporator size. Minimizing the heat exchanger sizes can reduce the heat exchanger cost for a system. Because the system cost is dominated by the heat exchangers, the overall cost of the vapor compression systems could thereby be greatly reduced. Therefore the main objective of the present investigation was to determine the minimum evaporator volume for a standard vapor compression cycle with a fixed performance. Two types of heat exchangers were focused on, plate frame and bar plate. In an effort to determine the evaporator size for the two heat exchangers, another objective of this investigation is to develop and validate detailed heat exchanger models for use as sizing tools. The models were validated against heat exchangers from an experimental facility. In the validation effort, a variety of correlations were tested to determine the most accurate combination for each heat exchanger type.

1.3. Thesis Organization

The following chapters will present the motivation, methodology, and results for the evaporator minimization research. Chapter Two provides a review of the current modeling and optimization techniques for vapor compression cycles and heat exchangers. The chapter also gives a review of the relevant heat transfer and pressure drop correlations which will be used in the heat exchanger modeling effort. Chapter Three describes the heat exchanger modeling method as well as the thermodynamic model of a simple vapor compression system. Chapter Four provides the experimental methods used to collect the data for the heat exchanger validation while Chapter Five presents the results of the comparison between heat exchanger model experimental data. Furthermore, the chapter presents the results of the evaporator minimization effort using the full vapor compression system thermodynamic model. Chapter Six provides concluding remarks,

presenting the key results and offering recommendations for future work. Chapter Seven lists citations of the previous works used in the present investigation. Finally the appendix shows a step by step hand calculation of the two heat exchanger models as well as the vapor compression cycle model.

Chapter 2. Literature Review

The previous chapter describes the need for high fidelity heat exchanger sizing tools for use in thermal energy system design, particularly compact evaporative heat exchangers in vapor compression systems. This chapter will first provide a literature review of current heat exchanger modeling techniques. The review will not be limited to compact evaporator modeling as many techniques can be modified to different heat exchanger types. The next portion of the chapter will be a correlation review split into correlations pertaining to plate frame and bar plate heat exchangers. Next a review of vapor compression cycle optimization studies is presented. Finally, the research needs will be outlined based on the current literature gaps.

2.1. Heat exchanger modeling and optimization

It is important to develop high fidelity heat exchanger models which can be used to design and size heat exchangers for given applications or determine how heat exchangers will function under off design conditions. These models can greatly reduce design time, cost, and increase system efficiency. The disadvantage is that there is no universal model: each style and application of heat exchanger must have a unique model. These unique models must be tested to truly be accurate. The following section will review relevant heat exchanger models found in the literature and their accuracy.

The first model type of interest is the discretization and thermal resistance network method. One investigation by Bansal and Chin [6] modeled a wire frame condenser with a single circular copper tube which serpentines to form a rectangular cross section, Figure 2-1a. Steel wire stretches across adjacent tube sections to act as an extended surface. The investigation divided the tube into sections each containing a single wire, Figure 2-1 b. The investigation focused entirely within the

vapor dome, and did not predict single phase refrigerant cooling. However, the model did account for the change in condensation flow regimes. At each element a thermal resistance network was constructed as a function of the refrigeration side convection, wall conduction, and air side convection. The refrigerant side convection resistance was calculated from empirical correlations based on the particular flow regime of the element. Here lies an advantage to the method, the fluid properties of the condensing refrigerant can be more accurately determined when the condensing region is divided up. Properties such as density and thermal conductivity which are used in heat transfer correlations can vary widely as a fluid passes under the vapor dome. The discretization allows for a more accurate heat transfer coefficient calculation compared to if the region was treated as a single unit due to the more frequent determination of fluid properties. The air side resistance was calculated from a single correlation through the heat exchanger, using the local air properties at each element. The refrigerant pressure loss was similarly modeled across each element and summed to determine the total pressure loss. Frictional, gravitational, and acceleration pressure losses were accounted for. The model was validated with experimental data.

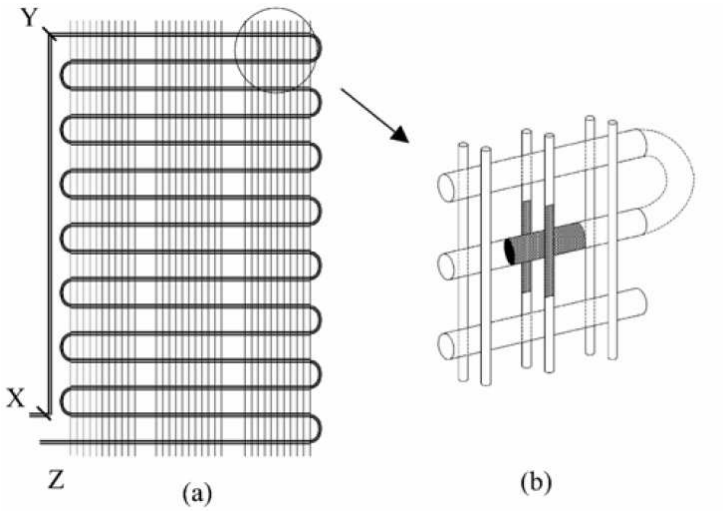

Figure 2-1. Wire tube condenser. (a) Whole heat exchanger Schematic, (b) Single control volume. Bansal and Chin [6]

The Jokar et al. [7] investigation is another example of the resistance network method but with a different discretization scheme than Bansal and Chin. The study sought to develop a heat transfer and pressure drop model for evaporation and condensation in a microchannel chevron plate heat exchanger. The investigation modeled each phase region as a single independent unit. This differs from Bansal and Chin [6] who sub divided further. This scheme reduced the complexity of the model but also does reduce the accuracy of heat transfer coefficient calculation. The experiment tested the evaporator and condenser on a small car air conditioning system, both liquid coupled to water glycol. The heat exchangers were tested at low R134a mass fluxes, $5 < G < 40$ kg m^{-2} s^{-1}, in single phase and two-phase, spanning the full range of quality. The number of channel sets was varied from 17, 20, and 27, while all the plates were 311 mm long. The investigation modeled each phase region and tested various correlations against collected data in each region. The Yan and Lin correlation as well as the Chen correlation were tested on the refrigerant boiling side. It was found that neither correlation was able to accurately predict the heat transfer effects. The Chen correlation resulted in an MEA equal to 31%, and no metric was given for the Yan and Lin correlation. The study attributes the error to the smallness of the channel sizes, believing that the surface tension has a larger impact on the heat transfer than what the correlation capture. Another potential cause was the discretization scheme. The boiling region was modeled as a single control volume, making large assumptions such as uniform properties in the region which is not true, leading to inaccurate correlation predictions.

The Picon-Nunez et al. [8] investigation looked into the effect of pressure drop on the volume of a plate fin heat exchanger core with respect to surface selection. Though not explicitly stated, the investigation used a thermal resistance network method to determine the core volume. No discretization was done, the core was assumed to be one control volume where the inlet and

outlet conditions were thermodynamically calculated. The selection of surfaces and fin types used in a heat exchanger core can cause an increase or decrease in pressure drop and heat transfer coefficient. In general, pressure loss and heat transfer coefficient are directly related, which can result in smaller core volumes for higher pressure loss. This investigation sought to predict this relation as a function of surface selection. Two flow configurations were tested, cross flow and counter flow. In the cross flow configuration, it was possible for both fluid streams to fully utilize the available pressure loss. This was due to the ability to independently change the flow path length of the two fluids. The counter flow configuration, however could not independently change the path lengths of the two fluid and there for only one fluid could fully utilize the available pressure loss. Unlike the Jokar et al. investigation, the assumption of a single control volume here was accurate because the core is entirely single phase heat transfer and the fluid properties vary little through the core.

The Corberan et al. [9] investigation is somewhat of a combination of the previous two studies. They developed a model to predict evaporation and condensation in compact heat exchangers similar to Jokar [7], however, the model was constructed similarly to Bansal and Chin [6]. The compact heat exchanger in this investigation is an air coupled, cross flow, horizontal, finned tube heat exchanger. The model divided the heat exchanger into discrete elements where the local parameters were constant and the heat transfer rate was calculated using the *UA LMTD* method. The model uses a correlation from Gray and Webb [10] to determine the air side heat transfer coefficient and the Dittus-Boelter [11] correlation to determine the single phase refrigerant heat transfer coefficient. The investigation neglects thermal conduction axially along the copper tubes, because the case study showed a negligible amount of heat transfer due to the small wall temperature difference. A variety of boiling and condensing heat transfer correlations were

analyzed for use in the model. The investigation used both homogeneous flow and separated flow frictional pressure drop correlations. The three homogenous correlations all gave nearly identical results and have a linear relation with increased vapor quality, under predicted the separated flow correlations. The Schlunder boiling correlation [12] was the best suited for the model because it had the highest accuracy and covered the whole range of qualities. For the evaporative pressure drop investigation the Martinelli and Nelson [13] correlation best predicted the experiment however the correlation is limited to qualities under 80%, therefore requiring another correlation to predict the qualities above that limit. The Schlunder correlation was chosen because it encompassed the whole quality range and predict the having good prediction to the experiment.

The above three models all use the thermal resistance network method. The disadvantages found for using this method is the need of heat transfer correlations. These correlations are empirically developed and therefor limited to valid operating ranges, requiring careful selection. The advantage to using this method is the ease of modeling. No complicated differential equations are required to solve the model.

One alternate method to the discretization and thermal resistance network is a finite difference nodal analysis which tracks heat transfer and pressure drop for plate heat exchangers between all plate sets and along each plate set. This finite difference nodal model allows for characterization of heat exchanger performance while accounting for phase change, misdistribution, and complex geometric configurations. Qiao et al. [14] analyzed one such finite difference nodal model that accounted for complex flow configurations, including multiple flow passes of both fluids. The key assumptions made by this investigation were as follows. All fluid properties were calculated based on the inlet conditions to each segment. The phase remains constant throughout a segment. Plate surface temperature was constant across the whole segment.

The heat exchanger was adiabatic and negligible longitudinal heat conduction along the plates of though the fluids. And the fluids were perfectly mixed at the end of each pass. The pressure drop across the heat exchanger is comprised of three parts: the loss across the inlet and outlet manifolds, the frictional loss across the core itself, and the gravitational effects. Frictional losses were calculated using the Shah and Sekulic [4] friction factor correlation. Heat transfer characteristics were predicted using the Yan and Lin [15] single phase correlation. Condensation heat transfer was not tested because the authors argued the boiling tests sufficiently demonstrated the capability of the model to accurately model phase change. This assumption however is not valid. The model was tested correlations for boiling heat transfer and therefore valid as an evaporator or boiler but not as a condenser. The modes of heat transfer are different between boiling and condensation therefore a separate study is required. Several two-phase boiling heat transfer correlations were tested: Yan and Lin [15], Hsieh and Lin[16], Ayub [17] , and Han et al. [18] correlations. Each correlation under predicted the heat transfer of the refrigerant. The Haung et al. [19] correlations, however, provide a more accurate heat transfer coefficient. Multiple cases were studied with all predictions being accurate for the heat load within 5% of the experiment. The advantage of the nodal method is the ability to predict more complex geometries and flow configurations than the discretization, as well as the ability to account for conditions such as misdistribution. This does however come at the cost of a more complex model and there is still the requirement of heat transfer correlations.

Glazar et al. [20] is an example of a study which developed a model using a finite element technique to analyze the effect of channel geometry on compact heat exchanger performance. The study developed a numerical performance model of an air coupled microchannel coil heat exchanger and validated the model with experimental data. The heat exchanger contained 68

parallel flat tubes connected with approximately 700 straight fins. Single phase distilled water flowed through the micro-channels while air passed over the straight finds in cross flow. The model eliminated any symmetric planes in the heat exchanger to reduce computational requirements. The remaining heat exchanger was then subdivided into 110 million three dimensional control volumes which allowed for a system of continuity equations to solve for the heat transfer. This eliminated the need for a thermal resistance network and heat transfer correlations. The model could accurately predict all experimental temperatures to within ±5 K. The investigation did not give any metric for pressure drop accuracy. The remaining portion of the investigation was performed using the empirical model. Six channel geometries were tested: square, barrel, circular, hexagonal, vertical rectangular, and square diamond. Heat transfer effectiveness and pressure drop were used as the metrics for comparing the geometries. Increases in air side velocity decreased the overall effectiveness which increase the effect of channel geometry. In the range of $0.6 < \varepsilon < 0.7$, channel geometry has the most impact on heat exchanger effectiveness, and the square diamond and hexagonal channels performed best in terms of heat transfer. In terms of pressure drop the square and circular channels had the lowest pressure drop.

The previously mentioned studies have all used discretization techniques that are inherently discontinuous. Gut and Pinto [21] developed a general model for predicting the performance of a plate frame heat exchanger with a continuous property distribution instead of a discretization method. The investigation only studied single phase heat transfer, but examined many different flow configurations. The key assumptions were the same as the Qiao investigation. The pressure drop was a function of frictional, manifold, and gravitational loss. The friction factor and Nusselt number were calculated using correlations proposed by Shah and Focke [22], Saunders [23], and Mehrabian et al. [24]. The model was not compared to any experimental data. The Gut and Pinto

model is a good example of an investigation which avoided discretization, however, even when modeling single phase heat transfer, the model was complex, so its use in two phase conditions would be impractical.

This section presents examples of various heat exchanger modeling methods. The methods presented were the, discretization and thermal resistance network, finite element, and continuous property distribution methods. The discretization and thermal resistance network method is simply molded but requires the use of empirical correlations. The finite element model requires some more complexity, however does not require the use of empirical correlations. And the continuous property distributions does remove the discontinuity of the previous two models but is more complex and also requires the use of empirical correlations, so as long as the discontinuity is acceptable this method is not preferred. Similarly each of the models described above are for different heat exchanger types and applications, none of which are similar to the heat exchangers of this investigation.

2.1.Correlation review

The heat exchanger models used in this study are built on the thermal resistance network method. This method uses empirical correlations to determine heat transfer coefficients. A literature review was used to narrow the vast number of correlations to a few that were applicable to the present study. The correlations that will be presented were developed specifically for single phase and boiling flow though plate frame heat exchangers, as well as through micro and mini channels. These correlations were developed empirically from data sets either collected specifically for the particular investigation or from a data bank of heat transfer experiments constructed from multiple previous investigations.

There are many metrics to record the accuracy of a correlation, however, this investigation will focus on mean absolute error and the percent of data within an error range. The mean absolute error (MAE) is calculated using the equation (2.1) below:

$$MAE = \text{Ave}\left(\text{abs}\left(Error\right)\right) \tag{2.1}$$

The other metric used to express accuracy is the percentage of predictions that fall within a given personage band of the data collected. For example 85% of the heat transfer coefficients calculated predicted the collected data within ±25% error.

2.1.1. Plate Frame Correlations

A plate frame heat exchanger consists of a stack of corrugated stainless steel plates separated by rubber gaskets and compressed in a frame. The plates have a stamped chevron corrugation pattern and the angle from the vertical defines the chevron angle, see in Figure 2-2 where β represents the chevron angle.

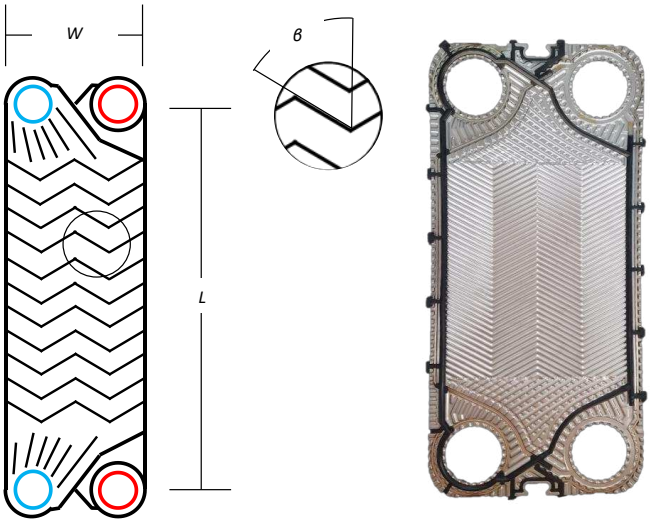

(a) (b)

Figure 2-2. Plate frame heat exchanger chevron plate, (a) geometry description, (b) Image of actual plate

Brazed plate heat exchangers follow a similar construction, but the plates are brazed together instead of gasketed. The same flow characteristics are exhibited in both heat exchangers, so both heat exchanger correlations were investigated. The fallowing sub sections will outline a correlation review for first boiling heat transfer and pressure drop, then single phase heat transfer and pressure drop in chevron plate heat exchangers with the intention of finding a set of correlations to be tested in the model.

2.1.1.1.Plate Frame Boiling

Correlations have been developed based on experiments [15,16,18,19,25–27], and based on data banks of heat transfer data collected over a field of experiments [17,28,29]. Experiments were carried out utilizing small bench top plate heat exchangers, some unmodified from their commercial form [16,18,19,26,28], some modified to allow for specialty analysis such as flow visualization [15,30]. Typical experiments collect temperatures and pressures at the inlet and outlets of the two fluid streams, along with the flow rates for the two fluids. The heat duty and heat flux were controlled using the hot side fluid, often water or a water-glycol mixture. The test heat exchangers in all of these studies are on the bench top scale, much smaller than the industrial sized heat exchangers used in vapor compression application. The experiments studied the effects of a range of parameters including: chevron angle, heat and mass fluxes, and fluids. The correlations presented below have been found to be relevant to the present study as either a potential correlation to be tested in the model, or as insight into the physics of the heat transfer and pressure drop characteristics in chevron plat heat exchangers. Many of the correlations and their developed parameter ranges are presented in Table 2-1.

Table 2-1: Plate frame boiling heat transfer correlation review.

Name	Working Fluid	# of Channels	Chevron Angle	mass flux		heat flux		T_{sat}		Quality		L	w	dh
	-	-	degree	kg /m2s		kW/m2		c		-		mm	mm	mm
Test	**R134a**	**150**	**60**	**5.8**	**6.8**	**2**	**2.8**	**10**	**15**	**0**	**1**	**1200**	**430**	**5.1**
Han et al. [18]	R22 / R410	3	20,35,45	13	34	2.5	8.5	5	15	0.9	0.95			
Hsieh and Lin [16]	R410	2	60	50	125	2	37	10	30	0	0.9	450	120	6.6
Huang et al.[19]	R134a / R507a / R12 / Ammonia	23	28,44,60	5.6	30.3	1.9	7	5	13	0.01	0.95	519	180	3.5
Lee et al. [25]	R134a / Water Glycol	33 / 39 / 53	60	45	268			-6	29			311	112	3.9
Longo Gasparella [27] [31]	R1233zd(E)	Unknown	60	5.5	27	6	49	105	105	0.01	0.6	357	103	4.4
	R410	9	65	4	50	3	21	5	20	0.45	0.7	278	72	3.2
Yan and Lin [15]	R134a / 410 / R245fa	9	65	4	50	3	21	5	20	0.45	0.7	278	72	3.2
Han et al. [18]	R134a	2	60	55	70	11	15	31	31	0.09	0.9	450	120	5.9

One such insight which has lead the search for potential correlation is that heat and mass fluxes had a significant impact on the heat transfer coefficient in plate heat exchangers [18,31]. In the Longo and Gasparella investigations [18,31], data was collected around a brazed plate heat exchanger with evaporating R134a, R410a, or R236fa refrigerant and a water-glycol coolant. The inlet quality of the refrigerant was controlled with a preheater, and the refrigerant exited as a superheated vapor. For a constant heat flux, the experimental data showed that as mass flux increased the average heat transfer coefficient increased. At low mass flux ranges, $G < 40$ kg m^{-2} s^{-1} , pool boiling correlations become valid [27,31] because flow convection heat transfer is significantly smaller than the nucleate boiling portion. The Longo and Gasparella [31] investigation collected data for a range of mass fluxes, $10 < G < 40$ kg m^{-2} s^{-1}, and compared the data from their study to the Cooper [32], Equation (2.2). and the Gorenflo [33], Equation (2.3) pool boiling correlations:

$$h_{\mathrm{nb}} = 55 \cdot P_{\mathrm{red}}^{0.12} \cdot \left(-\log_{10} P_{\mathrm{red}}\right)^{-0.55} \cdot MW^{-0.5} \cdot (q'')^{0.67} \tag{2.2}$$

$$h = h_{\mathrm{o}} \cdot 1.2 \cdot P^{0.27} + \left(2.5 + \frac{1}{1-P}\right) \cdot P \tag{2.3}$$

Where h_{o} in the Gorenflo correlation is a reference heat transfer coefficient. The Cooper correlation predicted the Longo and Gasparella data with a mean absolute deviation of 8.2%, 12.7%, and 34.5% for R134a, R410a, and R236fa, respectively. While the Gorenflo correlation predicted the data to an MAE equal to 12.3%, 23.9%, and 40.7% for R134a, R410a, and R236fa, respectively. The authors concluded that the R134a and R410a data collected was dominated by nucleate boiling heat transfer, while the R236fa data contained both nucleate boiling and convective boiling contributions. The investigation did not create a new correlation and only sought to determine the viability of a nucleate boiling correlation for predicting the heat transfer coefficients of flow boiling at low mass flux in a plate heat exchanger. It was concluded that both correlations were

adequate for use with R134a and R410a, with the Cooper resulting in slightly lower error, however both correlations significantly under predicted the R236fa results and were not recommended. The investigation tests at low mass fluxes, fluxes which are similar to the present investigation, see table 2-1, and because of the found accuracy of the Cooper pool boiling correlation at the low mass flux range, the correlation will be tested in the model and further test its viability in plate heat exchangers.

The Haung et al. [19] investigation is another good example of a nucleate boiling dominated correlation. The Nusselt correlation is a function of heat flux, enthalpy of vaporization, thermal diffusivity, saturation temperature, and liquid thermal conductivity. The low mass flux in the Huang et al. investigation caused the flow parameters (Reynolds number and chevron angle) to be less significant. Therefore, the heat transfer was dominated by nucleate boiling and the Nusselt correlation took the form of Equation (2.4).

$$Nu = \frac{h_r \cdot d_o}{k_r} = 1.87 \times 10^{-3} \cdot \left(\frac{q'' \cdot d_o}{k_r \cdot T_{sat}} \right)^{0.56} \cdot \left(\frac{i_{fg} \cdot d_o}{\alpha_r^2} \right)^{0.31} \cdot Pr_r^{0.33} \tag{2.4}$$

This correlation is unique because the characteristic length used is a bubble diameter, not hydraulic diameter. The bubble diameter is defined by Equation (2.5),

$$d_o = 0.0146 \cdot \theta \cdot \left[\frac{2 \cdot \sigma}{g \cdot (\rho_{sl} - \rho_{sv})} \right] \tag{2.5}$$

Where θ is the bubble contact angle and σ is the fluid surface tension. The heat transfer correlations was developed based on 222 data points with an associated 7.3% MAE. The pressure loss cannot be described independently of the fluid flow because flow properties are required for frictional pressure drop. Huang et al. correlated the two-phase friction factor, Equation (2.6), with the equivalent Reynolds number defined by equations (2.7) and (2.8).

$$f_{tp} = \frac{3.81\times10^{4}\cdot F_{rf}}{Re_{tp}^{0.9}\cdot\left(\rho_{sl}/\rho_{sv}\right)^{0.16}} \tag{2.6}$$

$$Re_{tp} = \frac{G\cdot Dh}{\mu_{tp}} \tag{2.7}$$

$$\mu_{tp} = \left[\frac{x_m}{\rho_{sl}} + \frac{1-x_m}{\rho_{sv}}\right]^{-1}\cdot\left[\frac{X_m\cdot\mu_{sl}}{\rho_{sl}} + \frac{\left(1-x_m\right)\cdot\mu_{sv}}{\rho_{sv}}\right] \tag{2.8}$$

The pressure drop was correlated to a MAE equal to 6.7%. The Huang et al. correlation was found relevant to the present investigation as a heat flux dominated correlation which was developed for lower mass flux ranges, 10.7 to 31.4 kg m^{-2} s^{-1}, and similar saturation temperatures for R134a, 5.9 – 13.0 °C, as the present study, see table 2-1. Due to this both the heat transfer and pressure drop correlations were tested in the plate frame model.

At higher mass flux ranges, correlations can account for both components using weights for the convective heat transfer and the nucleate boiling terms [16,19]. This can be done using enhancement and suppression factors multiplied by the convective and nucleate boiling contributions, respectively. The Hsieh and Lin [16] investigation used a data bank of heat transfer data to develop the correlation in this manner. The data ranged in mass flux between 50 to 100 kg m^{-2} s^{-1} .The convective portion in the correlation was the Dittus-Boelter [11] correlation and the pool boiling was represented with the Cooper [32] correlations. These correlations were not developed for use in plate heat exchangers and the Dittus-Boelter correlation requires turbulent flow, and yet the overall weighted correlation predicted the heat transfer coefficient for a large amount of the data bank, 74% to ±25% error. The frictional pressure drop equation developed from the same data bank was a function of equivalent Reynolds number and was correlated to an MAE of 18%. The accuracy of both the frictional pressure drop and heat transfer correlations makes

them attractive for use in the model. This correlation, though developed for mass fluxes higher than the present study it was developed for similar heat fluxes, and as found by Longo and Gasparella [27], heat flux can have a significant impact on the calculation of heat transfer coefficient. The Hsieh and Lin correlation was tested in the model due to its development for similar heat fluxes as well as its method of weighting terms.

There are numerous correlations which were developed empirically [17,18,25,26,29]. One of the primary difficulties in developing correlations empirically is the effect of vapor quality. The vapor quality was an important parameter for predicting the heat transfer and pressure drop across the plates because the proportion of vapor to liquid in a cross section has a large effect on fluid properties. Furthermore, as the quality increases, regardless of all other parameters, the heat transfer coefficient increases. The heat transfer will increase as a result of increased fluid velocity due to decreased fluid density. The higher fluid velocity will increase convective heat transfer [18]. There are a number of strategies to account for vapor quality. One method was to use equivalent parameters which are normalized by quality. A common example was the use of equivalent mass flux [26], expressed in equation (2.9).

$$G_{\mathrm{eq}} = \frac{\dot{M}}{A_{\mathrm{c}}} \cdot \left[\left(1 - X\right) + X \cdot \left(\frac{\rho_{\mathrm{sl}}}{\rho_{\mathrm{sv}}} \right)^{0.5} \right] \tag{2.9}$$

The equivalent mass flux is used in place of the mass flux term in dimensionless parameters such as Reynolds and boiling numbers.

The Han et al. [18] correlation is an example of a simple correlation. The correlation was considered due to its strong dependence on plate geometry, though it does not encompass many of the parameters, see table 2-1. The Nusselt correlation, Equation (2.10), is a function of equivalent Reynolds number, equivalent boiling number, and Prandtl number.

$$Nu = Ge_1 \cdot Re_{eq}^{Ge_2} \cdot Bo_{eq}^{0.3} \cdot Pr^{0.4} \tag{2.10}$$

$$Bo_{eq} = \frac{q''}{G \cdot \left[\left(1 - x_m\right) + x_m \cdot \left(\frac{\rho_l}{\rho_v}\right)^{0.5} \right] \cdot i_{fg}} \tag{2.11}$$

Where the Ge values are non-dimensional geometric parameters given by Equations (2.12) through (2.15).

$$Ge_1 = 2.81 \cdot \left(\frac{P_{co}}{d_h}\right)^{-0.041} \cdot \beta^{-2.83} \tag{2.12}$$

$$Ge_2 = 0.746 \cdot \left(\frac{P_{co}}{d_h}\right)^{-0.082} \cdot \beta^{0.61} \tag{2.13}$$

$$Ge_3 = 64,710 \cdot \left(\frac{P_{co}}{d_h}\right)^{-5.27} \cdot \beta^{-303} \tag{2.14}$$

$$Ge_4 = -1.314 \cdot \left(\frac{P_{co}}{d_h}\right)^{-0.62} \cdot \beta^{-0.47} \tag{2.15}$$

The frictional pressure drop was correlated using Equation (2.16).

$$f_{tp} = Ge_3 \cdot Re_{eq}^{Ge_4} \tag{2.16}$$

The study collected data from three corrugated plate evaporators, each with a different chevron angle, 70°, 55°, 45°. The developed correlation was able to predict 90% of the experimental data to within ±15% for both the Nusselt and friction factor correlations. The dependence on many geometric parameters potentially could be scalable and beneficial in the study of large industrial plate frame evaporators.

The Yan and Lin [15] investigation was considered because of it use of flow visualization and was a good example of an empirical correlation developed for evaporation heat transfer of R-134a in corrugated plate heat exchangers. The investigation tested two plate heat exchangers,

where the first had three steel plates for heat transfer and pressure drop analysis and the second heat exchanger had a transparent plate used for flow visualization. Each heat exchanger had a single cold side channel and a single hot side channel with 60˚ chevron angle. The evaporative heat transfer coefficient for R134a was determined from experimental data collected at two mass fluxes, 55 and 70 kg m^{-2} s^{-1} with the same heat flux. At vapor qualities less than 0.45, the mass flux does not have a significant effect on heat transfer coefficient. Thus, nucleate boiling was the dominant mode of heat exchange. When the vapor quality is greater than 0.45, the heat transfer coefficient grows exponentially with increasing vapor quality, leading to more convective boiling heat transfer. This distinction between flow regimes, nucleate and convective boiling, was further validated using flow visualization. At low vapor qualities, there was significant bubble generation which indicated flow boiling. At high qualities, turbulent vapor dominates the channel flowing over a liquid film, indicating convective boiling. The evaporative Nusselt correlation was a function of Reynolds number, Prandtl number, boiling number, quality, and density. The two-phase friction factor correlation was split into two regimes: one for equivalent Reynolds numbers below 6000 and another for equivalent Reynolds numbers above 6000. The two-phase friction factor is only a function of equivalent Reynolds number. The Yan and Lin investigation demonstrates the importance of quality on the heat transfer coefficient. The shift from nucleate to convective boiling at the quality of 0.45 is there for needed to be captured in the model developed. There for treating the boiling region of the evaporator as a single zone would introduce large error. This being said, the Yan and Lin investigation was not consider for testing in the present model. This was because the study focuses on the importance of vapor quality but only includes the parameter in the correlation as part of equivalent Reynolds number. This finding would represent itself better as a weighted convective, nucleate boiling correlation.

Lee et al. [25] investigated heat transfer and pressure loss of R1233zd(E) in a plate heat exchanger with high mass flux. Due to a push for lower global warming potential refrigerants, R1233zd(e) has been considered as a drop in replacement for R245fa in Organic Rankine Cycles (ORC). However there has been a limited amount of investigations of this fluid in plate heat exchangers. This investigation compared the characteristics of the two fluids and developed a boiling Nusselt correlation for R1233zd(e). The operating conditions for the experiment were similar to what would be experienced in an ORC, with saturation temperatures between 60˚C and 80˚C, and mass fluxes 32, 45, 58 kg m^{-2} s^{-1}. Each test experience forced convective boiling rather than pool boiling, implying the heat transfer had a greater dependence on mass flux than heat flux. Under the same conditions, the heat transfer coefficients of the two fluids, R1233zd(e) and R245fa, were similar at lower vapor qualities. However, at higher qualities the R1233zd(e) had roughly a 19% lower heat transfer coefficient due to a significantly lower vapor thermal conductivity. The investigation proposed a simple Nusselt number correlation which was a function of equivalent Reynolds and Prandtl numbers. The correlation predicted 97.8% of the data to ±20% error. At low qualities, the two fluids have similar friction factors. At higher qualities the friction factor of the R1233zd(e) becomes significantly higher than that of the R245fa due to a larger ratio of liquid to vapor densities. The data was used to empirically derive a friction factor correlation which is a function of equivalent Reynolds number, liquid Reynolds number, and liquid Prandtl number. The factor was correlated with 95.2% of the data within ±20% error.

The aim of this section was to find a group of boiling heat transfer correlations to be tested in the plate frame model. Not all of the above correlations were tested in the present study, and none of the correlations described above encompass all relevant parameter bound seen in Table 2-2. The four correlations selected were the Cooper [32], Huang et al. [19], Hsieh and Lin [16], and

Han et al. [18] were selected due to encompassment of at least one important parameter or due to some novel correlation method. None of the correlations selected were tested in a heat exchanger of the same scale as the present investigation, though through the review it was found no correlation has.

2.1.1.2.Plate Frame Single Phase

The heat transfer and pressure drop of single phase fluids have been widely studied. This section offers a brief review of the correlations developed in an effort to find several correlations to be tested in the model. Primarily water or a water mixture is used as the working fluid on both sides, and no correlation was found which used a refrigerant, therefore the following review was used to find correlations to be used on both the water-glycol and refrigerant sides of the plate frame model.

Much of the information about the heat transfer characteristics of plate heat exchangers is maintained as proprietary information by heat exchanger manufactures. Therefore there is a lack of this information in the open literature [17], and some information regarding develop correlations may be unknown. Table 2-2 depicts a review of single phase heat transfer correlations in plate heat exchangers, along with their associated valid ranges for relevant parameters such as Reynolds and Prandtl numbers, as well as chevron angle and hydraulic diameter. Several correlations included are of interest to the due to their closeness in parameter ranges to the present investigation. One such correlation is the Rosenblad and Kullendroff [34]. The correlation fully encompassed the required Reynolds number range of the water-glycol and nearly encompassed the range of the single phase refrigerant. The experiments used a mass transfer technique to determine the effect of geometric parameters on heat transfer. From the work the correlation was developed as a function of Reynolds and Prandtl numbers.

Table 2-2. Single phase Plate frame correlations and associated valid parameter ranges.

Name	Working Fluid	Chevron Angel	Re		Pr		dh
	-	degree	-		-		mm
Test Refrigerant	**R134a**	**60**	**130**	**3000**	**0.8**	**3.5**	**5.1**
Test Water-Glycol	**Water-Glycol**	**60**	**180**	**520**	**32**	**34**	**5.1**
Chisholm and Wanniarachchi [41]	Water	30-80	1000	40000	5	5	
Muley and Manglik [38]		30,45,60	600	10000	2	6	5.08
Kahn [36]		30,45,60	500	2500	3.5	6.5	3.9
Thonon [78]	water	30,45,60,75	60	2415			
Muely [39]		30-60	30	400			
Maslov and Kovalenko [35]	Water	60	50	20000			
Talik et al. [79]	Water-Glycol	60	10	720	70	450	4.65
	Water		14500	11460	2.5	50	4.65
Hessami		45,60	200	1800			11
Emerson [80]	Water		10	25			
			40	1000			
Longo and Gasparella [31]	Water	65	200	1200	5	10	
Kumar [81]	Water	60	20	400			
Rosenblad and Kullendorff [34]	Water	60	60	2415			4

The Maslov and Kovaleko [35]correlation is another of interest due to its development for Reynolds numbers encompassing both the single phase refrigerant and water-glycol requirements. The original source of the correlation could not be found, however it has been used widely in literature [17,36,37]. From those sources the correlations itself was found and took the same form as the Maslov and Kovaleko correlation. The source were also use to collect some of the information needed to fill out Table 2-2. Though the information about the development of the correlation is unknown, the correlation is appealing due to its wide Reynolds number range, largest of the review. This would allow for higher trust in future use of the developed model after validation.

The Focke et al. [30] investigation studied the effect of chevron angle on single phase heat transfer in plate heat exchangers. The study used plates with chevron angles equal to 0°, 30°, 45°, 60°, 72°, 80°, and 90°. Rather than using a two working fluid heat exchanger to examine the effects of chevron angle, the investigation used an electric heater to heat the water working fluid. The heat flux was controlled and plates were easily exchanged in this test setup. As the chevron angle increased from 0° to 80°, the pressure drop through the plate increased by 2.5 orders of magnitude while the heat transfer increased by a factor of 4 to 10, depending on flow conditions. The heat transfer was correlated using the Colburn factor and is a function of Reynolds number. The standard deviation between the Colburn correlation and the experimental data was less than 5%. The frictional pressure drop was correlated using a friction factor equation that was only a function of Reynold's number and the standard deviation of the pressure drop was less than 7%.

The Muley and Manglik [38] investigation studied the heat transfer and pressure drop of liquid water flowing through a plate heat exchanger. Three plate arrangements were tested: both plates with 30° chevron angle, both with 60° chevron angle, and one plate 30° and the other 60°. The correlations were developed for the ranges: $2 < Pr < 6$ and $600 < Re < 10^4$. The correlation was a function of Reynolds number, Prandtl number, chevron angle, and the viscosity ratio. The correlation accurately represented the data within ±10% error. The investigation also developed a friction factor correlation which was a function of chevron angle and Reynolds number. The friction factor correlation described the data to within ±5% error. In addition, Muley [39] developed a set of simplified correlations specifically for laminar flow where *Re* was less than 400. The simplified correlation is of interest to this investigation to represent the water-glycol side heat transfer coefficient. The correlation was developed for similar bounds to the present

experiment, with only a slight difference in fluid, the difference between water and water-glycol. The simple correlation will allow for easy model development and operation.

The Garcia-Cascales et al. [40] investigation presents a variety of single phase correlations developed for plate heat exchangers with the intention of model development. One correlation of interest is the Chisholm and Wanniarachchi [41]. The correlation was developed for laminar flow and as a function of Reynolds number Prandtl number and chevron angle. The correlation was tested against data from Focke et al. [30] and found agreement within ±20% error. Another correlation of interest presented was the Kim [42] correlation. The correlation was developed in a water to water chevron plate heat exchanger and was a function of the same parameters as the Chisholm and Wanniarachchi correlation. Both correlations are of interest in the present investigation due to their simple formulation and development for laminar flow. Garcia-Cascaes et al. presents the issue of correlation being developed for a small geometric bounds. The two correlations above do not present their heat exchanger sizes and therefor testing them at the industrial scale could expand their relevance.

The Khan et al. [36] investigation created a heat transfer correlation for water to water plate heat exchangers. The investigation operated with the same three plate arrangements as Muley and Manglik. The correlation was developed for the ranges: $3.5 < Pr < 6.5$, $500 < Re < 2500$ and used a conventional single phase Nusselt number which is a function of Reynolds and Prandtl number. Separate correlations were developed for the three plate configurations and each accurately predicted the experimental data to within ±0.3%. A fourth correlation was developed to encompass all configurations, which sacrificed some accuracy, but fit the data within ±2% for the 30° plates, ±1.8% for the 60° plates, and ±4% for the mixed plate configuration.

The Bogart and Bolcs [43] investigation examined the performance of single phase plate heat exchangers. The experiments were conducted on two brazed plate heat exchangers, where one had 14 plates and the other had 20 plates. The two working fluids were water for the cold side fluid and mineral oil for the hot side. The investigation performed two sets of experiments to determine pressure drop and heat transfer. The pressure drop experiments were performed isothermally. Data was collected for the overall heat exchanger pressure drop which includes the channel, port, and manifold losses. The investigation did not separate these losses, instead opting to determine the overall pressure loss. The resulting Fanning friction factor correlations were only a function of Reynolds number. Five correlations were developed for three Reynolds ranges. Two of the correlations were simplified at the expense of accuracy. The least accurate of these correlations was correlated to within 10% and the most to within 1%. A Nusselt number correlation was developed for Reynolds numbers greater than 2300 that is a function of Reynolds number, Prandtl number, and viscosity. Several more correlations were developed for laminar flow which have a similar form to the turbulent correlation. The errors range from 1% to 2.5% for the heat transfer correlations. Separating the correlations into flow regimes does allow for a simpler formulation and or a reduced error compared to a unified correlation across a larger range of Reynolds numbers. However by doing this, it makes developing a model more difficult, due to the need of logic to determine which correlation is needed, mitigating the gain of a simple correlation.

2.1.2. Bar plate heat exchanger

Bar plate heat exchangers are constructed by stacking sets of plates separated by fins as shown in Figure 2-3. These plate stacks are then brazed together to form a heat exchanger core. The space between the stacked plates and the fins forms the fluid channels. These channels alternated between two working fluids, a low boiling point refrigerant, and a water glycol mixture

which was used as the heat input. The geometry of a bar plate heat exchanger can be varied significantly and many flow orientations are possible: cross flow, co-flow, counter flow, or any combination of those. The channel geometries can be varied within the core; for example a channel cross-sectional area can increase along the flow path to accommodate fluid expansion during boiling. The fallowing section provide a literature review of boiling and single phase heat transfer and pressure drop correlations developed for use in mini/micro channels and bar plate heat exchangers.

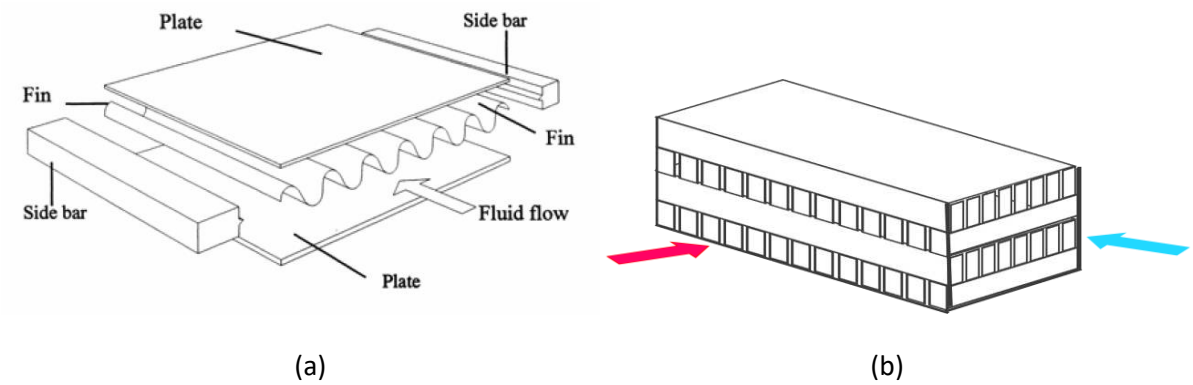

Figure 2-3. Bar plate heat exchanger construction. (a) Exploded view, Picon-Nunez [8]. (b) Cross flow cut away where red represents the hot flow path and blue the cold flow path.

2.1.2.1.Bar plate boiling

The present work focuses on compact evaporators with micro and mini channels. The hydronic diameter at which a channel is considered mini or micro versus a macro scale channel is inconsistent through the literature, where Bertsch et al. [44] defines the micro scale less than 2mm and no distinction between mini and micro scales. Fernando [45] defines the micro scale between 0.01 and 0.2 mm and the mini scale between 0.2 and 3mm. Thome [46] defines the micro scale as the diameter of the bubble formed when boiling. For the present investigations the Bertsch et al. consideration was used and channels less than 3 mm in hydraulic diameter will be considered micro channels. Table 2-3 presents the correlations discussed in this chapter.

Table 2-3. Microchannel boiling heat transfer correlation review.

Correlation	Fluid	Channel Shape	Hydraulic Diameter	Mass Flux Low	Mass Flux High	Heat Flux Low	Heat Flux High	Quality low	Quality High	T_{sat} low	T_{sat} High
	-	-	mm	Kg m^{-2} s^{-1}		W cm^{-2}		-		°C	
Agostini et al.	R134a	Rectangular	0.77,2.01	83	467	0.44	1.5	0	1		
[92,93]	Multi	Rectangular	0.34	281	1501	0.7	42	0.02	0.78	25	43
Bertch et al. [94]	R134a multi	Rectangular Rec /	0.54-1.09	20	350	0.5	22	0	0.95	8	30
Bertch et al. [44]	R134a	Circular	0.16-2.92	20	3000	0.3	115	0	1	-194	97
Cooper [32]	Multi	Pool		0	0	0.01	60	0	1		
Hamdar et al.[95]	R152a	Square	1	200	600	0.1	0.6				
Kandlikar [96]	Multi(8)		4.0-32	13	8179	0.03	228	0.001	0.987		
Kuznetsov et al. [49]	R134a	Rectangular	0.975	23	190	0.1	1.6	0	1		
Lazrek and Black [97]	R113	Circular	3.1	125	750	1.4	38	0	0.6		
Lee and Lee [98]	E113	Rectangular	0.78-3.63	50	200	0	1.5	0.15	0.75		
Li and Wu [52]	Multi	Rec / Circular	0.2-3	20	3500	0	800	0	1	0	31
Liu and Winterton [99]	Multi (9)	Circular	2.95-32	12.4	8179.3	0.035	262	0	0.948		
Lovegrov and Robertson[100]	R11	Serrated fin			150				0.04		
Raju et al.[101]	R134a	Offst Strip fins	1.1894	50	82	0.14	0.22	0.32	0.75	-1	5
Thome et al. [46]	Multi (9)	Circular	0.7-3.1	50	564	0.5	17.8	0.01	0.99		
Tran et al. [54]	R12	Rectangular	2.4	44	832	0.036	1.29	0	0.94		
Warrier et al. [53]	R84	Rectangular	0.75	557	1600	0	0.599	0	0.55	26	60
Yun et al. [102]	r410	Rectangular	1.36-1.44	200	400	1	2	0	0.85	0	10

The micro channel correlations were developed similarly to the plate frame correlations, as a weighted average of nucleate and convective boiling terms or as a single empirical correlation. The Bertsch et al. [44] investigation is an example of the weighted average format and collected heat transfer data from 14 studies found in literature on boiling heat transfer through micro channels. 3899 data points were used to develop a microchannel boiling heat transfer correlation. The correlation was developed on the basic Chen [47] flow boiling format which scaled nucleate and convective boiling coefficients. The correlation is shown in Equation (2.17), with weighted nucleate boiling and two-phase convective terms:

$$h_{\text{tp}} = h_{\text{nb}} \cdot S + h_{\text{conv,tp}} \cdot F \tag{2.17}$$

Micro channels have relatively short lengths and small diameters. Because of the high frictional pressure loss associated with the small diameters, the mass flux through the channels is reduced which often leads to low Reynolds numbers. The nucleate boiling term in the Bertsch et al. correlation was predicted by the Cooper [32] pool boiling correlation, shown in equation (2.18).

$$h_{\text{nb}} = 55 \cdot P_{\text{red}}^{0.12} \cdot \left(-\log_{10} P_{\text{red}}\right)^{-0.55} \cdot MW^{-0.5} \cdot (q'')^{0.67} \tag{2.18}$$

The Cooper pool boiling correlation is also used in the study by Hsieh et al. [26] and the two-phase convective heat transfer coefficient is calculated as a vapor quality scaled function of the single phase vapor and liquid Hausen correlation [48]:

$$h_{\text{conv,tp}} = h_{\text{conv,sl}} \cdot \left(1 - X\right) + h_{\text{conv,sv}} \cdot X \tag{2.19}$$

$$h_{\text{conv,sp}} = \left(3.66 + \frac{0.0668 \cdot \frac{Dh}{L_c} \cdot Re \cdot Pr}{1 + 0.04 \cdot \left[\frac{Dh}{L_c} \cdot Re \cdot Pr \right]^{2/3}} \right) \cdot \frac{K_1}{Dh} \tag{2.20}$$

The suppression factor and enhancement factor are calculated using equation (2.21) and (2.22), respectively.

$$F = 1 + 80 \cdot e^{-0.6 \cdot Co} \tag{2.21}$$

$$S = 1 - X \tag{2.22}$$

The suppression factor, *S,* is multiplied by the nucleate boiling heat transfer coefficient to account for the reduced liquid available as the vapor quality increases. The enhancement factor, *F*, is multiplied by the convective heat transfer coefficient to account for the increased flow velocity due to the decrease in fluid density. The resulting correlation has a mean absolute error MAE less than 28% and predicts 60% of the measurements with an uncertainty less than ± 30%. The correlation is valid over for mass fluxes from 20-3000 kg m^{-2} s^{-1}, heat fluxes from 0.4-115 W cm^{-2} s^{-1}, and saturation temperatures from -194 to 97 °C. This correlation is of particular interest to the present study, because it was developed off of a large data bank, the correlation encompasses a wide range of parameter values, including the range of heat and mass fluxes, saturation temperatures, fluids, and hydraulic diameters tested in the present study, see Table 2-3. Because of this the correlation was tested in the bar plate model.

The Kuznetsov et. al. correlation [49] is another example of a correlation developed from a data bank where the total heat transfer coefficient is a scaled composite of flow convection and nucleate boiling terms:

$$h^2_{tp} = \left(h_{nb} \cdot S\right)^2 + \left(h_{conv,tp} \cdot F\right)^2 \tag{2.23}$$

The correlation uses the Danilova [50] refrigerant pool boiling equation for the nucleate boiling term rather than the Cooper equation [32] and the flow convective term is calculated from a laminar liquid Nusselt number. The Nusselt number for this investigation was calculated using

Kays and Crawford [51] for laminar flow in rectangular channels. Furthermore, the suppression and enhancement factors, Equations (2.24) and (2.25), are defined differently.

$$F = \left[1 + X \cdot Pr_{sl} \cdot \left(\rho_{sl}/\rho_{sv} - 1\right)\right]^{0.35} \tag{2.24}$$

$$S = \left(1 + 0.55 \cdot F^{0.1} \cdot Re_{sl}^{0.16}\right)^{-1} \tag{2.25}$$

The study does not offer any correlation error or number of data points used. However its encompassment of all important parameters except hydronic diameter, makes it appealing for use in the model, Table 2-3. The hydraulic diameter tested is similar to the present study, only an 18% difference. Therefore, even in spite of a lack of accuracy given, the correlation was tested.

The previous correlations have been weighted functions of nucleate and convective boiling, however, several studies have focused on developing simple empirical equations correlations. A simple correlation could allow for quicker model development and run time. Li and Wu [52] developed a simple correlation for micro channel flow boiling by utilizing a data bank of heat transfer data containing 3700 points from twenty eight studies. The data was used to empirically develop a Nusselt correlation as a function of liquid Reynolds number, Bond number, and Boiling number. The data was used to determine constants used in the equation shown below:

$$Nu = 334 \cdot Bo^{0.3} \cdot \left(Bn \cdot Re_{l}^{0.36}\right)^{0.4} \tag{2.26}$$

The correlation predicted 65.5% of the data bank within ±30% which is significantly more accurate than other correlations of similar form. The Warrier et al. [53] correlation was tested against the same bank and always over predicted the Nusslet number, up to 325%. The accuracy of the correlation over a wide range of parameters is attractive because it allows has a wide use range. It was therefore tested in the bar plate model.

The Warrier et al. [53] investigation is another example of a correlation developed as a simple function. However this investigation did not use a data bank for validation. The heat transfer and pressure drop characteristics of flow boiling FC-84 through a multi mini channel test section were studied. The aluminum test section consisted of five rectangular channels placed in parallel. The dimensions of each channel were Dh = 0.75 mm and L = 307.35 mm. Experiments were conducted where the inlet temperature was varied between 26, 40, and 60˚C, the mass flux was varied from 557-1600 kg m^{-2} s^{-1}, and the heat flux was varied from 0-5.99 W cm^{-2} s^{-1}. Two phase boiling heat transfer correlations were developed for subcooled and saturated boiling. The subcooled boiling correlation was a function of boiling number and subcooled parameter, and developed off a small data set, therefore is limited to the bounds, $0.0<Sc<0.80$ and $0.00014<Bo<0.00089$. This correlation was validated from 200 data point collected, and found to match the experiment with 75% of the data falling within ±15% and all of the data falling within ±40%. The saturated boiling correlation is a function of boiling number and quality. Similar to the subcooled boiling data limitation, the saturated boiling correlation is limited to qualities between 0.0 and 0.55 and boiling number between 0.00027 and 0.00089. This correlation was found to deviate from the experiment by a maximum of ±28%. This correlation was developed based on a small sample of data and only a single test section geometry, therefore has limited use. Furthermore the separation of subcooled and saturated boiling presents a modeling difficulty which negates the benefit of a simple empirical correlation.

Tran et al. [54] investigated the frictional pressure drop for boiling refrigerant flow through small channels. Two refrigerants, R134a and R12, were tested in a 2.46 mm inner diameter, smooth walled brass tube. R12 was also tested in a brass rectangular channel with a hydraulic diameter of 2.40 mm. The study also considered a third fluid, R113, with supporting data from Wambsganss

et al. [55] which used a stainless steel circular tube with a diameter of 2.92mm. The proposed boiling pressure drop correlation was developed from Chisholm's B coefficient method [56]. The resulting correlation is a function of local vapor quality, confinement number, and liquid only frictional pressure drop. When comparing the correlation predicted pressure drops to the experimentally measured pressure drops, 93.8% of the data points were predicted to within ±30%.

The above section presents a review of heat transfer and pressure drop correlations which can be used in the bar plate model or present insight into the heat transfer and pressure drop characteristics of flow in the micro channels.

2.1.2.2.Bar plate single phase

Single phase heat transfer in micro and mini channels has been widely studied because these geometries are widely prevalent in advanced electronics cooling and engine radiator applications. The purpose of this review is to find potential correlations which can be tested in bar plate model to represent the single phase regions of the refrigerant side and or the water-glycol heat transfer. The current study is interested in mini and micro channels due to the experimental bar plate heat exchanger having comparable hydraulic diameters to a micro channels, less than 3 mm [44].

Garimella et al. [57] examined rectangular micro tubes to develop a correlation for tube side heat transfer in automotive style, air coupled heat exchangers. The experiment used a single tube test section, including air side louvered fins on both sides of the tube. A single test section was used to increase controllability. A water-glycol solution flowed through the tube side while cold water was passed in counter flow through a baffled shell. Water was used on the air side because it has excellent transport properties relative to air. The increased fluid properties along with the significantly larger heat transfer area on the air side, caused the thermal resistance to be much smaller than the tube side resistance which allowed for a focus on the tube side heat transfer.

Table 2-4. Single Phase Bar Plate Correlation Review.

Name	Working Fluid	Channel Shape	dh	Re		Pr	
	-	-	mm	-		-	
Test Refrigerant	**R134a**	**Rectangular**	**1.193**	**540**	**5400**	**0.82**	**3.5**
Test Water-Glycol	**Water-Glycol**	**Rectangular**	**0.950**	**55**	**205**	**30**	**67**
Shah and London [59]			>0.1	0	2300		
Sieder and Tate [63]			>0.1	0	2300	0.48	1670
Hartnett and Kostic [83]		Rectangular	>0.1	0	2300		
Dittus Boelter [11]		Circular		10000		0.7	160
Choi et al. [62]	Nitrogen	Circular	0.003-0.081	30	2000		
Churchill [65]		Circular		0	10^7	0.2	9810
Garimella et al. [64]	Water-glycol	Rectangular		118	10671	0.243	16.2
Peng and Peterson [61]		Rectangular	0.155-0.747	0	2200		
Stignor et al.[103]	Glycol	Rectangular	2.06-4.73	0	2300		
Benjan		Rectangular		0	2300	0.7	0.7
Kays and Crawford [51]		Rectangular		0	2300		
Gnielinski [64]		Circular		3000	5x10^6	0.5	2000

The heat transfer coefficient was calculated from the experimental data using a thermal resistance network. The correlation was continuous over the laminar, transitional, and turbulent regimes, using a weighted sum of the Nusselt numbers in these regions. The laminar, transitional, and turbulent Nusselt numbers are functions of the Reynolds number, Prandtl numbers, hydraulic diameter, flow length, and the viscosity. The correlation accurately predicted the test data within ±10% error. The correlation development is similar to the bar plate conditions and with its low error, the correlation is in consideration for use in the model.

Some investigations, rather than developing new correlations specifically for micro channel flow, investigate the use of previously developed correlations for similar geometries in micro channels. One such investigation is by Sahar et al. [58], where fluid was passed through a square micro channel with a hydraulic diameter ranging from 0.1 to 1 mm as well as a rectangular micro channel whose aspect ratio was varied from 0.39 to 10 with a hydraulic diameter fixed at 0.56 m. The investigation did not use experimental data to determine the correlation accuracy, but used a high fidelity simulation in Fluent. The simulation itself was validated using data collected from an identical test facility with a 0.56 mm hydraulic diameter. The Nusselt number from the collected data and the simulation was compared to correlation developed by Shah and London [59] and Bejan [60]. The Shah and London correlation had good agreement with the collected heat transfer data while the Bejan correlation slightly over predicted the Nusselt number. Because of this, the two correlations could be considered for use in micro channel heat exchanger modeling.

Another investigation which tests a multitude of correlations for their predictive ability in micro channels was the Fernando et al.[45] investigation. The study collected data around an array of multi-port extruded aluminum tube encased in a shell. Warm water was passed through micro channel sides and was cooled via cold water passed through the shell over the tubes. Several correlations include in Table 2-4 were tested by Fernando et al. It was found for the laminar test regions the Peng and Peterson [61] correlation best predicted the experimental Nusselt values. However this was only at the lower Reynolds numbers, below 1300. Others correlations such as Shah and London [59], Choi et al. [62], and Sider ant Tate [63] were test. It was found that the Chio et al. correlations under predicted the Nusselt number below a Reynolds number of 500 and over predicted the rest of the range slightly. The other two correlations did not capture the Nusslet Reynolds relation well, significantly over predicting the Nusselt number at low Reynolds number

and significantly under predicting the Nusselt number at high Reynolds numbers. Though the Fernando et al. investigation did not see good representation with the correlations mentioned above are of interest in the present investigation as representation for the water glycol side heat transfer. Particularly the Peng and Peterson correlation which did show fair representation at the Reynolds regions similar to those of the water-glycol in the bar plate heat exchanger. Fernando et al. also investigated turbulent heat transfer. The most interesting of which are the Gnielinski [64] and the Garimella et al. [57] correlations tested. The Gnielinski turbulent correlation was able to predict the heat transfer with the smallest maximum deviation, 6% difference. However the correlation was developed for Reynolds ranges significantly too high for the water-glycol side of the heat exchanger in this study and barley encompasses the high end of the single phase refrigerant. The Garimella et al. correlation also predicted the Fernando et al. Nusselt results well with a max difference of -19%. However the Garimella et al. correlation is valid or Reynolds ranges encompassing the required single phase refrigerant range. This is a further incentive to test the correlation for both sides of the heat exchanger model.

Though it was not developed specifically for the micro channel application, the Churchill [65] comprehensive heat transfer correlation may be of interest. Churchill sought to create a single correlation for all single phase flow in circular pipes. The correlation was developed with the ability to predict Nusselt numbers for laminar transitional and turbulent flow and was a function of three Nusselt numbers, the Reynold's number, the Prandtl number, and the friction factor. The three Nusselt number required are the laminar value, the value as Reynold's number approaches 2100 and Prandtl number approaches 0, and the value at Reynold's number equals 2100. The correlation is of interest to this investigation because the three Nusselt numbers can be recalculated for rectangular cross sections using the Kays and Crawford [51] values and the correlation can be

used to cover the entire scope of Reynolds numbers used in the model. Due to its comprehensive nature, the Churchill correlation will be tested in the evaporator model for both the water-glycol and the single phase refrigerant.

2.2.Vapor Compression Modeling and Optimization

Air conditioning and refrigeration systems can be a significant fraction of the total electrical consumption of industrial, commercial, and residential buildings. For this reason, extensive research has been performed into the optimization of vapor compression cycles (VCC), which is the primary method of producing space conditioning and refrigeration for these facilities. Investigations, such as Selbas et. al.[66], use exergy based optimization to determine the ideal state points and subsequent heat exchanger areas in a vapor compression cycle where the condenser provides some degree of subcooling and the evaporator superheats the refrigerant. Although many investigations focus on cycle state point optimization, there is a lack of studies which focus on heat exchanger size optimization [66–68]. Minimizing the size of the condenser and evaporator will reduce system volume and overall system cost. Some investigations did determine the required areas, [6,69–71], though most do not investigate actual heat exchanger sizing or configuration. Chen et. al. [69] compared the heat exchanger areas between an ideal Carnot cycle and vapor compression cycle with irreversibility. Bansal and Chin [6] also considered size and configuration of heat exchangers. The authors investigated optimizing a wire and tube condenser on an air-coupled VCC based on a ratio of heat duty and weight. However, there were no studies available that focus on the optimization of different types of liquid-coupled evaporators.

Though no studies have optimized the evaporators, the Shiba and Bejan [70] investigation determined the optimum condenser configuration for a vapor compression system. A heat exchanger model for a counter flow, tube in tube condenser was developed, with refrigerant

passing though the center tube and air through the annulus. Two global conditions were fixed in the study, the overall volume and weight of the condenser. The diameters of the inner and outer tubes were varied along with the tube length to determine system thermodynamic performance. As the diameter of the inner refrigerant tube decreased, the cross sectional area was decreased and length was increased. The decrease in cross sectional area lead to an increase in fluid velocity and, along with the longer path length, the pressure loss though the heat exchanger also increased. This subsequently increased the compressor work and was a detriment to system performance. The air side pressure loss was a function of the ratio of both diameters and was used to determine the required fan power. The refrigerant mass flow rate was adjusted to maintain an energy balance throughout the system, accounting for changes in compressor work. Similar type studies will be needed for the evaporator in the VCC for full system optimization.

2.3. Gaps in Literature

From the literature reviewed above, there are a few primary gaps in the body of work. The first research gap is that most studies in the literature use small scale heat exchangers or test sections with simple geometries to develop heat transfer and pressure drop correlations. It may be necessary to expand and test the validity of the correlations outside their original geometric conditions. Another, is that the heat exchanger models that are developed for plate frame heat evaporators do not incorporate a sub cooled component. There are situations in thermal energy system design where this component may become significant. The second research gap is that, in general, there are few studies that aim to optimize heat exchanger core volume with high fidelity heat exchanger models.

Previous investigations primarily use small heat exchangers with a small number of channel sets. The plate frame experiments in investigations [15,16,18,30,72,73] used 5 or fewer

channel sets while investigations [7,14,19,40,43] used fewer than 40 channel sets. The investigation from Sterner and Suden [74] was the only work with more than 40 channel sets. Furthermore, the plates used in these experiments are typically smaller; the largest was 519 mm by 180 mm [19]. This scale only encompasses the lower end of sizes of plate frame heat exchangers used in practice. These small scale correlations need to be tested against larger heat exchangers for validity. In previous bar plate experiments, only a few channel sets were used in one pass patterns up to 10 cm long. The Ahmadi et al. [75] investigation focused on a plate fin heat exchanger which is very similar to bar plate. Unfortunately, the study focused on a single pass unit, not the heat exchanger as a whole, and only studied single phase flow. Investigations into the accuracy of these correlations at a larger, more practical scale is necessary.

The study by Picon-Nunez et al. [8] was the only investigation to examine the relationship between pressure drop and core volume of a bar plate heat exchanger. There were no investigation of this type for plate frame heat exchangers. In addition, no investigation has been conducted into the relationship of pressure drop and core volume for a specific vapor compression cycle evaporator. Plate frame and bar plate heat exchangers are particularly absent from the literature. Although the Picon-Nunez et al. investigation chose surface enhancement factors as the independent variable, there are many other ways of adjusting pressure drop, such as changing the ratio of the number of channels to the area of each channel.

2.4. Specific aims of the present investigation

The review of the literature shows a need for further expansion in evaporator modeling for industrial scale devices. The present study seeks to develop a high fidelity heat exchanger model for two evaporators: plate frame, and bar plate. The models will utilize correlations found in the literature to predict heat transfer coefficients and refrigerant side pressure losses. A variety of

correlations will be tested against data collected from evaporators used in an industrial scale vapor compression system to determine the correlation's accuracy at the larger scale. Both models will be developed to allow for a sub cooled evaporator inlet. The two evaporator models will then be utilized to optimize a vapor compression cycle. Previous investigations focus on the effect of heat exchanger design on cycle performance, however, no investigations focus on minimizing heat exchanger size for a fixed performance. The following section will describe the heat exchanger and vapor compression system modeling approach.

Chapter 3. Modeling Approach

Heat exchanger models exist in the literature, however as discussed in the previous chapter, these models are specific to the application and heat exchanger type. This investigation is interested in compact liquid coupled evaporators, of which there are no current models in open literature. This investigation sought to develop a model for plate frame and bar plate evaporators. Many heat exchanger modeling methods described in the previous chapter were applied to this investigation. The discretization and thermal resistance network method was chosen due to its simplicity and quickness in calculation. The discretization strategy involved dividing the cores into a finite number of control volumes where the physical dimensions of the heat exchangers informed the discretization. The thermal resistance network employed empirical correlations, which were discussed in Chapter 2, to determine the heat transfer and pressure drop across each control volume. The second part of this study was to investigate how these heat exchangers perform in a vapor compression cycle. VCCs have been previously molded and studied, however, for the purposes of this study, a simple thermodynamic model was sufficient to determine the relationship between evaporator pressure drop and volume. The cycle model set the inlet and outlet conditions for the heat exchanger models. All models were developed in Engineering Equation Solver (EES) [76], which is a simultaneous systems of equations solver with thermodynamic fluid properties built in to the software. The methods and equations used to model the heat exchangers and the VCC will be described in the following sections.

3.1.Plate Frame Heat Exchanger

Plate frame heat exchangers are comprised of corrugated steel plates compressed together, with each plate separated by rubber gaskets. The space between two adjacent plates forms a

channel for fluid flow. These channels alternate between a hot side working fluid and a cold side working fluid, which allows for heat transfer between the two working fluids throughout each plate, as shown in Figure 3-1. The plate stacks can be separated easily to be cleaned, which is beneficial for certain applications including food processing. In these applications, the heat exchanger is liquid to liquid, however, plate frame heat exchangers can also be liquid to two phase. For the present study, the hot side working fluid was a 70-30 by volume water-propylene glycol mixture, and the cold side working fluid was evaporating R134a. The water-glycol flows from the top of the heat exchanger downward, in counter flow relative to the refrigerant, which flows from the bottom of the heat exchanger upward.

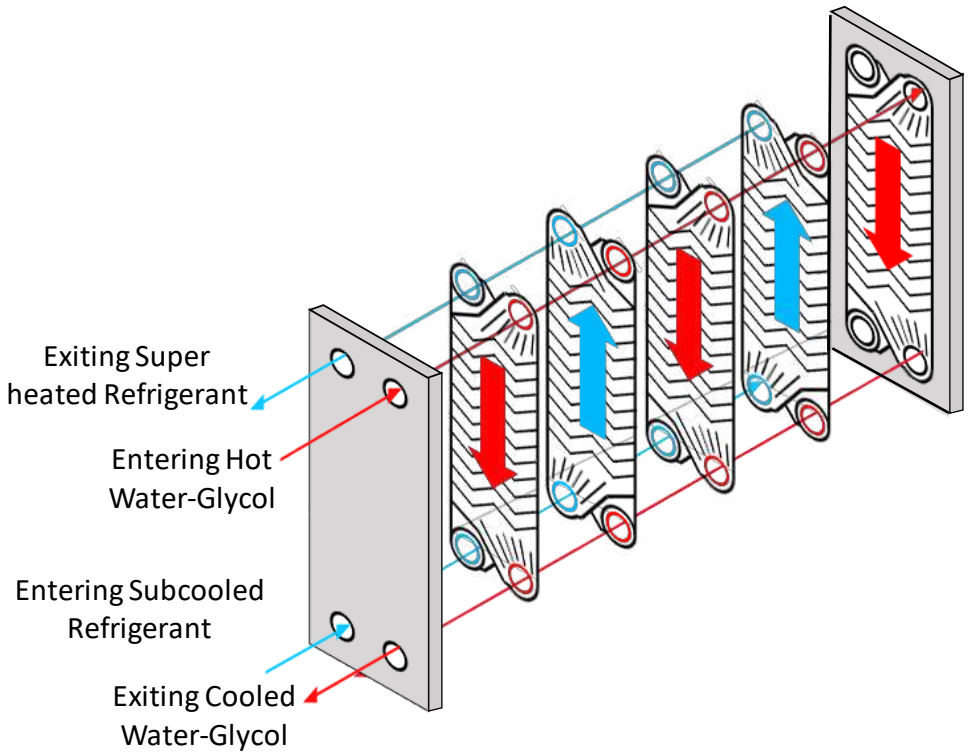

Figure 3-1. Exploded plate and frame heat exchanger.

3.1.1. Plate Frame Heat Exchanger Discretization

The model was designed to allow for easy manipulation of the heat exchanger discretization pattern. To account for variations in local pressure drop and heat transfer, the heat exchanger is subdivided to capture the effects of changing fluid transport and thermodynamic properties as well as the phase change nature of the evaporator. The heat exchanger as a whole is first divided into a single plate set, one hot side channel and one cold side channel. The analysis assumed that flow was uniformly distributed into each channel. The assumption is justified by comparing the predicted pressure loss though the manifolds relative to the total pressure loss for each side. The manifold pressure loss was 2.2% and 6.3% of the total pressure loss for the refrigerant and water-glycol sides respectively. Because the manifold pressure loss was a small portion of the total pressure loss for each side, the two fluids are evenly distributed across all the channel sets. Each channel set was then divided further into a finite number of control volumes. For the counter flow arrangement, the j=1 control volume is the water-glycol channel inlet and the refrigerant channel outlet, while the $j=j_n$ control volume is the refrigerant inlet and water-glycol outlet. In the parallel flow arrangement, both the water-glycol and refrigerant enter at the j=1 control volume and leave at the $j=j_n$ control volume.

The control volumes can be defined one of two ways. The first method is to fix the geometry of the heat exchanger, and input the inlet fluid conditions. This leaves the outlet fluid conditions to be calculated. The second method is to fix the heat duty of the control volume and calculate a required heat transfer area. If the width of the plates is fixed, then the length of the plates would be left to be calculated. For this study, the fixed geometry method was not chosen because it lacks sensitivity to a change in heat transfer coefficients; a large change in either refrigerant side or water-glycol side heat transfer coefficient leads to a negligible change in outlet

temperature. This was due to the high effectiveness of experimental heat exchanger and a small log-mean temperature difference. The fixed heat duty method was chosen because it is sensitive to a change in heat transfer coefficient. A large change in heat transfer coefficient leads to a large change in predicted length.

The control volumes span all three regions of the heat exchanger: subcooled liquid, two-phase boiling, and superheated vapor. The enthalpy change across each of the liquid control volumes is defined by Equation (3.1).

$$\Delta i_{\mathrm{l}} = \left(i_{\mathrm{r,sl}} - i_{\mathrm{r,in}} \right) / \left(j_{\mathrm{f}} - j_{\mathrm{n}} \right) \tag{3.1}$$

The saturation enthalpy was calculated using the saturation pressure which was calculated from the inlet pressure and pressure drop. The pressure drop was determined using empirical correlations.

The enthalpy change across each two phase control volume was calculated using the difference between the saturated vapor and liquid enthalpies divided by the number of control volumes in the two phase region, see Equation (3.2).

$$\Delta i_{\mathrm{tp}} = \left(i_{\mathrm{r,sv}} - i_{\mathrm{r,sl}} \right) / \left(j_{\mathrm{f}} - j_{\mathrm{g}} \right) \tag{3.2}$$

Like the saturated liquid enthalpy calculation Equation (3.1), the saturated vapor enthalpy was defined by the predicted pressure at the saturated vapor point. The enthalpy change was calculated using the difference between the saturated liquid and vapor enthalpies, accounting for the pressure drop between the two points. When analyzing a P-H diagram, Figure 3-2, the zero pressure drop chiller line, shown in green, is slightly longer than the chiller line which includes pressure drop, shown in blue. The shape of the vapor dome reduces two-phase heat transfer in the chiller with the use of pressure drop.

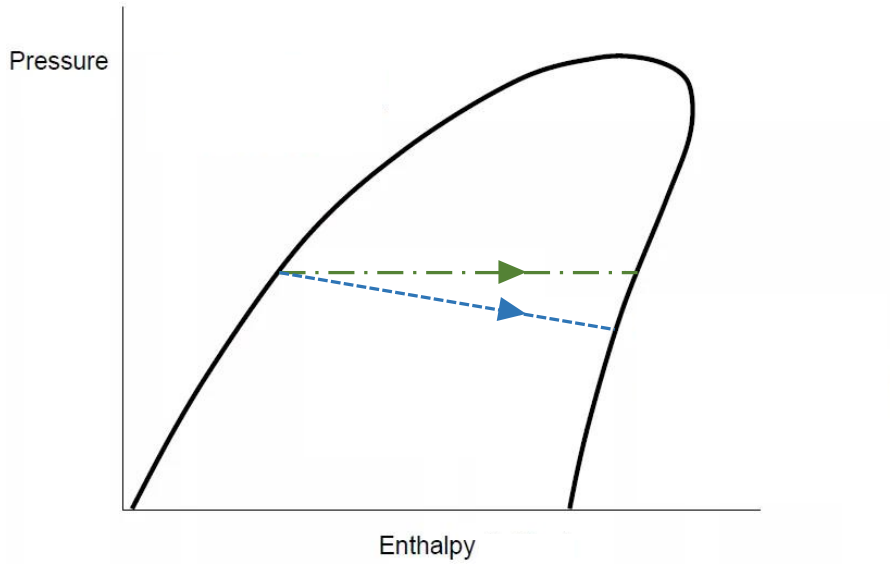

Figure 3-2. Pressure-enthalpy diagram showing pressure loss through the two phase region. Green represents no pressure loss, blue represents some pressure loss.

Finally the enthalpy change across the superheat control volumes is calculated using Equations (3.3), which is the difference in exit and the saturated vapor enthalpy divided by the number of superheated control volumes.

$$\Delta i_g = \left(i_{r,out} - i_{r,sv} \right) / \, j_g \tag{3.3}$$

The plate frame heat exchanger in this investigation was divided into 20 control volumes. The model can accommodate up to 40 control volumes which could improve mesh convergence. A mesh sensitivity analysis was performed, there was a 0.48% change in predicted heat exchanger length when the number of CVs was increased from 30 to 40, compared to a 0.1% change in predicted heat exchanger length when the number of CVs increase from 20 to 30. Though at the smaller mesh sizes, the length prediction was less than half as sensitive, the increased number of CVs increased the running time of the model. 20 CVs was determined to be the optimal compromise between mesh convergence and operating time.

A sensitivity study was performed resulting in the following number of discrete control volumes for each refrigeration region: 3 for superheated vapor, 12 for two-phase, and 5 for subcooled, see Figure 3-3. The number of control volumes in each region was determined by an estimated proportion of the present flow area. In standard refrigeration applications, the refrigerant is not subcooled and the fluid enters the heat exchanger as a two-phase fluid. In the experimental test facility, the refrigerant entered as a subcooled liquid which was modeled accordingly.

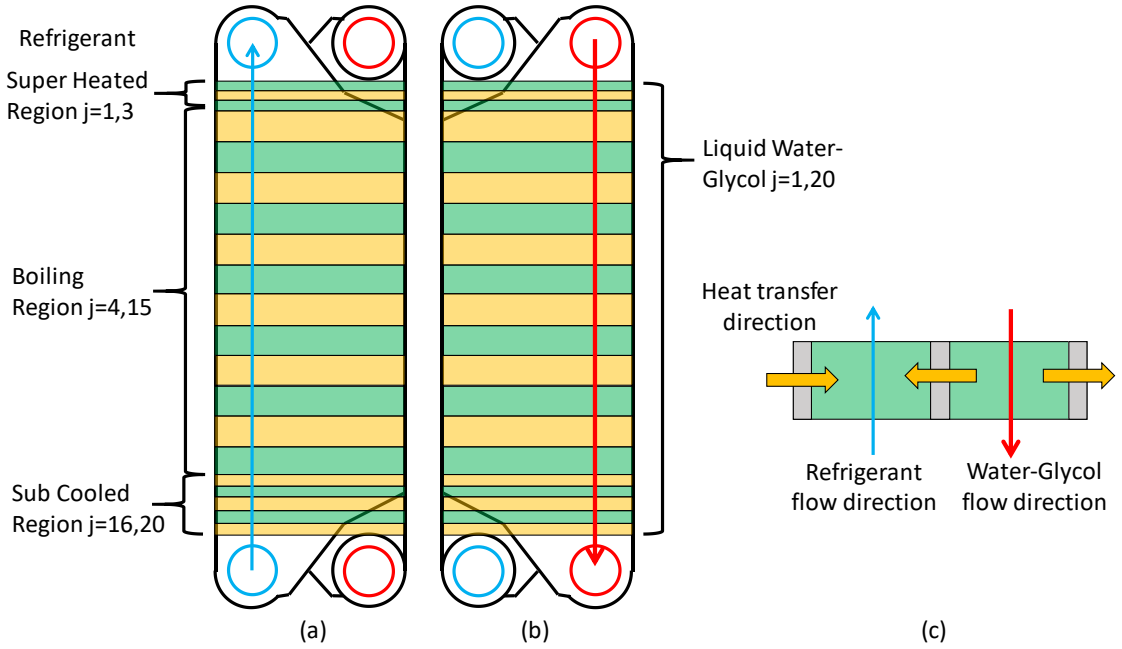

Figure 3-3. Plate frame heat exchanger control volume discretization, (a) refrigerant side, (b) water glycol side. (c) Single control volume showing fluid and heat flow directions and heat transfer area.

3.1.2. Plate Frame Heat Exchanger Geometries

The plate frame heat exchanger is comprised of corrugated stainless steel plates stacked on one another and separated by rubber gaskets. The space between two adjacent plates forms a channel for fluid to pass. These channels alternate between a hot side working fluid, and a cold

side working fluid so that heat is exchanged between the two working fluids throughout each plate. The plate stack is placed into a frame and compressed between two steel end support pieces.

The corrugated plates are sheets of stamped steel as shown in Figure 3-4. The plates include fluid inlet and outlet ports, a diffuser and reducer with guide vanes, and a corrugated chevron pattern heat transfer surface. The diffuser distributes the fluid to the bulk of the plate. The chevrons are used to generate turbulence and increase local fluid velocity to increase the heat transfer coefficient [25]. If the chevron angle is increased, the heat transfer coefficient and pressure drop will increase [77]. The plate frame heat exchanger used in this study has a double V chevron pattern at a 60° angle, a steep angle to increase heat transfer. In smaller devices the chevron pattern is a single V, and in all sizes the angle can be stamped between 30° and 60°. The plates in this study have a 0.432 m wide flow path that is 1.2 m long, see Figure 3-4.

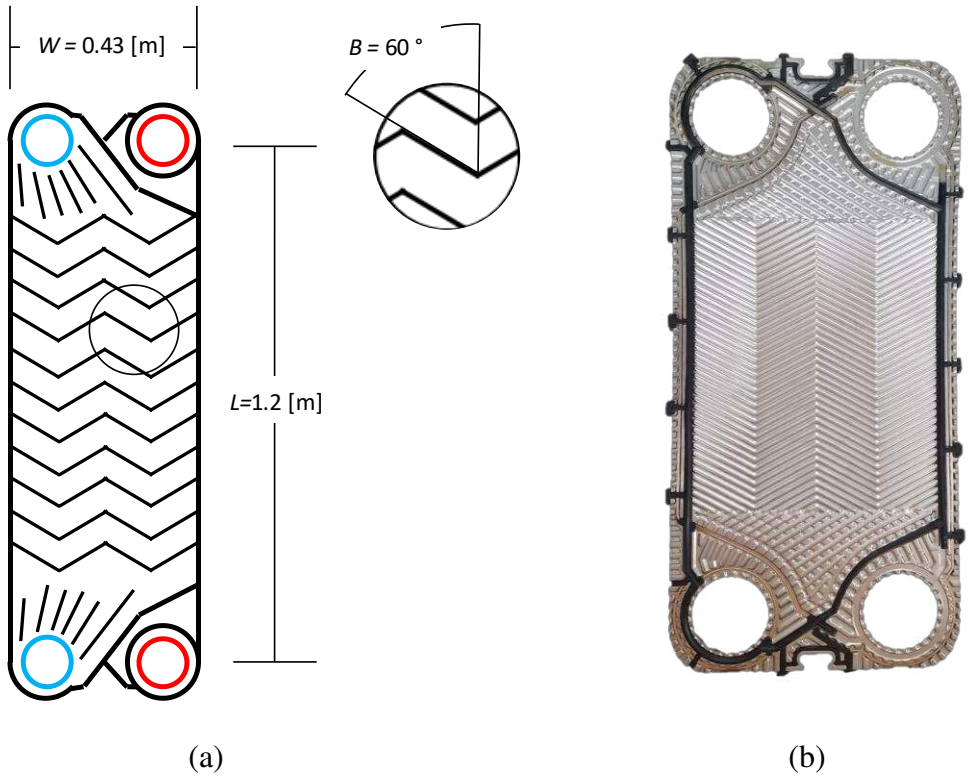

Figure 3-4. Plate in plate frame heat exchanger investigated in the current study, (a) geometry description, and (b) photographic image of plate.

3.1.3. Plate Frame Heat Exchanger Correlations

Chapter 2 presents a literature review of heat transfer and pressure drop correlations developed for plate frame heat exchangers. Not all correlations discussed were valid for the present investigation and therefore were not implemented in the model development. Table 3-1 found at the end of the chapter, shows relevant correlations and their valid parameter ranges for boiling flow in plate heat exchangers. The parameters highlighted in green indicate that the study fully encompasses the range tested in the present study. The parameters highlighted in blue indicate the study partially encompasses the range tested in the present study. There were three correlations of interest for the two phase boiling region, the Huang et al. [19], Hsieh et al. [26], and Han et al. [18] correlations.

Though no correlation fully encompasses every flow and thermodynamic parameter in the present study, Huang et al. [19] appears to be the closest: it fully covers heat and mass fluxes ranges, nearly captures all saturation temperatures, was evaluated with R134a, and the plates had a 60° chevron angle. The low mass flux in the Huang et al. investigation cause nucleate boiling to be the dominant heat transfer mechanism and made the flow parameters (i.e. Reynolds number and chevron angle) less significant. Therefore, the heat transfer was dominated by nucleate boiling, and it thus of interest to this investigation.

The studies by Longo and Gasparella [27,31] encompassed many of the required parameters including mass flux, saturation temperature, and fluid type. Similar to Huang et. al., their investigation was conducted at low mass fluxes, and they found that nucleate boiling was the dominate mode of heat transfer in the two-phase region. For example, Longo and Gasparella found that their data compared favorably to the Cooper pool boiling correlation [32], with a mean absolute deviation of 8.2%.

Table 3-1: Plate frame boiling correlation review highlighted. Green represents parameters that the correlation fully encompasses the present investigation's test parameters, Blue represents correlations which only partially encompass the test parameters.

Name	Working Fluid	Number of Channels	Heat Transfer Correlated	Pressure Drop Correlated	Chevron Angle	mass flux		heat flux		T_{sat}	
	-	-			degree	kg /m2s		kW/m2		c	
Test	**R134a**	**150**			**60**	**5.8**	**6.8**	**2**	**2.8**	**10**	**15**
Han et al. [18]	R22 / R410	3	X	X	20,35,45	13	34	2.5	8.5	5	15
Hsieh and Lin [16]	R410	2	X	X	60	50	125	2	37	10	30
Huang et al.[19]	R134a / R507a / R12 / Ammonia	23	X	X	28,44,60	5.6	30.3	1.9	7	5	13
Lee et al. [25]	R1233zd(E)	Unknown	X	X	60	5.5	27	6	49	105	105
Longo Gasparella [27] [31]	R410	9	X		65	4	50	3	21	5	20
	R134a / R410 / R245fa	9	X		65	4	50	3	21	5	20
Yan and Lin [15]	R134a	2	X	X	60	55	70	11	15	31	31

The Hsieh et al. [26] investigation encompassed even fewer parameters: heat flux, saturation temperature, and chevron angle. They developed a correlation that combined liquid convective and pool boiling heat transfer. The convective contribution was calculated using the Dittus-Boelter correlation [11] multiplied by an enhancement factor, whereas the pool boiling contribution was calculated by multiplying the Cooper correlation by a suppression factor. Similar to Huang et al., they also developed a friction factor correlation as a function of equivalent Reynolds number.

Almost all the other correlations presented in Table 3-1 were not tested in the present investigation due to not encompassing enough important parameters. For example, the Yan and Lin [15] correlation, though tested with R134a, tested at far higher heat and mass flux ranges. However, the correlation presented by Han et al. [18] was considered due to its dependence on plate geometry, even though it does not encompass many of the parameters of the present investigation. The Nusselt correlation is a function of equivalent Reynolds number, equivalent boiling number, and Prandtl number. Non-dimensional parameters based on the plate geometry are used as the multiplier and Reynolds number exponent.

In the present study, both the refrigerant and water-propylene streams flow as single-phase fluids. A review of correlations developed for single phase heat transfer in plate heat exchanger is summarized in Table 3-2 found at the end of the chapter. All of these correlations were developed for water or a water-glycol mixture, and no correlations were found for single phase refrigerant in plate heat exchangers. However, some of the studies do cover the Reynolds and Prandtl numbers for the fluids investigated here. Table 3-2 depicts the valid parameter ranges for several heat transfer correlations developed for single phase flow in chevron plate heat exchangers.

Table 3-2. Single phase plate frame correlations and associated valid parameter ranges, highlighted. The green highlighting indicates that the correlation fully encompasses both the water-glycol and single phase refrigerant ranges tested in this investigation. The Blue indicates the parameter partially encompasses both fluids. The purple indicates the parameter fully encompasses only the Water-glycol and the red indicates the parameter partially encompasses the refrigerant but not the water-glycol.

Name	Working Fluid	Heat Transfer Correlated	Pressure Drop Correlated	Chevron Angel	Re		Pr		dh
	-			degree	-		-		mm
Test Refrigerant	**R134a**			**60**	**130**	**3000**	**0.8**	**3.5**	**5.1**
Test Water-Glycol	**Water-Glycol**			**60**	**180**	**520**	**32**	**34**	**5.1**
Chisholm and Wanniarachchi [41]	Water	X		30-80	1000	40000	5	5	
Muley and Manglik [38]		X	X	30,45,60	600	10000	2	6	5.08
Kahn [36]		X		30,45,60	500	2500	3.5	6.5	3.9
Thonon [78]	water	X	X	30,45,60,75	60	2415			
Muely [39]		X	X	30-60	30	400			
Maslov and Kovalenko [35]	Water	X		60	50	20000			
Talik et al. [79]	Water-Glycol	X	X	60	10	720	70	450	4.65
	Water	X	X		14500	11460	2.5	50	4.65
Hessami		X		45,60	200	1800			11
Emerson [80]	Water	X			10	25			
		X			40	1000			
Longo and Gasparella [31]	Water	X		65	200	1200	5	10	
Kumar [81]	Water	X		60	20	400			
Rosenblad and Kullendorff [34]	Water	X		60	60	2415			4

The green highlighting indicates that the correlation fully encompasses both the water-glycol and single phase refrigerant ranges tested in this investigation. The Blue indicates the parameter partially encompasses both fluids. The purple indicates the parameter fully encompasses only the Water-glycol and the red indicates the parameter partially encompasses the refrigerant but not the water-glycol. As noted in Table 3-2, the Maslov and Kovalenko [35] correlation was developed for the same chevron angle as the present study, and the valid Reynolds range encompasses both working fluids. In addition, none of the investigations that report a Prandtl number range fully encompass the ranges of either fluid in the present study. This is due to the limited fluids used in the investigations. Adding propylene glycol to water dramatically increases the Prandtl number. The Talik et al. [78] investigation does use a water-glycol mixture; however, they utilize a higher glycol concentration than the present study. As discussed below, the correlations tested for this investigation were the ones that most encompassed either fluids tested or Reynolds ranges.

Seven single phase correlations developed for plate heat exchangers were tested to predict the water-glycol side heat transfer coefficient the: Muley [39], Thonon et al. [79], Maslov and Kovalenko [35], Rosenblad and Kullendroff [34], Emerson [80], Talik et al. [78], and Kumar [81]. The single phase correlations were tested for the water glycol heat transfer. The seven single phase correlations were selected because of the valid Reynolds numbers are similar to the operating Reynolds numbers of the present study. Of the correlation tabulated, all by Kumar fully encompass the water-glycol Reynolds number. The Kumar correlation was also considered for this study because the valid range encompassed the majority of the test conditions. None of the seven correlations considered were developed for valid Prandtl number. This was due to all but the Talik et al. being developed with water. The Talik et al. was developed for water-glycol however it was at larger concentrations resulting in a larger Prandtl number.

Table 3-2 at the end of the chapter, shows potential correlations to predict the single phase refrigerant. Three of the correlations were selected for testing: Thonon et al. [79], Maslov and Kovalenko [35], and Rosenblad and Kullendroff [34]. Thonon et al., and Maslov and Kovalenko encompassed the required Reynolds number range and the Rosenblad and Kullendroff encompassed the majority of the required range. Because the correlations were developed for water none of the selected correlations meet the Prandtl number range.

3.1.4. Plate Frame Pressure Drop

In addition to heat transfer, the pressure drop must be carefully considered as a design aspect. The pressure drop through a heat exchanger is important because it could have a large impact on system components and overall system performance. The total pressure loss across the heat exchanger was input to the model from experimental data. The experimental pressure loss was divided by number of control volumes to set the pressure loss across each control volume:

$$\Delta P = \frac{\Delta P_{\text{total}}}{20} \tag{3.4}$$

Distributing the pressure loss like this does cause some error. It is likely that the pressure loss is greater toward the end of the refrigerant flow path where the specific volume is larger. However it is impossible to experimentally determine how this changes with the current experimental set up. Therefor the linear pressure loss was accepted.

At the single phase control volume the pressure loss is calculated in two parts: the frictional, and gravitational pressure losses. For the control volumes with two phase refrigerant, a third loss was calculated, the acceleration pressure loss due to an increased volume flow rate. The frictional pressure loss was calculated using a friction factor from the frictional pressure loss correlations

described in section 3.1.3. The friction factor was then used in Equation (3.5) to calculate the frictional pressure loss across each control volume.

$$\Delta P_{\text{fric}} = \frac{f \cdot L \cdot \bar{V}^2 \cdot \rho}{2 \cdot Dh} \tag{3.5}$$

The friction factor in the above equation was calculated using correlations from literature. The Thonon et al. single phase correlation, Equation (3.6), was used to determine the friction factor for the single phase refrigerant because its valid Reynolds numbers and chevron angle encompasses the experiments.

$$f = 0.6857 \cdot Re^{-0.25} \tag{3.6}$$

The Huang et al. [19] correlation was used to determine the two phase frictional pressure drop through the core. As discussed in the following chapters, the refrigerant side pressure drop could not be validated, therefore the Huang et al. correlation was selected because the development encompasses the majority of the desired operating parameters. The correlation used equations (3.7) through (3.8) to calculate the friction factor.

$$FR = 0.183 \cdot \left(\frac{\beta}{30}\right)^2 - 0.275 \cdot \left(\frac{\beta}{30}\right) + 1.1 \tag{3.7}$$

$$f = \frac{38100 \cdot FR}{Re_{\text{eq,r}}^{0.9} \cdot \left(\frac{\rho_{\text{r,sl}}}{\rho_{\text{r,sv}}}\right)^{0.16}} \tag{3.8}$$

The gravitational pressure loss was calculated as a function of density, gravity, channel length, and the change in vertical head, see Equation (3.9).

$$\Delta P_{\text{grav}} = \rho \cdot g \cdot L_{\text{plate}} \tag{3.9}$$

The acceleration pressure loss in the two phase control volumes was calculated using Equation (3.10). This loss accounts for the increase in fluid volume as more refrigerant changes form liquid to vapor. The equation is a function of inlet and outlet quality to the control volume, the mass flux *G,* and the saturated liquid and vapor densities. The increase volume leads to an increased fluid velocity and subsequent pressure loss.

$$\Delta P_{\text{accel}} = G^2 \cdot \left(X_{\text{out}} - X_{\text{in}} \right) \cdot \left(\rho_{\text{sv}}^{-1} - \rho_{\text{sl}}^{-1} \right) \tag{3.10}$$

The sum of all the pressure losses from the model was the predicted pressure loss of the evaporator plate, Equation (3.11).

$$\Delta P_{\text{total}} = \Delta P_{\text{fric}} + \Delta P_{\text{accel}} + \Delta P_{\text{grav}} \tag{3.11}$$

The core pressure drop portion of the model was primarily used in the evaporator optimization effort as opposed to the model validation effort.

The second part of the pressure drop predictive capabilities of the model was the manifold pressure loss portion. For the model validation effort, the predicted manifold pressure loss was compared to the measured manifold pressure loss to justify the uniform distribution assumption. If the manifold pressure was loss small relative to the total pressure loss, the assumption could be made. In the evaporator optimization effort, the manifold pressure loss was included in the heat exchanger pressure loss and was used when reconsidering the uniform distribution for some of the conditions calculated.

The manifold pressure loss was calculated as the sum of two parts, the frictional loss from the fluid flowing through the manifold, and the minor loss from the fluid separating in a “T”, see equation (3.12) below. For ease of modeling, both contributions were calculated based on the

average conditions of the manifold, and the flow rate used in the calculations was assumed to be half of the total flow rate.

$$\Delta P_{\text{manifold}} = 0.5 \cdot K_{\text{T}} \cdot \rho_{\text{r}} \cdot \overline{V_{\text{r}}^2} + f_{\text{manifold}} \cdot \rho_{\text{r}} \cdot \overline{V_{\text{r}}^2} \cdot \frac{Depth}{D_{\text{manifold}}} \tag{3.12}$$

In the frictional loss portion of the calculation, the friction factor was determined using the Fanning friction factor correlation, shown in Equation (3.13).

$$f_{\text{manifold}} = 0.316 \cdot Re_{\text{r}}^{-0.25} \tag{3.13}$$

The Fanning friction factor correlation used in the present investigation is for Reynold's numbers greater than 2300, and for both the inlet and outlet manifolds in both the model validation and the optimization study, the refrigerant in the manifolds was turbulent. Therefore, the pressure drop was calculated this way for both the inlet and outlet manifolds.

3.1.5. Property Distribution and Thermal Resistance Network

A thermal resistance network was developed at each control volume that related the geometric characteristics of the heat exchanger core to the thermodynamic fluid changes. The thermal resistance network concept was described in Incropera and Dewitt [82]. A thermal resistance is analogous to an electric resistance network where voltage differential drives current across a resistance, govern by Ohm's law. Current is analogous to heat transfer rate, voltage differential analogous to a log mean temperature difference, and the resistance analogous to the inverse of UA, a function of heat transfer coefficient and geometry. The UA LMTD thermal resistance equation can then be described with Equation (3.14).

$$q = UA \cdot LMDT \tag{3.14}$$

An alternative thermal resistance equation for relating the fluids' temperatures is to use the ε-NTU method, Equation (3.15), which relates the maximum amount heat transfer to the actual amount by using effectiveness (ε). The effectiveness value is used to calculate the UA though the counter flow ε-NTU correlation (3.16) and then the NTU Equation (3.17).

$$q = \varepsilon \cdot C_{\min} \cdot \left(T_{\mathrm{g}} - T_{\mathrm{r}}\right) \tag{3.15}$$

$$NTU = \frac{1}{Cr - 1} \ln\left(\frac{\varepsilon - 1}{\varepsilon \cdot Cr - 1}\right) \tag{3.16}$$

$$UA = NTU \cdot C_{\min} \tag{3.17}$$

Where $C_{\min}$ and Cr are defined by Equations (3.18) and (3.19) respectively.

$$C_{\min} = \min\left(\dot{m}_{\mathrm{g}} \cdot Cp_{\mathrm{g}}, \dot{m}_{\mathrm{r}} \cdot Cp_{\mathrm{r}}\right) \tag{3.18}$$

$$Cr = \frac{C_{\min}}{C_{\max}} \tag{3.19}$$

Each control volume is defined by a change in refrigerant enthalpy, and because the mass flow rate of the refrigerant remains constant throughout the heat exchanger, the heat transfer rate for each control volume in each phase region is the same. The heat transfer rate can be calculated as shown below:

$$q = \dot{M} \cdot \left(i_{\mathrm{r,out}} - i_{\mathrm{r,in}}\right) \tag{3.20}$$

Now that the heat transfer rate is known, the change in glycol temperature across each control volume is calculated using the Equation (3.21).

$$q = \dot{M}_{\mathrm{g}} \cdot cp_{\mathrm{g}} \cdot \left(T_{\mathrm{g,in}} - T_{\mathrm{g,out}}\right) \tag{3.21}$$

The minimum heat capacitance rate, $C_{\min}$, was calculated, and by knowing the heat transfer rate and entering temperature difference, equation (3.15) was solved for effectiveness.

Subsequently, the *UA* was calculated using equations (3.16) and (3.17). The *UA* was then used along with a thermal resistance network and heat transfer coefficients calculated from correlations to predict the length of the heat exchanger, all further discussed below.

There are five factors that will resist the transfer of heat between the water-glycol and the refrigerant: the convective heat transfer between the water-glycol and the plate wall, the fouling on the water-glycol side wall, the conduction through the plate wall, the fouling on the refrigerant side of the wall, and the convective heat transfer from the wall to the refrigerant. For this investigation, the two fouling resistances were neglected because the heat exchanger is new and has had limited time for fouling to occur. Thus, the two convective resistances and the conductive resistance need to be determined to calculate *UA* or overall conductance. The flow of heat modeled is shown in Figure 3-5, where the three resistances are in series, because the heat transfer does not split between resistances.

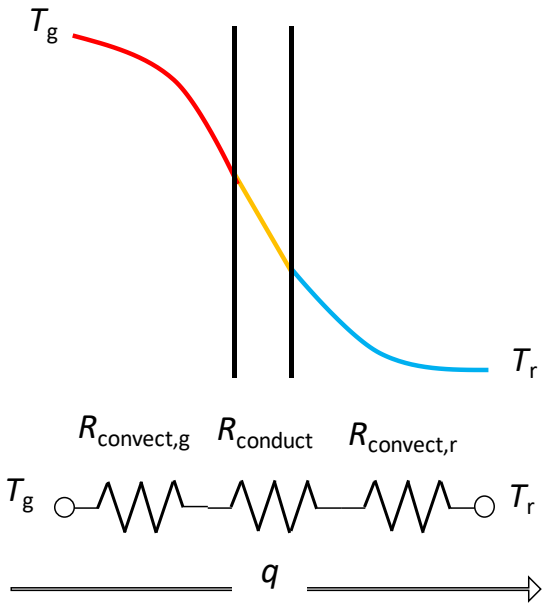

Figure 3-5. Plate frame thermal resistance network.

Therefore the total resistance is simply the sum of the three individual resistances and the UA can be calculated using Equation (3.22).

$$UA = \frac{1}{R_r + R_{wall} + R_g} \tag{3.22}$$

The convective thermal resistances, R_r and R_g, are calculated using Equation (3.23), and are a function of heat transfer coefficient and area. Correlations found from literature are used to predict the heat transfer coefficients as was discussed previously. Separate correlations are required for the glycol and refrigerant side heat transfer coefficients as well as for single and two phase refrigerant coefficients. The heat transfer area is the plate area in each control volume, where L is the control volume length, and W is the effective plate width as is shown in the equation below:

$$R = \frac{1}{h \cdot A_{ht}} = \frac{1}{h \cdot L \cdot W} \tag{3.23}$$

The wall thermal resistance due to conduction was calculated using the Equation (3.24), which is a function of steel thermal conductivity, heat transfer area, and the plate thickness (δ_{wall}).

$$R_{wall} = \frac{\delta_{wall}}{K_{wall} \cdot A_{ht}} = \frac{\delta_{wall}}{K_{wall} \cdot L \cdot W} \tag{3.24}$$

The UA can be represented as a single variable, the inverse of the total resistance, or in special cases as two separate variables multiplied together, total heat transfer coefficient multiplied by area. To split the variables, the heat transfer areas in all of the resistances must be equal to be factored out.

$$UA = \frac{L \cdot W}{\left(\frac{1}{h_r} + \frac{\delta}{K_{wall}} + \frac{1}{h_g} \right)} \tag{3.25}$$

The area portion of the *UA* becomes equal to the heat transfer area and the *U* portion can be described using Equation (3.26).

$$U = \frac{1}{\left(\frac{1}{h_r} + \frac{\delta}{K_{wall}} + \frac{1}{h_g} \right)} \tag{3.26}$$

This special case can be applied to this investigation because the heat transfer area for all three resistances is equal to the plate area of each control volume, Equation (3.27).

$$A = L \cdot W \cdot 2 \tag{3.27}$$

Equation (3.27) was used to calculate the length of each control volume, and by summing all control volume lengths, the predicted length of the heat exchanger was calculated and then compared to the actual length.

It was assumed that all of the heat transfer was between the two fluids and no heat was lost to the ambient. To prove this assumption valid, an order of magnitude calculation was made to determine the magnitude of heat that left the plate frame core due to natural convection compared to the amount of heat transferred between the two working fluids. Radiation heat loss was neglected because the 5 °C temperature difference between the ambient and the water-glycol was too small for any significant radiation heat transfer. The heat loss due to natural convection was the sum of three components, the heat loss through the sides of the heat exchanger through the splash shield, the heat lost through the front and back through the end plates, and the heat lost through the top of the core. Figure 3-6 shows the thermal resistances accounted for in this analysis.

The natural convection heat transfer coefficients were calculated using the Churchill and Chu [110] vertical plate, and Lloyd and Moran [111] horizontal plate correlations. The case with the largest temperature difference was used for this analysis because it would lead to the most heat lost. The outside wall temperature of the core was assumed to be the high side temperature of the water-glycol for a conservative calculation. It was found that the heat loss to the environment was less than 0.1% of the heat transferred between fluids, meaning the assumption is valid.

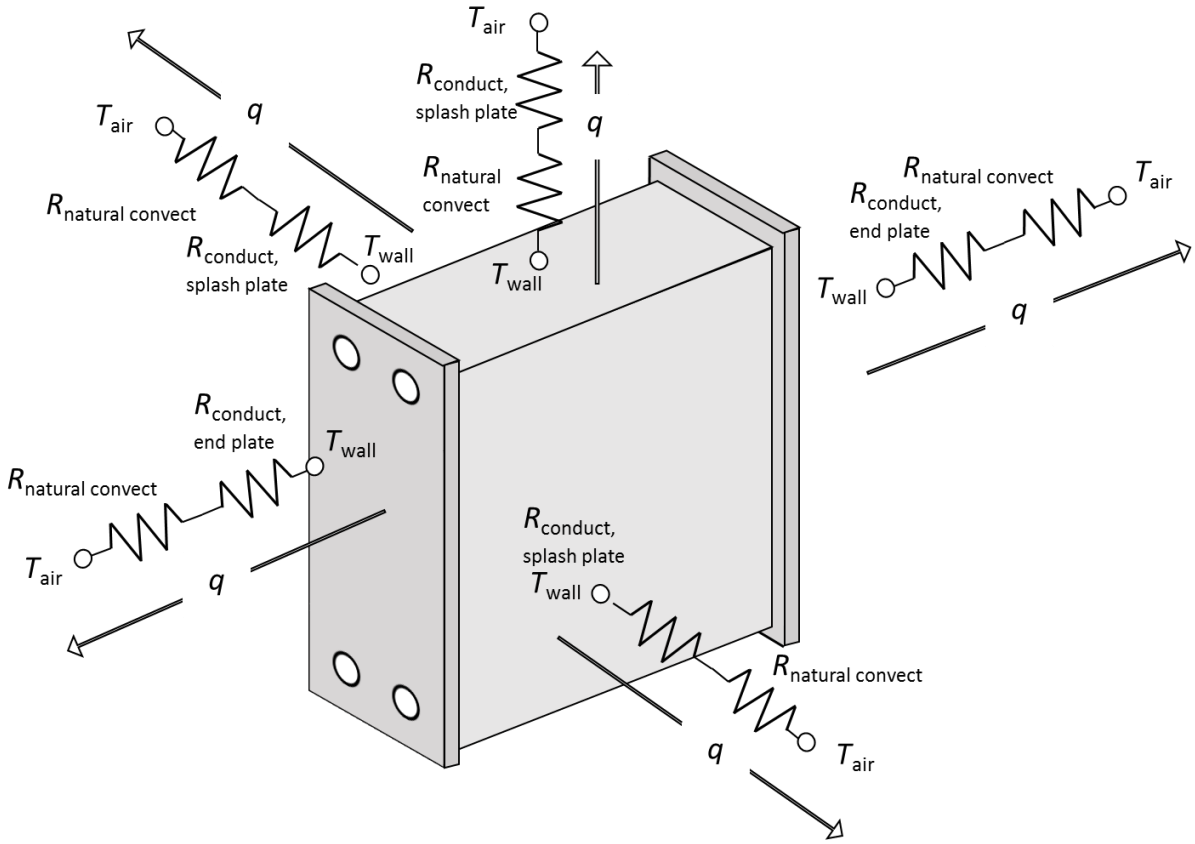

Figure 3-6. Plate frame ambient heat loss thermal resistance networks

3.2.Bar Plate Heat Exchanger

The bar plate evaporator consists of a heat exchanger core, inlet and outlet refrigerant manifolds, and water-glycol inlet and outlet diffusers. The bar plate core is comprised of aluminum plates separated by serpentine fins that create fluid channels, shown in Figure 3-7.

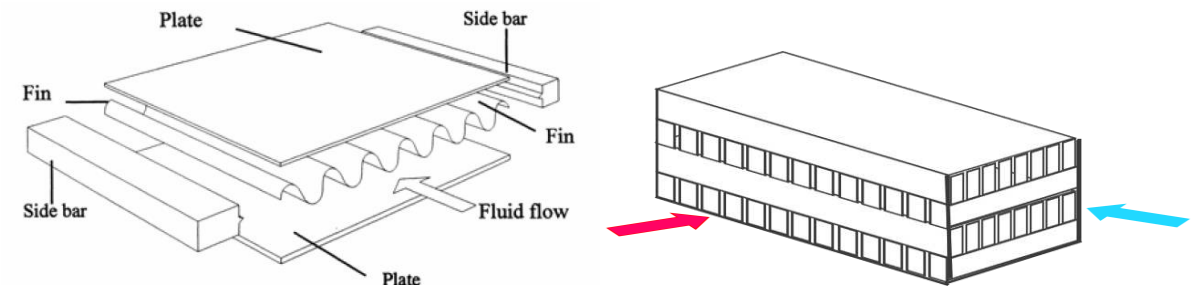

(a) (b)

Figure 3-7. Bar plate heat exchanger construction. (a) Exploded view, Picon-Nunez [8]. (b) Cross flow cut away where red represents the water-glycol flow path and blue the refrigerant flow path.

These channels alternate between a propylene glycol water mixture and R134a. The water-glycol side channels run straight from the inlet expander of the heat exchanger to the outlet diffuser, denoted by the red arrows in Figure 3-8.

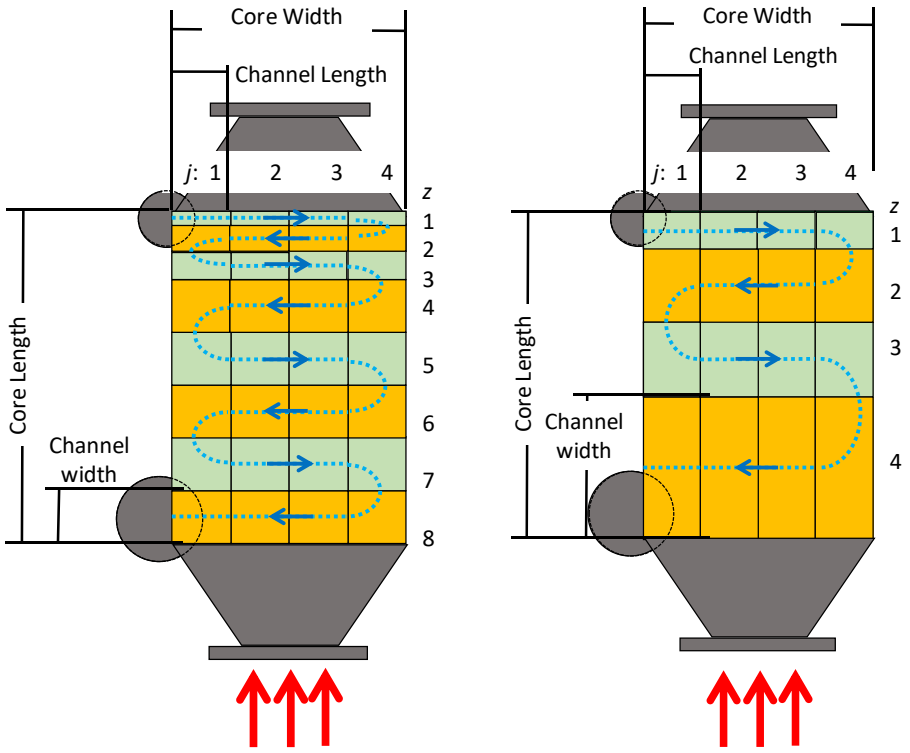

(a) (b)

Figure 3-8. Bar plate heat exchanger control volume discretization pattern and fluid flow directions. Red represents water-glycol and blue represents refrigerant. (a) Discretization pattern for model validation. (b) Discretization pattern for vapor compression cycle evaporator optimization.

The refrigerant flows in a cross-counter pattern compared to the water-glycol channels, as shown by the blue arrows in Figure 3-8. The refrigerant heats as it enters the evaporator core and becomes a two-phase fluid. As the refrigerant flow, the density decreases as more of the fluid becomes vapor which would increase pressure drop. To accommodate fluid expansion and reduce the pressure drop, the cross sectional area of the serpentine refrigerant channels increases along the length of the core. The refrigerant enters at the bottom of the heat exchanger and moves upward against gravity, and the water-glycol enters the core from the top moving in the direction of gravity. Figure 3-8 is shown upside down with respect to orientation in the facility, so the refrigerant inlet is denoted as [1, 1].

3.2.1. Bar Plate Heat Exchanger Discretization

To account for variation in local pressure drop and heat transfer, the evaporator was subdivided to capture the effects of changing fluid transport and thermodynamic properties as well as to capture the serpentine cross counter flow configuration. Uniform distribution of flow into each channel was assumed for each side. The assumption was justified by comparing the total pressure loss to the predicted manifold pressure loss for both sides. The manifold pressure loss was 2.2% and 6.3% of the total pressure loss for the refrigerant and water-glycol sides respectively. Because the manifold pressure loss was a small portion of the total pressure loss for each side, the two fluids are evenly distributed across all the channel sets. Each channel set was then divided further into a finite number of control volumes. Two control volumes account for the inlet subcooled liquid, twenty-six control volumes account for the two-phase region, and four account for the superheated refrigerant. The division of control volumes was based on estimated portions of heat transfer area.

The thirty-two control volumes form a four by eight grid. The CVs in the grid were named based on their vertical and horizontal position. The z direction indicates a single refrigerant row and vertical position. The rows alternated flow directions, left to right then right to left. The horizontal CVs are denoted as j, and the number of horizontal CVs was j_h. The discretization pattern was slightly changed from the model validation effort to the evaporator optimization effort. Adding multiple control volumes along each refrigerant channel was necessary to accurately account for phase change. When looking at figure 3-8, the liquid CVs were set between $j = 1$ and $j = 2$ for $z = 1$. The subcooled heat duty is minimal in the evaporator, likely limiting itself to the first refrigerant row. The two phase region was between [1,3] and [7,4]. This leaves the last refrigerant row for superheated vapor.

The number of refrigerant rows, the control volumes in the z direction, was decreased from 8 to 4 for the optimization effort, Figure 3-8 shows the modified discretization pattern. The heat exchanger in the test facility contains 8 refrigerant rows, however, 8 rows lead to an unrealistically slim core in the optimization process. Therefore, the reduction in rows allowed for a more realistic aspect ratio when determining the core volume in the simple vapor compression cycle. Furthermore, all of the control volumes in pattern contain two phase refrigerant.

Similarly to the plate frame model, the bar plate model fixed the heat duty at each control volume to calculate a required geometry which was compared to the actual heat exchanger geometry. The heat duty was not divided evenly between every control volume. The subcooled control volume heat duties were defined by the difference between inlet enthalpy and saturated liquid enthalpy divided by the number of subcooled control volumes as seen below:

$$q = \left(\frac{i_{sl} - i_{in}}{CV_l} \right) \cdot \dot{m}_r \tag{3.28}$$

The superheated control volumes were calculated similarly with the saturated vapor and the outlet enthalpies:

$$q = \left(\frac{i_{sv} - i_{out}}{CV_v} \right) \cdot \dot{m}_r \tag{3.29}$$

The heat duty for the two-phase control volumes did not fallow this same pattern. If the heat duty of the two phase region were evenly distributed, the predicted areas at low vapor qualities would be much smaller than the areas for higher vapor qualities. This results in an unrealistic property profile of the refrigerant relative to the water-glycol. Therefore the two phase heat duty at each control volume was defined by Equation (3.30), where the heat duty is larger at lower vapor qualities, or at smaller i values, and decreases along the length of the core.

$$q[z, j] = \left(\frac{\left(i_{sv} - i_1\right) \cdot z}{\left(\sum_{y=sl}^{y=sv} z_y \right) \cdot j_{ov} - j_{sl} - j_{sv} \cdot z_{ov}} \right) \cdot \dot{m}_r \tag{3.30}$$

In Equation (3.30), z_{ov} and j_{ov} are the total number of control volumes in the vertical and horizontal directions, 8 and 4 respectively. This uneven distribution of heat duties prevents the first channels from being predicted much smaller than the last. The model calculated a lower heat duty earlier in the core for control volumes with a low vapor quality, and the heat transfer coefficient generally increases as the refrigerant boils.

3.2.2. Bar Plate Heat Exchanger Geometries

The bar plate heat exchanger is constructed by stacking aluminum plates with fins separating each plate. The space between the plates form fluid channels which alternate between water-glycol and refrigerant. On the water-glycol side, the fins run straight from the top of the core

to the bottom. On the refrigerant side the fins are accompanied by bars and form a serpentine flow pattern in either cross counter or cross parallel flow relative to the water-glycol channels. As the refrigerant boils in the evaporator, the density decreases which will increase the volume flow rate for a fixed mass flow rate. As the volume flow rate of the refrigerant increases, the pressure drop through the core will also increase. To accommodate the higher volume flow rate and pressure drop, the cross sectional area of the channels increases along the core length by increasing the channel width.

3.2.3. Bar Plate Correlations

Some of the correlations discussed in chapter two for micro channel heat transfer were used to predict the heat transfer coefficients used in the thermal resistance calculations. Table 3-3 depicts relevant heat transfer correlations for the boiling heat transfer in micro channels. The parameters which are highlighted in green encompasses the range tested in the present investigation. Parameters highlighted in blue only partially encompass the present study range. Three correlations, Bertsch et al. [44], Kuznetsov et al. [49], and Li and Wu [52], were selected to predict the two phase refrigerant heat transfer coefficient. The Bertsch et al. and Li and Wu correlations encompassed all parameters and were therefore chosen to be tested. The Kuznetsov et al. correlation encompassed every parameter except hydraulic diameter which differed by 18%.

Table 3-3. Microchannel boiling heat transfer correlations, highlighted. Green represents parameters that the correlation fully encompasses the present investigation's test parameters, Blue represents correlations which only partially encompass the test parameters.

Correlation	Fluid		Channel Shape	Hydraulic Diameter	Mass Flux Low	Mass Flux High	Heat Flux Low	Heat Flux High	Quality low	Quality High	T_{sat} low	T_{sat} High
	-		-	mm	Kg m^{-2} s^{-1}		W cm^{-2}		-		°C	
Test conditions	**R134a**		**Rectangular**	**1.193**	**25**	**115**	**0.3**	**0.5**	**0**	**1**	**5**	**20**
Agostini et al.	R134a		Rectangular	0.77,2.01	83	467	0.44	1.5	0	1		
[92,93]	R236Fa	R245fa	Rectangular	0.34	281	1501	0.7	42	0.02	0.78	25	43
Bertch et al. [94]	R245Fa	R134a	Rectangular	0.54-1.09	20	350	0.5	22	0	0.95	8	30
Bertch et al. [44]	multi (14)	R134a	Rec / Circular	0.16-2.92	20	3000	0.3	115	0	1	-194	97
Cooper [32]	Multi		Pool		0	0	0.01	60	0	1		
Hamdar et al.[95]	R152a		Square	1	200	600	0.1	0.6				
Kandlikar [96]	Multi(8)			4.0-32	13	8179	0.03	228	0.001	0.987		
Kuznetsov et al. [49]	R134a	r21	Rectangular	0.975	23	190	0.1	1.6	0	1		
Lazrek and Black [97]	R113		Circular	3.1	125	750	1.4	38	0	0.6		
Lee and Lee [98]	E113		Rectangular	0.78-3.63	50	200	0	1.5	0.15	0.75		
Li and Wu [52]	Multi	R134a	Rec / Circular	0.2-3	20	3500	0	800	0	1	0	31
Liu and Winterton [99]	Multi (9)		Circular	2.95-32	12.4	8179.3	0.035	262	0	0.948		
Lovegrov and Robertson[100]	R11		Serrated fin			150				0.04		
Raju et al.[101]	R134a		Strip fins	1.1894	50	82	0.14	0.22	0.32	0.75	-1	5
Thome et al. [46]	Multi	R134a	Circular	0.7-3.1	50	564	0.5	17.8	0.01	0.99		
Tran et al. [54]	R12		Rectangular	2.4	44	832	0.036	1.29	0	0.94		
Warrier et al. [53]	R84		Rectangular	0.75	557	1600	0	0.599	0	0.55	26	60
Yun et al. [102]	r410		Rectangular	1.36-1.44	200	400	1	2	0	0.85	0	10

Table 3-4 presents single phase correlations relevant for use in the present study. The green highlighted parameters indicates the correlation fully encompasses both the required refrigerant and water-glycol ranges, the brown indicates the refrigerant range is fully encompassed, the purple indicates the water-glycol range is fully encompassed, the red indicates the refrigerant range is partially encompassed, and the blue indicates the water-glycol range is partially encompassed.

Table 3-4. Single phase bar plate correlation review, highlighted. The greed highlighted boxes indicate the correlation encompasses both the water-glycol and single phase refrigerant test conditions for the parameter. The purple highlight indicates the parameter is fully encompassed for the water-glycol. The brown highlight indicates the parameter is fully encompassed for the water-glycol. The blue highlight indicates the parameter is partially encompassed for the water-glycol. The red highlight indicates the parameter is partially encompassed for the refrigerant.

Name	Working Fluid	Channel Shape	dh	Re		Pr	
	-	-	mm	-		-	
Test Refrigerant	**R134a**	**Rectangular**	**1.193**	**540**	**5400**	**0.82**	**3.5**
Test Water-Glycol	**Water-Glycol**	**Rectangular**	**0.950**	**55**	**205**	**30**	**67**
Shah and London [59]			>0.1	0	2300		
Sieder and Tate [63]			>0.1	0	2300	0.48	1670
Hartnett and Kostic [83]		Rectangular	>0.1	0	2300		
Dittus Boelter [11]		Circular		10000		0.7	160
Choi et al. [62]	Nitrogen	Circular	0.003-0.081	30	2000		
Churchill [65]		Circular		0	10^7	0.2	9810
Garimella et al. [64]	Water-glycol	Rectangular		118	10671	0.243	16.2
Peng and Peterson [61]		Rectangular	0.155-0.747	0	2200		
Stignor et al.[103]	Glycol	Rectangular	2.1-4.7	0	2300		
Benjan		Rectangular		0	2300	0.7	0.7
Kays and Crawford [51]		Rectangular		0	2300		
Gnielinski [64]		Circular		3000	5x10^6	0.5	2000

As discussed further in the Chapter 4 Section 3, the correlation used to represent the water-glycol side heat transfer coefficient could not be experimentally validated. Therefore a correlation was selected based on similarities in heat exchanger geometry and flow conditions. Correlations considered for the water-glycol heat transfer were Churchill [65], Hartnett and Kostic [83], Garimella et al. [57], Shah and London [59], Bejan et al. [60], and Sieder and Tate [63], and Peng and Peterson [61]. These correlations were selected due to the closeness in their valid parameter ranges compared to the operating ranges for the present study. However, the Hartnett and Kostic correlation was selected because it accounted for the aspect ratio of the channels, where the other correlations only accounted for the hydraulic diameter.

The single phase refrigerant region was represented by the Garimella et al. [57] correlation. Due to its small contribution to the total heat transfer, the single phase correlation was not varied, and only the boiling correlations were tested for accuracy. A 10% change in single-phase heat transfer coefficient leads to less than a 0.5% change in weighted average heat exchanger width. The correlation was selected because it encompassed the entirety of the refrigerant side Reynolds numbers, and was development for rectangular channels. It was developed using water-glycol and not refrigerant, but no correlation was found that tested R134a under the required conditions, and the valid Prandtl ranges for the correlation encompassed the refrigerant tested range.

3.2.4. Bar Plate Heat Exchanger Pressure Drop

When validating the model for accuracy, the refrigerant pressure loss though the core was set to the experimental value and the pressure loss was evenly divided between all control volumes. Though this did present a level of error, it significantly aided in the ease of model operation, reducing diverging results and run time. The model calculated the total core pressure loss as the sum of the predicted pressure loss across each control volume. At the single phase control volumes

the pressure loss is simply the frictional and gravitational losses, while at the two phase control volumes the pressure loss is the sum of the frictional and acceleration losses. Because the refrigerant rows run parallel to the ground, the gravitational losses are not accounted for at each control volume. Only where the refrigerant turns into a new row, moving vertically, was the gravitational loss accounted for. The empirically developed Tran et al. [54] correlation was used to determine the frictional pressure losses. The Tran et al. pressure drop correlation, Equation (3.31), is a function of the liquid only frictional pressure drop, the confinement number, the quality, and a Gamma squared parameter. The liquid only pressure drop is calculated by the laminar flow in circular tubes as shown in Equation (3.32). The confinement number relates the bubble diameter with the hydraulic diameter and accounts for the micro size of the channels. The Gamma squared parameter is the ratio of gas only pressure loss to liquid only pressure loss.

$$\Delta P_{\text{fric}} = \Delta P_{\text{fric, sl}} \cdot \left(1 + 4.3 \cdot \left(\Gamma^2 - 1\right)\right) \cdot \left(Co \cdot X^{0.875} \cdot \left(1 - X\right)^{0.875} + X^{1.75}\right) \tag{3.31}$$

$$f_{\text{sl}} = 64 \cdot Re_{\text{sl}}^{-1} \tag{3.32}$$

The same gravitational and acceleration pressure loss equations used in the plate frame model were used for the bar plate model, but the geometric parameters and the gravitational components were altered.

It was also important for the model to be able to predict the pressure drop through the inlet and outlet manifolds. For the model validation effort it was important because the model assumed uniform distribution of flow, which can only be assumed when the manifold pressure loss is small relative to the core pressure loss. In the VCC optimization study it could be the case that the manifold pressure loss is significant when the number of channels becomes large.

The manifold pressure loss was calculated as the sum of the frictional loss of fluid flowing through the header and the minor loss of fluid leaving through a “T”, Equation (3.33) below. For

ease of modeling the average of the manifold was used in the calculation, ie the flow rate of fluid was assumed to be half of the total flow rate.

$$\Delta P_{\text{manifold}} = 0.5 \cdot K_{\text{T}} \cdot \rho_{\text{r}} \cdot \overline{V_{\text{r}}^2} + f_{\text{manifold}} \cdot \rho_{\text{r}} \cdot \overline{V_{\text{r}}^2} \cdot \frac{Depth}{D_{\text{manifold}}} \tag{3.33}$$

In the equation above, the minor loss coefficient, K_{T}, was determined using the minor loss calculator within Engineering Equation Solver [76]. The Fanning friction factor correlation was used to determine manifold friction factor, and shown in Equation (3.34) below.

$$f_{\text{manifold}} = 0.316 \cdot Re_{\text{r}}^{-0.25} \tag{3.34}$$

The Fanning friction factor correlation used in the present investigation is for Reynold's numbers greater than 2300, and for both the inlet and outlet manifolds in both the model validation and the optimization study, the refrigerant in the manifolds was turbulent. Therefore, the pressure drop was calculated this way for both the inlet and outlet manifolds.

3.2.5. Thermal resistance network

A thermal resistance network was constructed at each control volume and used with the three energy conservation equations to connect the geometry of the heat exchanger to the thermodynamic profile. The continuity equations described in section 3.2.3 result in an effectiveness that was used to calculate the *NTU* and subsequently a *UA*. The *ε-NTU* relations were used in the bar plate design as opposed to the *UA-LMTD* method because of the inaccuracy of calculating the log mean temperature difference in cross flow. The cross flow *ε-NTU* relationship, shown in equation (3.35) was used in this investigation:

$$\varepsilon = 1 - \exp\left[\left(\frac{1}{C_{\text{r}}}\right) \cdot NTU^{0.22} \cdot \left\{\exp\left[-Cr \cdot NTU^{0.78}\right] - 1\right\}\right] \tag{3.35}$$

Where C_r is the ratio of C_{min} over C_{max}. The UA was then calculated from the NTU using equation4.19:

A thermal resistance network was constructed at each control volume alongside the three energy equations to connect the geometry of the heat exchanger to the thermodynamic profile. The network consists of three thermal resistances in series: water-glycol convection including fin effects, conduction through the aluminum wall, and refrigerant convection including fin effects. The convection resistances, *R*, were calculated using Equation (3.36), where *h* is the water-glycol heat transfer coefficient. The conductive wall resistance was calculated using Equation (3.37). Fouling resistance was neglected from the resistance network. Fouling resistance was neglected from the resistance network due to the test heat exchanger being new and having few operating hours.

$$R_{conv} = \left[h \cdot (A_b + A_f \cdot \eta_f)\right]^{-1} \tag{3.36}$$

$$R_{wall} = \frac{\delta_{wall}}{K_{wall} \cdot A_{base}} \tag{3.37}$$

The three thermal resistances are inversely summed to calculate the *UA*, as shown in Equation (3.38), then the *UA* was related to the *NTU* with Equation (3.39).

$$UA = \frac{1}{R_r + R_{wall} + R_g} \tag{3.38}$$

$$NTU = \frac{UA}{C_{min}} \tag{3.39}$$

The resistance network equations above are used to solve for the required heat transfer area. Because the model has a fixed row width and depth, the row length of each control volume is easily calculated. The thirty two calculated row lengths where combined to form a single metric

of comparison, the weighted width Equation (3.40). The weighted width could be compared to the actual core width. Although the model determines the required heat transfer area, the total heat transfer area is difficult to visualize because the area per unit channel length changes as the channel width increases through the core. As such, the weighted average core width was used as a proxy metric to determine model accuracy as shown below:

$$W_{\text{weighted}} = \frac{\sum W_{\text{c}} \cdot L_{\text{c}}}{L_{\text{HX}}} \tag{3.40}$$

It was assumed that all of the heat was transferred between fluids, and that there was no ambient heat loss from the heat exchanger. This assumption was proven valid by performing an order of magnitude heat transfer calculation on the walls of the bar plate heat exchanger to the environment at a high temperature difference condition. Even at the condition, temperature difference of 18 °C, radiation heat transfer was negligible due to the temperature difference being relatively small for radiation to occur. Therefore only natural convection was accounted for. The laminar flow Nusselt correlation for natural convection on vertical plate presented by Churchill and Chu [110] was used to determine the natural convection heat transfer coefficient. The total heat transfer calculated to be lost to the ambient was 143 W. This was less than 0.2% of the total heat transfer between the fluids, an insignificant amount, allowing for the assumption to be made.

3.3.Vapor Compression Model

The goal of this portion of the investigation was to determine the optimum size and configuration of evaporating heat exchanges in a vapor compression cycle. This section elaborates on the methods and assumptions used in the cycle modeling. Two types of evaporators were

modeled: bar plate and plate frame compact heat exchangers. The core pressure loss was used as the optimization parameter for the evaporator size within a vapor compression cycle (VCC) model.

The VCC model was developed using Engineering Equation Solver [76]. The present cycle consists of four components: compressor, condenser, expansion valve, and evaporator, as shown in Figure 3-9.

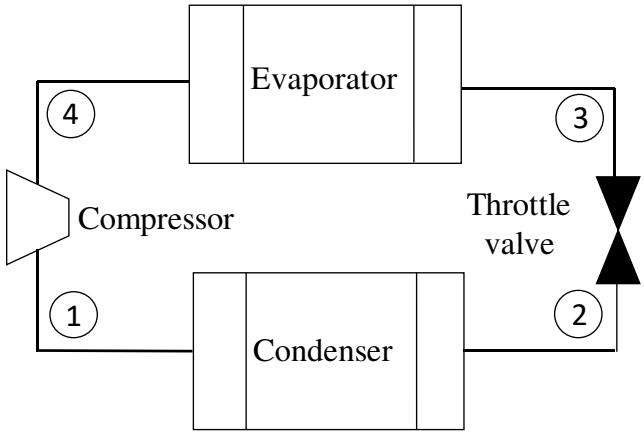

Figure 3-9. Schematic of a simple vapor compression cycle used in the current study.

The state points are listed in Table 3-5. The condenser was assumed to be ideal, where there was no pressure loss through the device, and the refrigerant exiting was fixed as a saturated liquid. The compressor was assumed to have an isentropic efficiency equal to 0.675, comparable to centrifugal compressors [84], and a fixed work which allowed for the cycle to have a COP equal to 5.

Table 3-5. Vapor compression cycle state points.

State Points	Temp	Pressure
	°C	°C
1	52.43	1,222
2	47.01	1,222
3	Floating	Floating
4	5.5	356

The evaporator was set so that the refrigerant exiting the device was a saturated vapor. Points one, two, and four were there by fixed in the model, so that the compressor and condenser performances

were not affected by the changing evaporator conditions. Point three was varied depending on the evaporator pressure loss, thus, the expansion valve accommodated the remaining pressure drop not lost through the evaporator. The input parameters to the cycle model are listed in Table 3-6.

Table 3-6. Vapor compression cycle conditions.

COP	5
Refrigerant Mass Flow Rate [kg s^{-1}]	2.27
Evaporator Water-Glycol Mass Flow Rate [kg s^{-1}]	16
Condenser Water-Glycol Mass Flow Rate [kg s^{-1}]	11.85
Evaporator Water-Glycol Temperature in, out [°C]	12, 7
Condenser Water-Glycol Temperature in, out [°C]	29, 37
Compressor Efficiency	67.5%
Evaporator Heat Duty [kW]	306

It was assumed that this change in pressure drop does not affect the expansion valve size. The throttle valve was assumed to be isenthalpic. Each component in the cycle was modeled with the inlet fluid conditions set equal to the outlet conditions of the previous component along the refrigerant flow path, neglecting the effects of pipe roughing.

The thermodynamics of the evaporator were modeled first. The coolant was a 70-30 by volume mixture of water and propylene glycol. The evaporator heat duty was calculated using the equation below:

$$q_{\text{Evap}} = \dot{m}_{\text{g}} \cdot Cp_{\text{g}} \cdot \left(T_{\text{g,in}} - T_{\text{g,out}}\right) \tag{3.41}$$

The water-glycol inlet and outlet temperature were set to 12°C and 7°C, respectively, which are standard for space conditioning applications [85]. The water glycol flow rate was fixed to 16 kg s^{-1} thereby setting the heat duty of the evaporator to 305.8 kW. All heat transfer occurred

while the refrigerant was a two-phase mixture, since the outlet quality was set to 1.0. Therefore, only one set of continuity equations was required, shown in Equations (3.41) - (3.43).

$$q_{\text{Evap}} = \dot{m}_{\text{r}} \cdot \left(i_{\text{r,4}} - i_{\text{r,3}} \right) \tag{3.42}$$

The enthalpy at the heat exchanger inlet, h_{r3}, was set via the outlet enthalpy of the expansion valve, state point 3. The exiting enthalpy, $h_{\text{r4,}}$ was determined using the saturation condition at the outlet temperature of the evaporator. Equation (3.42) was used to calculate the refrigerant mass flow rate through the vapor compression cycle. The final continuity equation, Equation (3.43), was used to couple the thermodynamic model and heat exchangers via the evaporator effectiveness. In Equation (3.43), minimum heat capacity rate (C_{min}) was the water-glycol stream because the refrigerant side is a two-phase mixture which has a heat capacity rate diverging to infinity.

$$q_{\text{Evap}} = Cp_{\text{g}} \cdot \dot{M}_{\text{g}} \cdot \varepsilon \cdot \left(T_{\text{g,in}} - T_{\text{r,3}} \right) \tag{3.43}$$

After the refrigerant exits the evaporator, it enters the compressor, labeled as state point 4 in Figure 3-9. The compressor efficiency, 67.5%, along with the inlet enthalpy, is used to determine the compressor outlet enthalpy in Equation (3.44).

$$\eta_{\text{Com}} = \frac{i_{\text{2,s}} - i_{\text{1}}}{i_{\text{2}} - i_{\text{1}}} \tag{3.44}$$

The isentropic enthalpy was calculated using the entropy at state 4 and the pressure at state 1. The high side pressure at state 1 was determined from the condenser.

The condenser was a liquid coupled heat exchanger and used a coolant loop of 70-30 by volume mixture of water propylene glycol. The inlet and outlet temperatures were set for the water-glycol side, 29°C and 37°C respectively. The heat exchanger was split into two regions, super-heated and two phase, requiring two sets of continuity equations. Equations (3.45) through (3.47)

were solved simultaneously to determine the state points into and out of the condenser superheated region along with the mass flow of the water-glycol.

$$q_{\text{Con,Sh}} = \dot{m}_{\text{r}} \cdot \left(i_{\text{r,1}} - i_{\text{r,sv}} \right) \tag{3.45}$$

$$q_{\text{Con,sh}} = \dot{m}_{\text{g}} \cdot Cp_{\text{g}} \cdot \left(T_{\text{g,mid}} - T_{\text{g,out}} \right) \tag{3.46}$$

$$q_{\text{Con,Sh}} = C_{\text{min}} \cdot \varepsilon \cdot \left(T_{\text{g,mid}} - T_{\text{r,1}} \right) \tag{3.47}$$

The condenser two phase region was solved for using Equations (3.48) through (3.50).

$$q_{\text{Con,tp}} = \dot{m}_{\text{r}} \cdot \left(i_{\text{r,sv}} - i_{\text{r,sl}} \right) \tag{3.48}$$

$$q_{\text{Con,tp}} = \dot{m}_{\text{g}} \cdot Cp_{\text{g}} \cdot \left(T_{\text{g,in}} - T_{\text{g,mid}} \right) \tag{3.49}$$

$$q_{\text{Con,tp}} = C_{\text{min}} \cdot \varepsilon \cdot \left(T_{\text{g,in}} - T_{\text{r,sl}} \right) \tag{3.50}$$

After the condenser, the refrigerant passes through the expansion valve. The valve is assumed to be isenthalpic, so Equation (3.51) is used to close the cycle.

$$i_{\text{r,2}} = i_{\text{r,3}} \tag{3.51}$$

The coefficient of performance was fixed at 5, and defined using Equation (3.52).

$$COP = \frac{q_{\text{evap}}}{\dot{W}_{\text{comp}}} \tag{3.52}$$

The previous sections presented the methods and equations used to develop the two evaporator models, one for a plate frame heat exchanger and one for a bar plate heat exchanger, as well as the methods and equations used to develop a vapor compression cycle model. The chapter also presented several correlations to be tested in the heat exchanger models. The next step in this investigation was to experimentally test the heat exchangers and compare the results to the empirical correlations found from literature. The following chapter will elaborate on the test facility as well as the testing methods used to collect the necessary data around the evaporators.

To determine the pressure drop, core volume relationship for the bar plate and plate frame heat exchangers operating in both parallel and counter flow, the heat exchanger models were integrated into the full vapor compression cycle system model. The state points at 3 and 4 were entered as boundary conditions to each heat exchanger model which calculated the length, width, and depth of the required core size.

The water-glycol side boundary conditions were set and held constant throughout the optimization. The outlet of the refrigerant was also set, leaving the inlet, state 3, to be varied. State 3 was varied by parametrically increasing the pressure drop through the core. This was accomplished physically by decreasing the number of channel sets, which decreased the core depth. To accommodate the required heat transfer area, the length of the plate frame core and the width of the bar plate core increases. As the pressure drops were parametrically tested for each core configuration, the core volume was calculated. This effort lead to the determination of the configuration and pressure drop resulting the minimum evaporator core volume.

Chapter 4. Experimental Set Up

This study aims to develop validated heat exchanger sizing models which required experimental data collection. The data collected for this study was from two evaporative heat exchangers in a preexisting turbo-compression cooling test facility which employed real world constraints. A turbo-compression cooling system (TCCS) is a thermally activated cooling system that is designed to generate cooling from low grade waste heat [86]. The system operates as an organic Rankine cycle (ORC) directly coupled to a vapor compression cycle (VCC) as shown in Figure 4-1. The test facility was designed to recover waste heat from the flue gas exhaust of a power plant to generate cooling which can offset water consumption of evaporative cooled power plants.

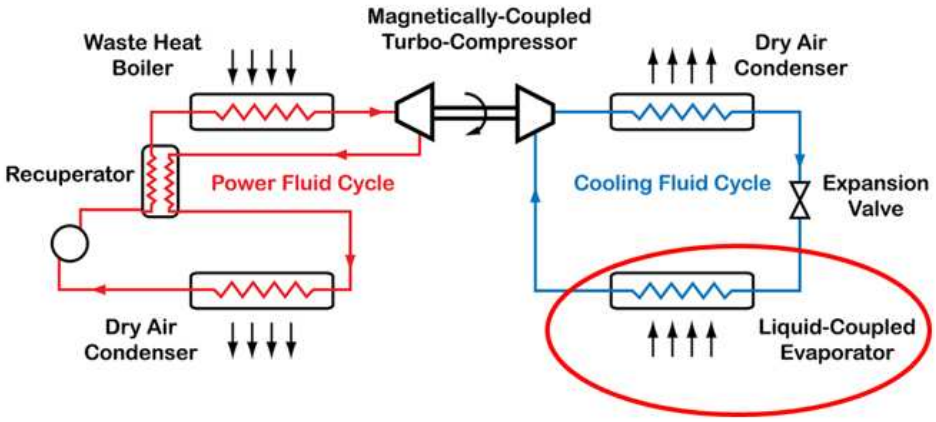

Figure 4-1. Turbo-Compression Cooling System test facility block diagram. The liquid-coupled evaporator is the primary focus of the present investigation, circled in red.

The organic Rankine power cycle in the facility consists of a waste heat boiler, centrifugal turbine, air coupled condenser, side channel pump, and recuperative heat exchanger. A flue gas simulation loop adds heat energy to the cycle which is used to vaporize the working fluid. The superheated working fluid is expanded through a centrifugal turbine which generates mechanical

power. The mechanical power generated from the ORC turbine directly drives a centrifugal compressor on the vapor compression cycle. The superheated working fluid at the turbine outlet preheats the subcooled fluid entering the waste heat boiler in a recuperative heat exchanger. Next, the fluid is condensed using air-coupled heat exchangers and then pressurized with the pump.

The vapor compression cycle in the facility generates the useful cooling effect. After the working fluid is compressed to a high pressure, it is passed through air coupled condensers to reject heat to the ambient. The condensers on the power and cooling cycles have a similar design. The R134a working fluid is then throttled in an expansion valve and sent to the evaporators. The test facility employs two expansion valves, one for each evaporative heat exchanger. One evaporator is an aluminum bar plate style device and the other is a stainless steel plate frame type heat exchanger. The working fluid evaporates in the heat exchangers which generates a cooling effect for an external water stream. After the working fluid is evaporated, it is sent back to the compressor.

This study focuses on the evaporators in the VCC. The cold, vapor compression side of the evaporators uses an R134a refrigerant, while the hot side consists of a 70-30 by volume mixture of water and propylene glycol. The water-glycol circulation skid consists of a centrifugal pump, two flow control valves, the evaporators, and a heater. The flow control valves were used to modulate the flow rate of the water-glycol through each heat exchanger. The heater was a simple plate frame type heat exchanger that was connected to a hot water circulation loop as shown in Figure 4-2. Both evaporators were oriented vertically in the loop. Water-glycol flowed down through the cores, while the refrigerant entered the bottom of the cores and flowed upward as it evaporated. Figure 4-3 shows photos of the two evaporates integrated into the test facility.

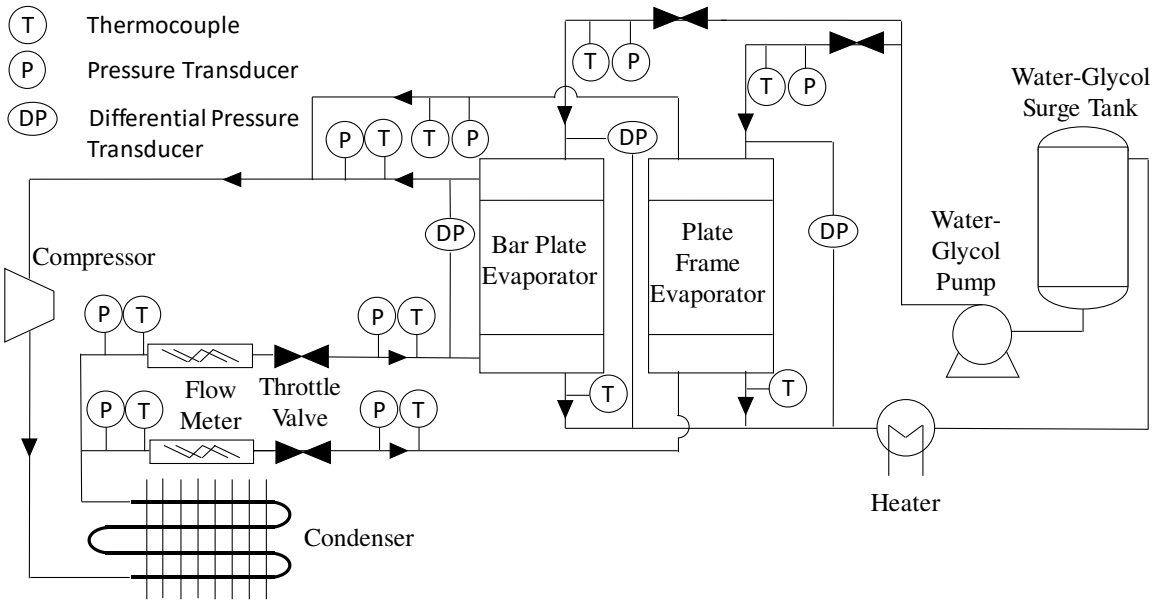

Figure 4-2. Facility process flow diagram of the vapor compression cycle and chilled water circulation loop. Positions of measurements shown.

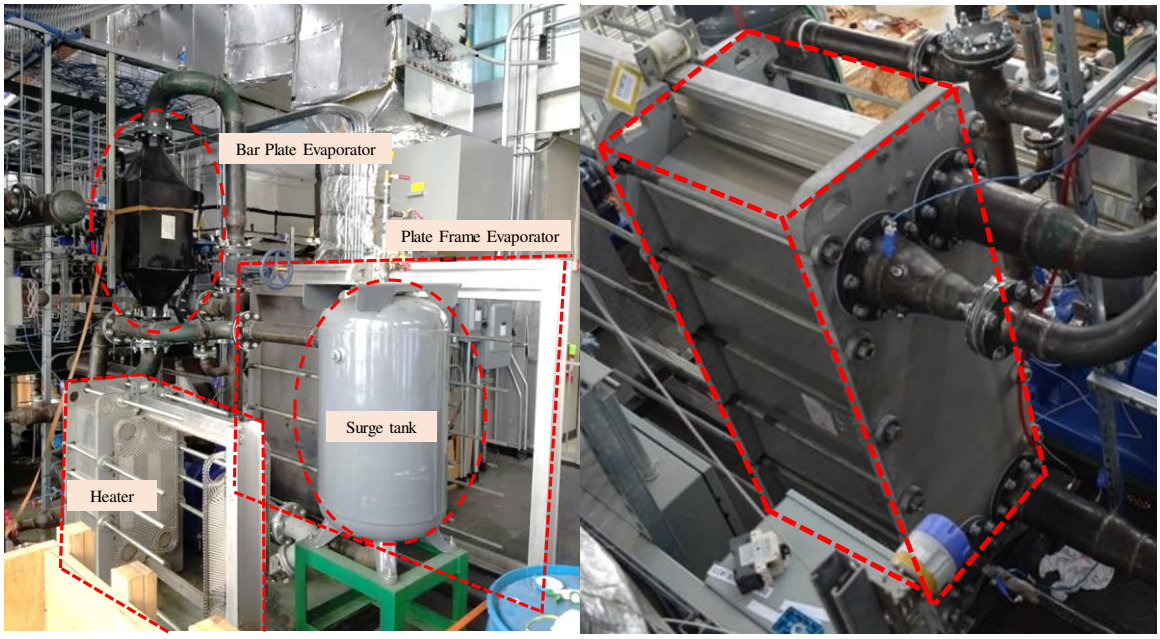

(a) (b)

Figure 4-3. Test facility photos. (a) Evaporator images in the facility, also showing the water-glycol circulation loop. (b) Plate Frame frontal view.

The facility was instrumented with T-type thermocouples on the heat exchanger inlets and outlets as well as before the expansion valve. Absolute pressure measurements were made with Ashcroft type G1 pressure transducers at both evaporator inlets and before the expansion valve. It is important to know the conditions before the expansion valve because the refrigerant at the evaporator inlet was theorized to be two-phase. Therefore, the enthalpy cannot be determined from temperature and pressure alone. However, in all cases for the TCCS operation, the refrigerant enters the evaporator slightly sub-cooled and therefore the inlet temperature and pressure were sufficient to determine inlet enthalpy. Another absolute pressure measurement was taken at the plate frame evaporator outlet to determine refrigerant pressure drop. On the bar plate evaporator, refrigerant pressure drop was measured with a differential pressure transducer. The refrigerant mass flow was measured using an inline Coriolis mass flow meter placed just upstream of each expansion valve.

The water-glycol sides of the evaporators were similarly instrumented with T-type thermocouples placed at the inlet and outlet of the heat exchanger. An Ashcroft type G1 pressure transducer was placed at the inlet and a differential pressure transducer was placed between the inlet and outlet of the water-glycol side to measure pressure drop through the device. The flow rate of the water-glycol was measured using a paddle wheel volumetric flow meter. The meter was calibrated to the 5" pipe diameter and was placed at the outlet of the evaporator. However, it was found that the paddle wheel volumetric flow meter presented too much uncertainty in measurement, discussed further below, so the mass flow rate of the water-glycol was calculated using an energy balance around the heat exchanger.

4.2. Data collection

During prior investigations [86], the TCCS test facility was operated under a specific power plant system design condition which resulted in the refrigerant outlet temperature converging to the inlet water-glycol temperature in both evaporators. This implied that the evaporators were oversized for this design point. Data collected under these conditions did not allow for model validation because instruments were only placed at the inlets and outlets of the heat exchangers. Therefore, the exact location in the heat exchanger where the temperatures converged is unknown. Figure 4-4 presents possible temperature profiles for an oversized heat exchanger where only the endpoint conditions are measured.

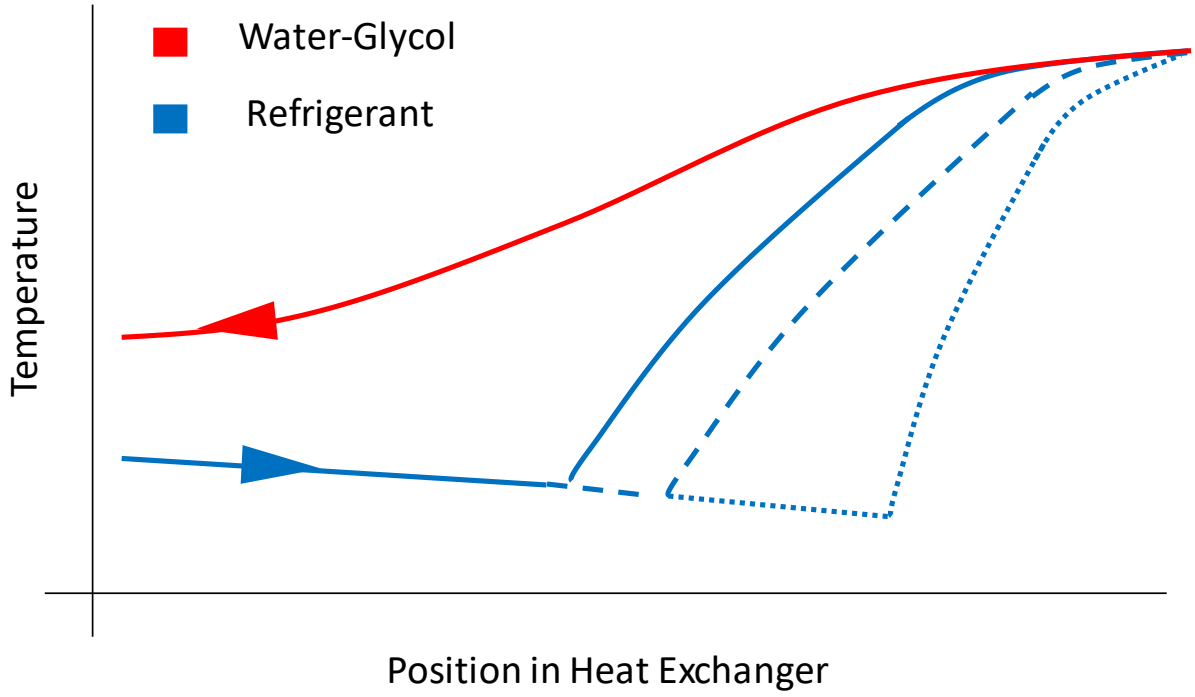

Figure 4-4. Counter flow temperature profile of an oversized evaporative heat exchanger where the temperatures converge.

Each of the blue lines represent a potential temperature profile along an arbitrary counter flow heat exchanger. The position at which the refrigerant reaches its maximum temperatures, the point after

which no appreciable heat transfer occurs, is unknown, removing one of the required boundary conditions required for model validation. In the case where the temperatures do not converge, the position where the refrigerant reaches a maximum energy value is known to be the outlet and all of the heat exchanger length is utilized. Slight modifications to the previous investigation's [86] testing procedure were required to collect data which could be used for model validation. In the test facility, the refrigerant mass flow rate was maximized to prevent temperature convergence while maintaining superheat entering the compressor. This was achieved with a balance of two operations: increasing compressor work via an increase in power cycle power output and opening the expansion valve. This maximization was performed over a range of water-glycol inlet temperatures and heat loads: 15°C – 25°C and 60 kW – 95 kW. The refrigerant and water-glycol temperatures often converged at heat loads below 60 kW and when the temperature difference between the water-glycol and the ambient temperature fell below 2 °C.

Not all steady state data points collected were used in model validation due to the temperature convergence phenomenon. The only steady state data points used were points in which the water-glycol inlet temperature was at least 0.5°C higher than the outlet refrigerant temperature and the outlet water-glycol temperature was at least 0.5°C higher than the inlet refrigerant temperature.

4.3. Wilson Plot Experiments

A Wilson plot experiment [87,88] was used to determine the water-glycol side heat transfer coefficient. The experiment varied the water-glycol flow rate over a range of conditions, while maintaining the same refrigerant side conditions. If the refrigerant convective resistance and wall conductive resistance remain constant across all of the collected points, then the water-glycol convective resistance would be the only resistance that will change in the overall thermal resistance

calculation as a function of the water-glycol flow rate. The method then reduces the water-glycol flow rate to a velocity term and plots the overall thermal resistance of the heat exchanger as a function of the water-glycol velocity to the power of negative N, for all the points collected. A linear regression was then performed on the data. The value of N was varied in order to maximize the R^2 value of the regression, this results in the best fit for the data. The regression was then set equivalent to Equation (4.1).

$$R_{ov} = \frac{1}{C_2 \cdot A_g} \cdot \frac{1}{\bar{V}_g^N} + C_1 \tag{4.1}$$

The regression was used to determine C_1 and C_2. The sum of the refrigerant and wall resistances is equal to C1, Shown in Equation (4.2).

$$C_1 = R_r + R_{wall} \tag{4.2}$$

The C_2 parameter was used to determine the water-glycol heat transfer coefficient for each of the data points collected, using Equation (4.3).

$$h_g = C_2 \cdot \bar{V}_g^N \tag{4.3}$$

The coefficients were then compared to coefficients calculated for the same data points using the single phase correlations discussed in Section 2.

To collect the data for the Wilson plot experiment, the TCCS test facility was brought to a steady state condition. It was important that for the entirety of the experiment the outlet refrigerant temperature did not converge to the inlet water-glycol temperature, as described above. With a non-converging evaporator steady state condition met, data were collected for three minutes. After the three minutes, the next condition was set. This was accomplished by closing the water-glycol throttle valve, decreasing the mass flow rate. Heat was added to the water-glycol to raise the inlet temperature, accounting for the decrease in mass flow to maintain a constant heat duty. The

condition was held for three minutes, then the next condition was set in the same manner. For all the points collected, the refrigerant side inlet and outlet conditions, as well as the refrigerant mass flow rate were held as constant as the facility could allow. The minimal variability allowed for the assumption that the refrigerant thermal resistance was constant across the experiment. This assumption was also made by Yanik and Webb [89] when performing similar experiments.

4.4. Uncertainty Analysis

The uncertainty of the experimentally calculated values used in the model validation effort was an important aspect in determining the relevance of the effort. The four parameters of interest for the uncertainty propagation study were: the overall heat transfer rate, the water-glycol side heat transfer coefficient, the water-glycol mass flow rate, and the refrigerant pressure drop. The overall heat transfer rate was of interest because it added certainty to the refrigerant heat transfer correlation comparisons. The two water-glycol parameters were added to the uncertainty study to determine the reliability of the Wilson plot experiments. Finally the refrigerant pressure drop measurement was added to determine if a pressure drop analysis could be performed. To determine the uncertainty of these parameters, the built in uncertainty propagation function in Engineering Equation Solver [76] was used. The function uses the standard method of error propagation in Equation (4.4).

$$S_y = \sqrt{\sum_{i=1}^{n} \left(\frac{\partial y}{\partial x_i} \right)^2 S_{x_i}^2} \tag{4.4}$$

In this equation, S_y represents the variable of interest and S_x represents each variable used in the calculation of S_y. Table 4-1 presents the uncertainty associated with the instruments used in data collection.

Table 4-1. Instrumentation uncertainty.

Instrument Type	Range	Accuracy
Thermocouple	All	0.6 °C
Diff. Pressure Transducer	0-15 PSI	1.5 %FS
	0-35 PSI	1.5 %FS
Pressure Transducer	0-200 PSI	0.25 %FS
Mass Flow Meter	0-7.5 kg s^{-1}	0.15 %MV

These uncertainties, along with the actual data collected were used as inputs to the uncertainty analysis. These inputs were propagated through to calculate the uncertainty of the three experimentally determined parameters of interest. For example, to calculate the overall heat transfer rate of either heat exchanger, the measured refrigerant temperature and pressure were used to determine the enthalpies at the heat exchanger inlet and outlet. The uncertainty of the measured values was propagated through to the enthalpy calculations. Next, the inlet and outlet enthalpies, along with the measured refrigerant mass flow rate were used to calculate the total heat transfer rate using Equation (4.5).

$$q = \dot{m}_{\mathrm{r}} \cdot \left(i_{\mathrm{r,out}} - i_{\mathrm{r,in}} \right) \tag{4.5}$$

The three parameters and associated uncertainties, are used as inputs into the right hand side of Equation (4.4) to determine the uncertainty of the experimentally calculated heat transfer rate. A similar process was performed to determine the uncertainty of the water-glycol flow rate calculation, and water-glycol heat transfer coefficient calculated from the Wilson plot experiment.

Table 4-2 presents the results of the uncertainty study for the plate frame heat exchanger. When analyzing the plate frame heat exchanger, the uncertainty of the heat transfer rate was small, 0.54% to 0.55% for the data. This level of uncertainty supports that the calculated parameter accurately represents the experimental data.

Table 4-2. Plate frame heat exchanger uncertainty results.

Total heat transfer Rate [kW]		Water-Glycol mass flow rate [kg s^{-1}]		Water-Glycol heat transfer coefficient [kW m^{-2} k^{-1}]		Refrigerant Pressure drop [kPa]	
Value	Uncertainty	Value	Uncertainty	Value	Uncertainty	Value	Uncertainty
185	1.016	66.61	94.03	3.602	2.369	7.459	4.23
186.4	1.016	55.29	60.35	3.282	1.71	7.067	4.23
187.9	1.023	43.93	36.01	2.925	1.166	7.04	4.23
186.3	1.013	22.16	8.749	2.078	0.4073	7.005	4.23
215.7	1.173	22.12	7.499	2.076	0.35	6.337	4.23
213.3	1.17	31	15.11			7.465	4.23
215.5	1.183	44.71	32.04			6.906	4.23
215.2	1.182	49.36	39.63			6.74	4.23
214.4	1.18	52.42	45.3			6.256	4.23
211.3	1.17	53.81	48.78			7.167	4.23

The accuracy of the water-glycol flow rate measurement was unknown due to the position of the measurement device. The paddle wheel flow meter was placed soon after a large bend, not allowing for fully developed flow at the point of measurement. Further the measurement device was never calibrated. The random error associated with the device was low, ± 1.8 [kg s^{-1}], however because the device was not calibrated, the bias uncertainty was unknown, and the actual flow rate could be significantly different from the measured flow rate. An alternative to using the paddle wheel flow meter, would be to determine the flow rate from the pump curves. This could be accomplished for the plate frame heat exchanger because the tests were conducted with only the one evaporator in use, therefore all of the flow went through the pump and the plate frame heat exchanger. Differential pressure measurements were not taken around the pump, but the power draw from the pump was measured. Accounting for motor efficiencies provided by the pump manufactures, the volumetric flow rate of the water glycol could be graphically determined. However when using this method of determining flow rate, the same trend between data points was not shown as it was from the flow meter. Figure 4-5, shows the predicted water glycol flow

rates using the two methods as well as an energy balance method. The pump curve method does not show any variability in flow rates across the data while the other two methods do.

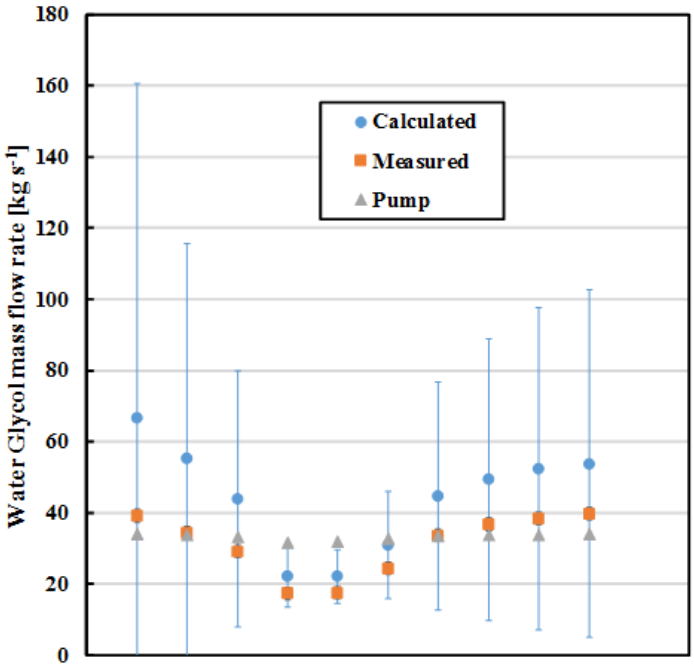

Figure 4-5. Predicted plate frame water glycol mass flow rates using energy balance calculations, paddle wheel flow meter measurements, and pump curves.

Because of the unknown uncertainty of the paddle wheel flow rate measurement and the lack of variability of the pump curve calculation, the water-glycol flow rate was calculated via an energy balance across the heat exchanger. This had an uncertainty larger than the heat transfer rate. The lowest uncertainty was 33% while the highest was over 100%. The lower uncertainty occurred when the water-glycol mass flow rate was small, which allowed for a larger temperature change between the inlet and outlet. Because the flow rate was calculated through an energy balance around the heat exchanger, the parameters and associated uncertainties used on the right had side of Equation (4.5) are the heat transfer rate, water-glycol specific heat, and the water-glycol temperature difference. As discussed above the uncertainty of the heat transfer rate was low, and therefore was not the cause of the high uncertainty of the flow rate. The uncertainty of the specific

heat was less than 1% but the uncertainty of the temperature change was high. The change had an absolute uncertainty equal to that of the thermocouples, ±0.6 ºC, and when the temperature change was 2 ºC, the relative uncertainty was 30%. However, when the temperature change was 0.5 ºC, as it was in some for the data, the relative uncertainty of the change exceeds 100%. This high uncertainty was propagated through to the water-glycol mass flow calculation. The implications of this high uncertainty was that it lead to an uncertainty in determining the water-glycol heat transfer coefficient, both in the Wilson plot experiment, discussed below, and the correlation calculated coefficient. There are two solutions to reduce the uncertainty for future work. The first would be to run experiments at much lower flow rates, allowing for a larger temperature change to occur. This would require an increased temperature differential between the refrigerant and the water-glycol to maintain the high heat transfer rate. All of which would change the system operating conditions significantly away from its realistic operation. The second solution would be to use more accurate thermocouples. If the thermocouples were calibrated to ±0.1 ºC, the relative uncertainty of the flow rate calculation can be reduced to ±5% to ±20%. Realistically T type thermocouples could not achieve this accuracy, however with the use of thermistors the high level of accuracy can be achieved.

The third parameter of interest in the uncertainty study was the water-glycol heat transfer coefficient calculated from the Wilson plot experiment. This uncertainty ranged from 16% to 65%, where the higher uncertainty occurred when the water-glycol mass flow rate was highest. The uncertainty of the flow rate was the largest contributor to the coefficient uncertainty. The uncertainty is high, and its significance is discussed further in the following section. The uncertainty could be reduced with the same methods described for the water-glycol mass flow rate.

The final parameter studied in this analysis was the refrigerant side pressure drop. The pressure drop across the refrigerant side of the plate frame heat exchanger was measured with two absolute pressure transducers. Each had an absolute uncertainty of 3 kPa. This resulted in a differential uncertainty equal to 4.23 kPa. With the absolute values of the pressure drop calculations ranging from 6.2 kPa to 7.5 kPa, the uncertainty of the measurement is larger than the deviation of the data. This did not allow for an accurate calculation and therefore the pressure drop for the plate frame heat exchanger could not be experimentally validated and had to be assumed. In a future study, the uncertainty of the pressure drop calculation could be reduce with the use of a differential pressure transducer measurement, rather than two absolutes.

Table 4-3 presents the results of the uncertainty study for the bar plate heat exchanger for the data collected in the Wilson plot experiment.

Table 4-3. Uncertainty results for the bar plate heat exchanger Wilson plot experiment.

Total heat transfer Rate [kW]		Water-Glycol mass flow rate [kg s^{-1}]		Water-Glycol heat transfer coefficient [kW m^{-2} k^{-1}]		Refrigerant Pressure drop [kPa]	
Value	Uncertainty	Value	Uncertainty	Value	Uncertainty	Value	Uncertainty
76.1	0.4	25.0	31.3	1.57	2.22	9.04	0.225
73.3	0.4	23.8	29.4	1.49	2.07	9.48	0.225
72.9	0.4	21.7	23.8	1.34	1.66	9.51	0.225
71.1	0.4	20.4	21.4	1.26	1.48	8.87	0.225
71.6	0.4	19.2	18.5	1.17	1.27	8.76	0.225
71.2	0.4	16.7	13.8	1.01	0.93	8.84	0.225

This is used as a representation of the uncertainty for the rest of the collected data. When analyzing the heat exchanger, the uncertainty of the heat transfer rate was small, 0.53% to 0.56% for the data. This level of uncertainty supports that the calculated parameter accurately represents the experimental data.

In the same way that the uncertainty in the water glycol mass flow rate was high for the plate frame heat exchanger, the uncertainty was high for the bar plate. The flow rate was determined using an energy balance around the bar plate heat exchanger as opposed to the paddle wheel flow meter or the pump curves. Like with the plate frame heat exchanger the flow meter was not calibrated and the bias uncertainty was unknown. However unlike the plate frame heat exchanger, the bar plate heat exchanger was always operated in parallel with the plate frame heat exchanger, not allowing for the use of pump curves to predict the flow rate. The relative uncertainty when using the energy balance method was almost at or above 100% for the data collected. The same factors such as the small water-glycol temperature change lead to the high uncertainty here as they did with the other heat exchanger. However, it was more significant because the bar plate heat exchanger operated with an even smaller temperature change in the water-glycol temperature. This lead to significant uncertainty in the water-glycol heat transfer coefficient calculation for the Wilson plot experiments. The uncertainty of the calculated heat transfer coefficients was larger than the difference between data points. This meant that the Wilson plot could not be used to validate the water-glycol heat transfer coefficient correlation. Due to difficulties operating the facility for the Wilson plot experiments, particularly varying the water-glycol flow rate over a large enough range, the experiment could not be reconducted, and the heat transfer coefficient had to be assumed. Thermistors could be used at the water-glycol inlet and outlet to reduce the uncertainty. Even then, if the thermistors had an accuracy to ±0.1°C, the uncertainty would be ±16% to ±20% and the difference between points is ±5% to ±7%, and the experiment would still not be reliable. The only way to reduce this uncertainty to a necessary level would be to install a reliable flow rate measurement device. To use the paddle wheel flow meter, a long strait section of pipe would be required for fully developed flow at the point of measurement.

Because the bar plate heat exchanger was instrumented with a differential pressure transducer on the refrigerant side, the pressure drop could be accurately measured. The uncertainty of the device is ±0.225 [kPa]. The uncertainty of the pressure loss measurement was tabulated in Table 4-3. The error of the measurement is small relative to the distribution of the data leading to a strong belief in the measurement. This allowed for an accurate pressure drop study to be conducted for the bar plate evaporator.

Chapter Four described the turbo-compression cooling system test facility, particularly the vapor compression cycle component and the water-glycol circulation loop in detail. The Wilson plot method was used to determine the water-glycol side heat transfer coefficient correlation. Finally, the data selection technique was presented that allowed for refrigerant side heat transfer validation. The following chapter presents the results of the data collection, how each correlation compared to the data, and which correlations were selected for the models. The chapter will also present the result for the evaporator minimization effort in a standard vapor compression cycle, determining the evaporator core volume versus pressure loss relationship.

Chapter 5. Results

The following chapter will present the results for the model validation for the plate frame and bar plate evaporators as well as the optimization results for the simple vapor compression cycle.

5.1. Heat Exchanger Validation

The two heat exchanger models developed in the present investigation were compared to data collected in the TCCS test facility. For the plate frame evaporator, the model was compared using the required plate length, while for the bar plate heat exchanger, the weighted core width was compared. After the bar plate model was validated, the total pressure drop on the refrigerant side was compared to the pressure drop predicted by the model. The following sections will describe the model validation in terms of each correlation tested, as well as the final combination of correlations which was chosen to represent the heat transfer and pressure drop of the two heat exchangers.

5.1.1. Plate Frame Heat Exchanger

The water-glycol side and refrigerant side heat transfer had to be experimentally validated which was accomplished by comparing the experimental data to predictions from the empirical correlations discussed in Chapter 3.

The model was first validated for the water-glycol side heat transfer coefficient using the Wilson plot experiment. Several steady state data points were collected and the overall thermal resistance was plotted as a function of the water-glycol velocity to the negative *N* power, as shown in Figure 5-1.

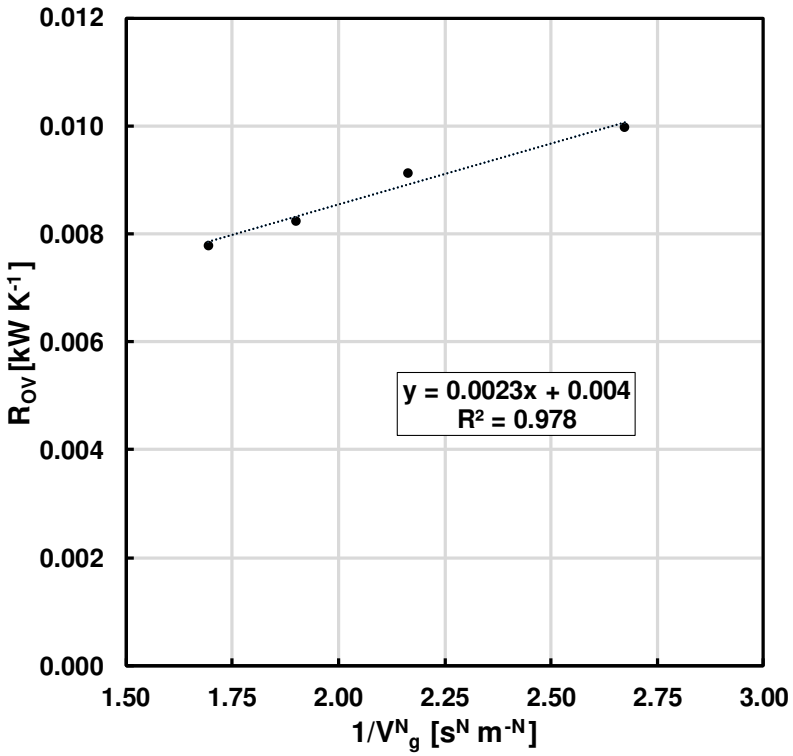

Figure 5-1. Plate Frame Wilson plot results; overall thermal resistance vs the inverse water-glycol velocity to the power of N.

N was first assumed to be 0.8 and then was varied until the linear regression achieved an R^2 value greater than 97.5%. The resulting N value was equal to 0.5. The water-glycol heat transfer coefficient was then calculated from the regression equation. These coefficients were then compared to seven single phase heat transfer correlations: Muley [39], Thonon et al. [79], Maslov and Kovalenko [35], Rosenblad and Kullendroff [34], Emerson [80], Talik et al. [78], and Kumar [81] as presented in Chapter 3. Table 5-1 shows the mean absolute error (MAE) of the model predicted heat transfer coefficient compared to the Wilson plot generated coefficients. Muley [39] resulted in the lowest MAE, equal to 0.136%. As discussed in the Chapter 4 section 4, the uncertainty in the water-glycol heat transfer coefficient calculated from the Wilson plot was high, reaching 65%. This was considered when comparing correlations.

Table 5-1. Plate frame single phase heat transfer correlation predictions compared to Wilson plot results.

Wilson Plot	Thonon	Muley	Talik et al.	Kumar	Maslov & Kovalenko	Emerson	Rosenblad & Kullendroff
3.629	6.51	3.62	7.650	6.886	4.935	6.544	6.264
3.317	5.77	3.32	6.719	6.104	4.520	5.888	5.558
2.957	4.92	2.96	5.663	5.202	4.032	5.124	4.743
2.596	4.10	2.60	3.405	3.231	2.871	3.388	2.958
2.101	3.06	2.11	3.464	3.290	2.896	3.435	3.011
%MAE	64.7	0.14	80.183	66.149	31.408	65.023	51.565

Figure 5-2 shows the water-glycol heat transfer coefficient as a function of water glycol velocity for each of the correlations tested as well as the four Wilson plot points with associated error bars.

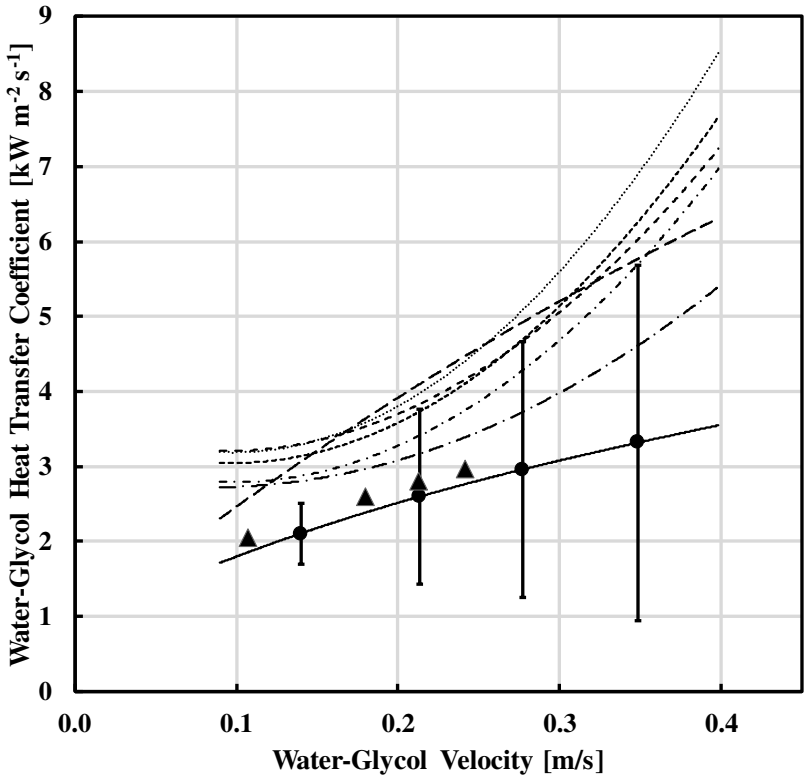

Figure 5-2: Comparison of Wilson Plot calculated water-glycol heat transfer coefficient to correlation calculated coefficients as a function of water-glycol fluid velocity. The dots represent the Wilson plot calculated heat transfer coefficients based on an energy balance calculated water-glycol flow rate. The triangles represent the Wilson plot calculated heat transfer coefficients based on the flow meter measured water-glycol flow rate.

Though some of the correlations, particularly Rosenblad and Kullendroff [34], and Maslov and Kovalenko [35], are within the upper end of three of the error bars, the correlations fail to capture

the lowest coefficient. Furthermore, the lowest coefficient is the most significant to accurately predicting the trend because this point has the least uncertainty. The Muley correlation followed the trend of both the energy balance calculated and flow meter measured water-glycol flow rate to the highest level of accuracy, so further model validation was performed using the Muley correlation to represent the water-glycol side heat transfer coefficient.

Wall resistance was calculated from known parameters so the refrigerant side thermal resistance was the only remaining variable to be experimentally validated in the heat transfer model. Three single phase heat transfer correlations and four boiling heat transfer correlations were tested in a matrix to determine the most accurate combination. The correlations were used to predict the required plate length of the heat exchanger core which was compared to the actual plate length for the collected working fluid conditions. The three single phase correlations tested were Thonon et al. [79], Maslov and Kovalenko [35], and Rosenblad and Kullendroff [34]. The single phase heat transfer coefficient had a minor impact on the predicted plate length relative to the boiling heat transfer coefficient. This is because less than 1% of the heat transfer occurs in the single phase region, and a change in single phase correlation only resulted in about a 0.2 m change in predicted plate length. The boiling correlations discussed next used the Maslov and Kovalenko single phase correlation for representative result values. This is because the correlation was a part of the combination resulting in the lowest MAE.

Four two phase heat transfer correlations, discussed in Chapter 3, were tested for accuracy within the model: Huang et al [90], Cooper [32], Hsieh et al. [26], and Han et al. [18]. The correlations were used to predict the required plate length of the core for given inlet and outlet conditions. The Huang et al. [19], and Hsieh et al. [26], correlations were chosen because their boundary conditions were representative of at least three of the following test parameters; heat

flux, mass flux, and saturation temperature, seen in Table 3-1 found at the end of the chapter. The Han et al [18] correlation was selected because of its strong dependence on geometric parameters. The Cooper correlation was tested because of its recommendation by Longo and Gasparella [31], who tested the pool boiling correlation against data collected for low mass flux boiling in plate heat exchangers.

Figure 5-3 presents the results comparing the matrix of refrigerant heat transfer correlations tested. In the box and whisker plots, the center 'X' represents the mean of the data points and the center horizontal line represents the median of the data. The box represents the variability of the data within one quartile on either side of the median and the whiskers show the variability of the outer two quartiles of results. Any statistical outliers are represented with the black dots outside the whiskers.

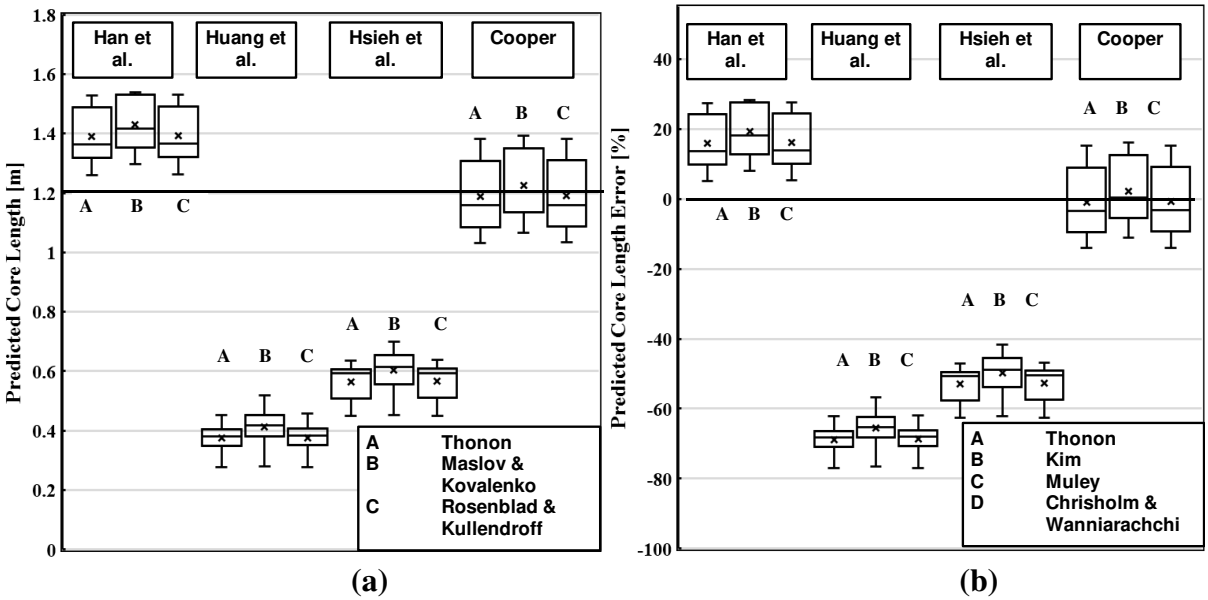

(a) **(b)**

Figure 5-3. Results of boiling heat transfer correlations tested for the plate frame heat exchanger. (a) Figure showing results as predicted plate length with the black bar at 1.2m represents actual heat exchanger length. (b) Present error comparted to the actual plate length. Black bar at 0% error.

Of the four boiling correlations selected, Huang et al. and Hsieh et al. correlations under predicted the heat exchanger plate length. When used to represent the two-phase boiling region,

the Huang et al. correlation predicted the plate length on average to be 0.413 m, 65.6% lower than the actual length. The Hsieh et al. correlation predicted the plate length on average to be 0.603 m, 49.8% lower than the actual length. The Han et al. correlations over-predict the core length as shown in Figure 5-3. The correlation over predicted the plate length due to an under prediction of the heat transfer coefficient, and not due to temperature converging. As shown in Table 5-2, the effectivenesses of each of the three regions were between 0.2 and 0.7.

Table 5-2. Effectiveness values for the subcooled, two phase, and superheated regions of the plate frame evaporator for the data.

ε Sub cooled	ε Two Phase	ε Super Heated
0.22	0.24	0.05
0.24	0.27	0.62
0.24	0.32	0.59
0.20	0.46	0.49
0.26	0.49	0.70
0.27	0.43	0.50
0.30	0.35	0.60
0.30	0.33	0.55
0.29	0.32	0.42
0.27	0.32	0.11

Figure 5-4 shows the two phase region dominates the UA requirement of the heat exchanger. This means the large predicted plate lengths were not caused by small differences in high effectivenesses resulting from the uncertainty of the heat transfer rate calculation. For heat exchangers with high effectiveness values, small changes in the effectiveness will result in a large change in required heat transfer area. Therefore, if in this study the effectiveness was on the order of 0.95, a large deviation in overall heat transfer rate could lead to a change in effectiveness, and subsequently the cause for the over prediction in plate lengths. However, because the effectiveness and uncertainty of the overall heat transfer rate are low, this could not be the case. The Han et al.

correlation likely under predicts the heat transfer coefficient due to extrapolation errors associated with using the correlation outside of the developed heat and mass flux range.

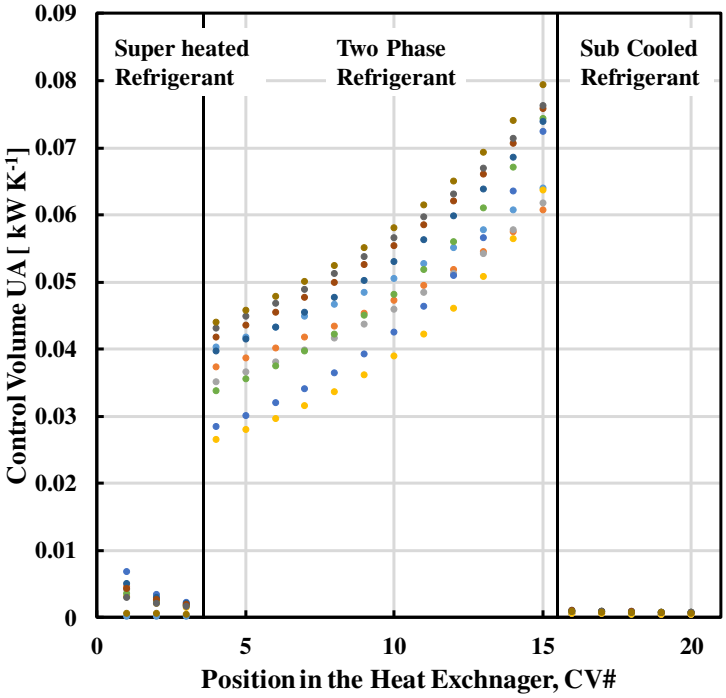

Figure 5-4. Distribution of UA along the heat exchanger control volumes for a single plate set. The different colors represent separate data points. The three refrigerant phase regions are separated by the vertical black bars. The majority of the overall heat exchanger's UA is in the two phase refrigerant region.

The Cooper correlation was able to accurately predict the plate length of the core. The core length was predicted to be 1.23 m with a MAE equal to 7.9%. Longo and Gasparella accredit its use in plate evaporators at low mass fluxes, and the current experiment further justifies its use. It is likely the case that the two phase refrigerant heat transfer is dominated by nucleate boiling. The Hsieh et al. correlation does account for a weighted proportion of nucleate and convective boiling, even using the Cooper correlation to predict the nucleate component. However the correlation was developed at a much higher mass flux range. This means the weighting function based on quality, does not accurately represent the proportions of each component.

The Huang et al. correlation was developed for similar mass flux ranges as the experiments, however did not predict the data well. It is unclear to why this correlation under predicts the data. Like the Longo and Gasparrella investigation, the Huang et al. study found that at low mass flux ranges the two phase heat transfer is dominated by nucleate boiling. The correlation was therefore developed with no flow parameters such as Reynolds number, and focused on parameters such as enthalpy of vaporization and thermal diffusivity.

The combination of a Cooper [32] boiling, and Maslov and Kovalenko [35] single phase heat transfer correlation, were used to represent the refrigerant side heat transfer, while the water-glycol side was represented with the Muley [39] single phase correlation. The combination resulted in the lowest MAE of any other, MAE equal to 7.9%, and was therefore chosen to represent the plate frame heat exchanger in the optimization study.

5.1.2. Bar Plate Heat Exchanger

As described in Chapter 4, the uncertainty of the calculated water-glycol heat transfer coefficients from the Wilson plot experiment were unacceptably high. As shown in Figure 5-5, the error bars for each of the collected points vary more than the deviation of the points themselves. Therefore there is little certainty in the calculated coefficients. To move forward with the investigation, heat transfer coefficients were assumed based on the Hartnett and Kostic [83] single phase heat transfer correlation. The correlation was chosen because it was developed for laminar flow through rectangular channels. Many correlations are developed for these conditions, but the Hartnett and Kostic correlation was the only to include an aspect ratio term, accounting for more detail about the heat exchanger geometry when calculating the heat transfer coefficient.

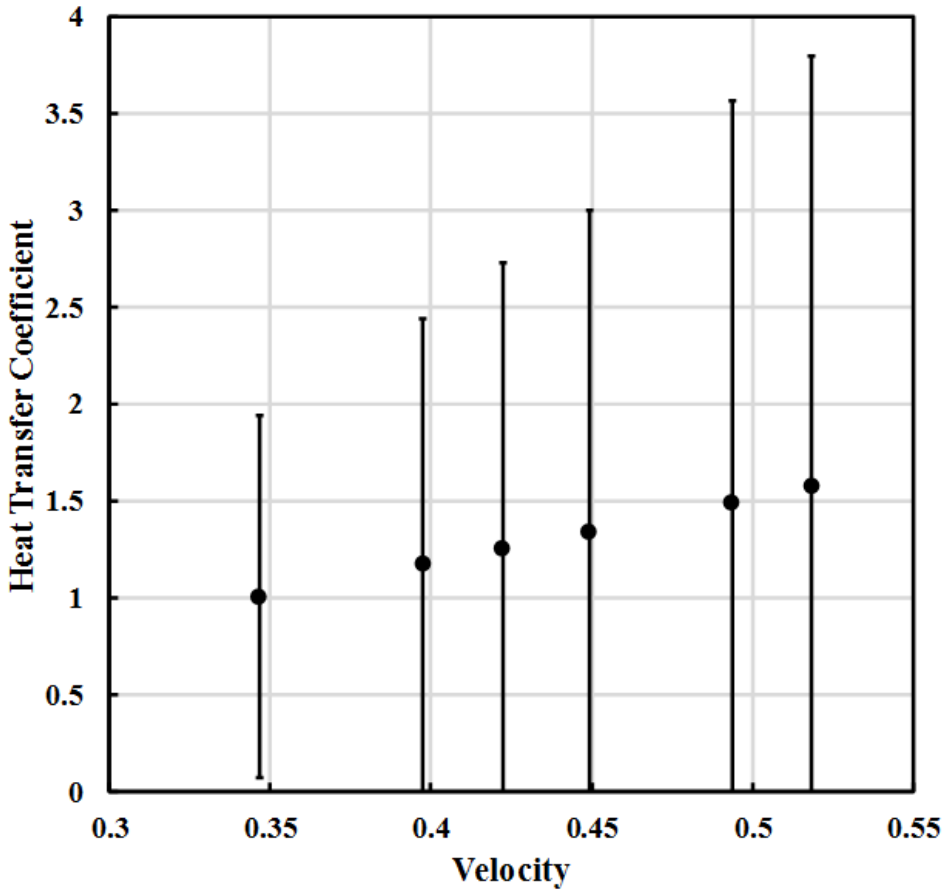

Figure 5-5. Bar plate Wilson plot results, water-glycol heat transfer coefficient as a function of water-glycol velocity. The associated error bars are for the heat transfer coefficients are large and encompass the deviation of the collected data points.

With the wall resistance calculated from known parameters, the refrigerant side convection resistance is the only remaining parameter to be validated for the heat transfer model. The single phase refrigerant heat transfer was represented with the Garimella et al. [57] correlation for flow in rectangular micro channels, because it encompassed the experienced range of the Reynolds numbers, as seen in Table 3-4. This leaves only the boiling refrigerant resistance. The data collected around the heat exchanger were used as inputs into the model to calculate the weighted width of the heat exchanger core. As described in Chapter 3, the primary method used to determine model accuracy was to compare the model-calculated weighted average of row lengths and the

actual heat exchanger core width. The weighting was used to normalize the row lengths to the row widths, as shown in Equation (5.1).

$$W_{\text{weighted}} = \frac{\sum W_{\text{c}} \cdot L_{\text{c}}}{L_{\text{HX}}} \tag{5.1}$$

The total heat transfer area was difficult to visualize, while a width dimension can be easily understood not unlike the length term for the plate frame model. As such, the weighted average core width was used as a proxy metric to determine model accuracy. Figure 5-6 depicts the model predicted heat exchanger core width for each boiling correlation tested. The actual heat exchanger width is represented by the solid black line across the Figure at 0.385 m. All three boiling correlations under predicted the heat exchanger core width. It was unlikely that the under prediction was caused by an added fouling or brazing resistance. The core was cleaned before installation and has less than 100 operating hours. It was also unlikely that the cause to the under predicted core width was due to the flow distribution assumption. To determine the accuracy of the assumption the manifold pressure loss was calculated and compared to the channel loss. It was found that the manifold pressure loss was between 35 and 70 Pa, nominally one-percent of the total loss. The small percentage supports the assumption of well distributed flow. Thus, the model had to be over predicting the refrigerant side heat transfer coefficient. Figure 5-6 presents the MAE of each prediction method. The Kuzentsov et. al. [49] boiling correlation leads to the closest width prediction on average, however does have the greatest variability in results. On the other hand, the Li and Wu [52] correlation significantly under predicts the core width by an average error equal to 89.1%, but had the lowest variability. The Bertsch et. al. [44] correlation was in the middle of the other two for error and variability.

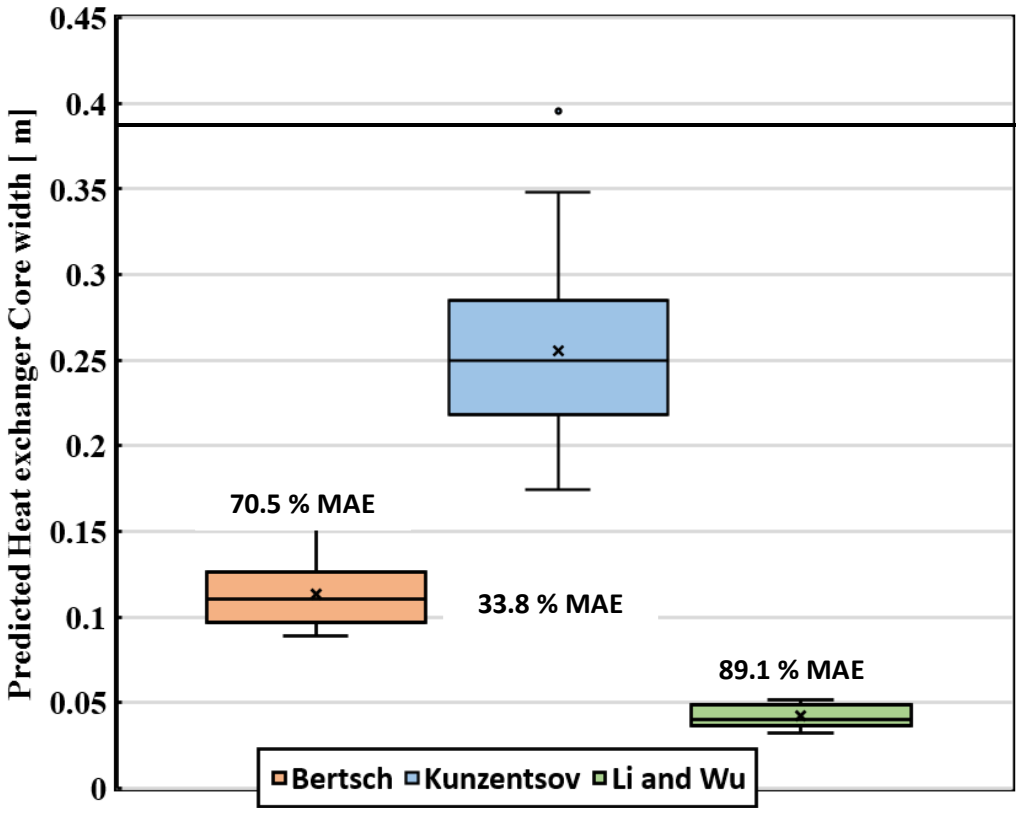

Figure 5-6. Predicted bar plate heat exchanger core width for each boiling heat transfer correlation tested. Black bar represents the actual core width at 0.38 m.

The Bertsch et al. correlation is a weighted proportion of convective and nucleate boiling components. When used, the convective heat transfer term dominates over the nucleate boiling heat transfer term throughout the two-phase region. This is supported by a large enhancement factor because the bubble diameter is large relative to the channel size, represented by a Confinement number > 0.5.

The Kuzentsov et al. correlation is also a weighted correlation like the Bertsch et al. The Kuzentsov et al. correlation however offers additional multiplication factors for the nucleate boiling term. This investigation used the developing and suppression factors but omitted the secondary suppression factor. The secondary suppression factor requires further understanding or boundary layer characteristics, which were not experimentally measured as part of this study.

Though the correlation was developed with some or all of the additional factors, the secondary suppression factor could help reduce error, or reduce the variation of the results. In future investigations the secondary suppression factor could be tested when the boundary layer information could be experimentally collected.

The Li and Wu correlation under predicted the required core width on average to 0.0421m, 11% of the actual width, 0.385 m. It is likely that the correlation over predicted the heat transfer coefficient which is caused by a high variance of the development of the correlation. The present investigation uses Reynolds, Boiling, and Bond Numbers within the recommended correlation bounds and yields predicted Nusselt numbers comparable to those found in the original study. In the development of the correlation, 85.8% of the data used in the correlation development was within ±50% error, some approach 100% error with the MAE for the data bank equal to 26.1%. It is likely that the data collected in this investigation is on the outer bounds of the correlation.

In an effort to continue on to the optimization effort with an accurate model, a correction factor was applied to each correlation to match the average predicted core width with the actual core width of 0.385 m. Table 5-3 shows each correction factors and associated results for the three correlations centered on the actual width.

Table 5-3. Bar plate refrigerant heat transfer coefficient correction factor and associated error.

Two Phase Boiling Correlation	Correction Factor	% MAE
Bertsch et. al.	0.365	13
Kuzentsov et. al.	0.61	14
Li and Wu	0.085	13

Figure 5-7 depicts the distribution of the corrected width prediction. The corrected Kuzentsov et al. correlation resulted in 91% of the data falling within ±25% error which was similar to the other two correlations, however the correlation required the least amount of correction with a factor

equal to 0.61. The Kuznetsov et al. [49] correlation was therefore selected for use in the heat exchanger model.

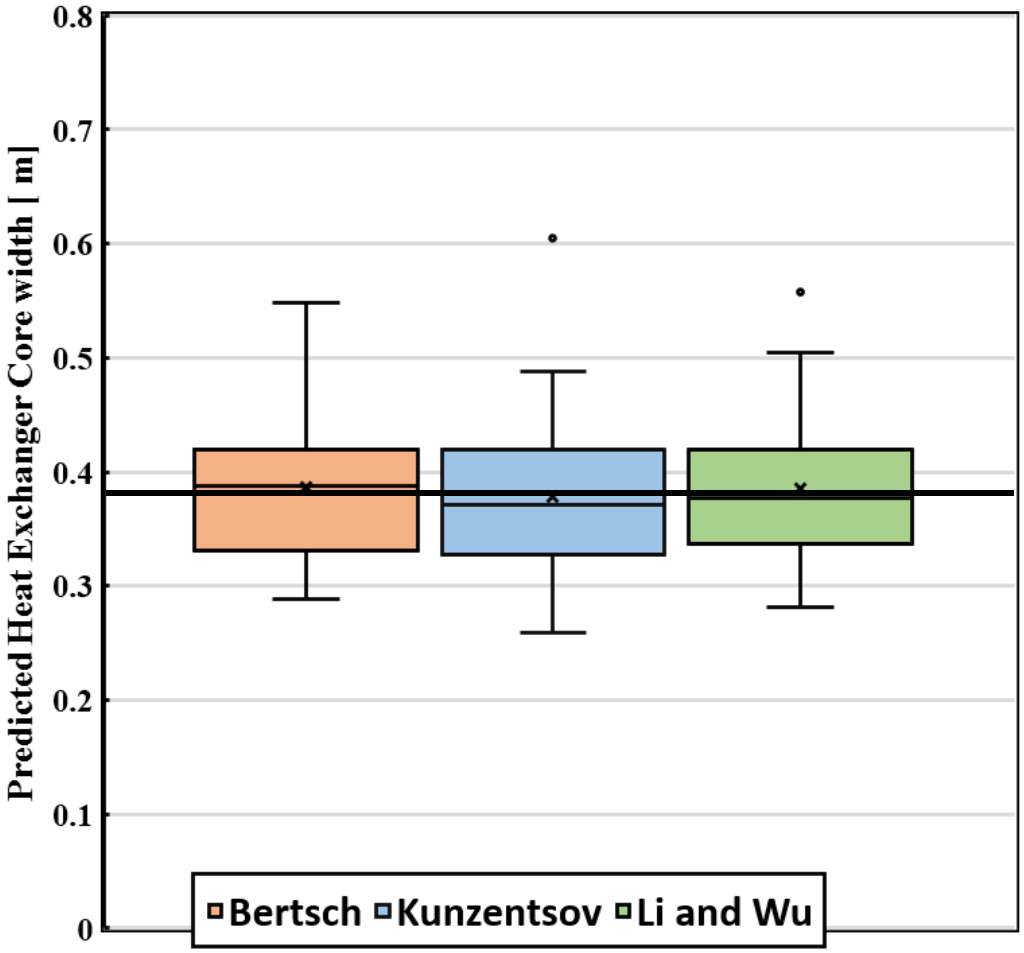

Figure 5-7. Bar plate exchanger core width for each boiling heat transfer correlation tested including correction factor. Black bar represents the actual core width at 0.38 m.

The resulting bar plate heat transfer model used the Hartnett and Kostic correlation to represent the water-glycol heat transfer and Garimella et al. correlation to represent the single phase heat transfer coefficient calculations. A corrected Kusentsov et al. correlation was used to represent the refrigerant two phase region. The following pressure drop validation used these heat transfer correlations.

The refrigerant pressure drop was calculated and compared to the total pressure loss across the bar plate evaporator. The predicted pressure loss was the sum of the calculated pressure losses of each control volume. This analysis was not performed until after heat transfer model was validated because the fluid travel length is a key factor in determining pressure loss. The three heat transfer correlations Kuznetsov et al. [49], Bertsch et al. [44] and Li and Wu [52], did not include pressure loss correlations. The pressure loss correlation from the Tran et al. [54] investigation was evaluated to calculate the boiling pressure drop through each two phase control volume of the bar plate design. In the single phase regions, the Churchill friction factor correlation [65] was used to determine pressure loss. Figure 5-8 depicts the measured refrigerant pressure drop against the model predicted pressure drop.

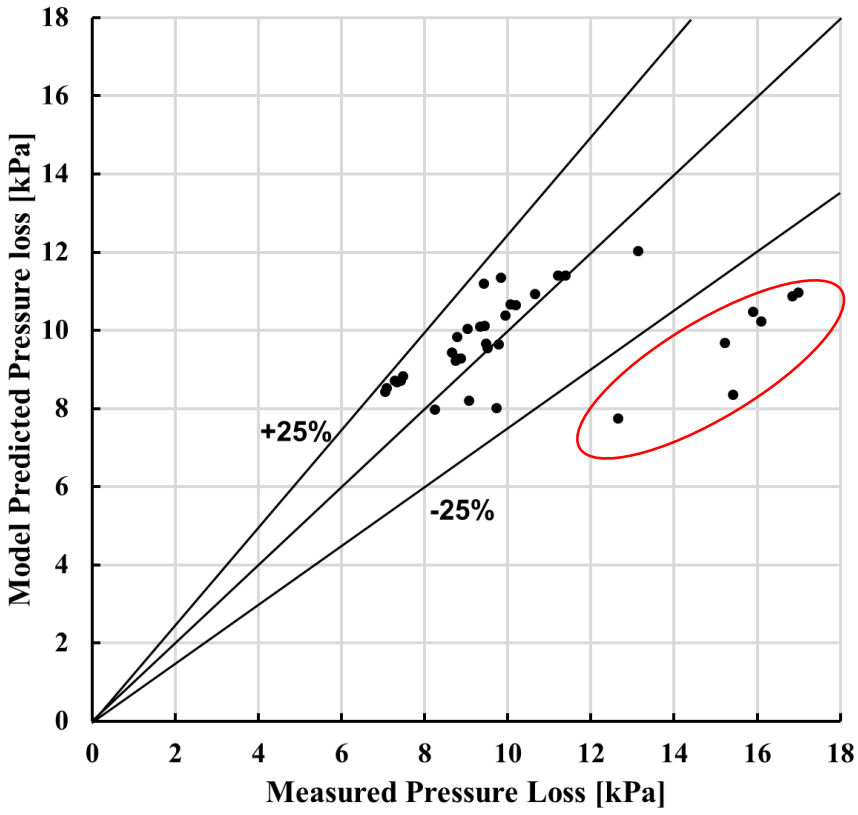

Figure 5-8. Measured refrigerant pressure loss versus predicted refrigerant pressure drop. The red circle indicates points that lie outside the 25% error bars.

The 0% and ±25% error bars are shown. 85.7% of the collected data lay within ±25% error and the MAE = 13.9%. At higher pressure losses, above 15 kPa, the model significantly under predicts the experiment. The seven measured data points collected at the high pressure loss do not have the same linear relationship to mass flow rate or heat flux as the rest of the data set does, seen in Figure 5-9 (a) and (b). It is not the case that the high measured data points are a result of increased fictional loss due to a large mass flux or caused by an increased acceleration loss due to a high heat flux evaporating the fluid earlier in the heat exchanger. This trend is not accounted for by the model. This investigation lies on the bounds of the valid parameter ranges for the Tran et al. correlation. The mass flux is close to the lower bound of the correlation, leading to a strong dependence on mass flux. However as a whole the correlation was able to predict a high percentage of the data within ±25% error, and therefore the correlations were accepted for the model.

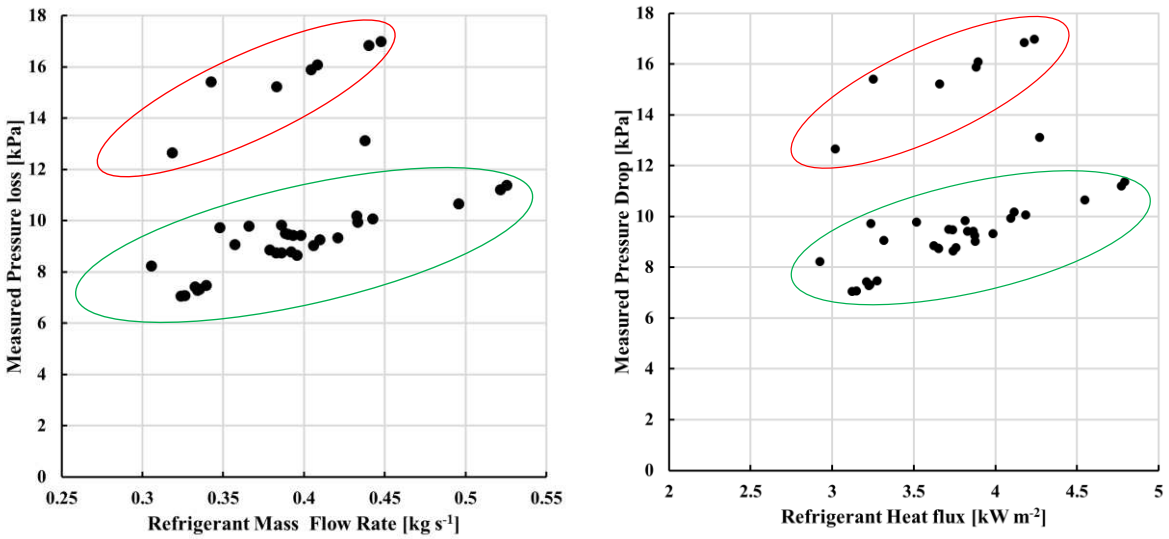

Figure 5-9. Bar plate heat exchanger pressure drop analysis. (a) Measured refrigerant mass flow rate versus measured refrigerant pressure drop. The green circle indicates the data exhibiting a linear relation and the red circle indicates data not exhibiting the linear relation. (b) Measured refrigerant pressure loss versus refrigerant heat flux.

The validated model utilized a combination of correlations to accurately predict performance. For the water-glycol heat transfer, the correlation selected was the Hartnett and

Kostic [83] laminar flow correlation in rectangular channel. The single phase region of the refrigerant was represented by the Garimella et al. correlation and for the boiling region, the Kuznetsov et al. [49] correlation was used to predict the heat transfer and calculate the required width of the core. Correction factors were added to the water-glycol and two phase refrigerant heat transfer coefficients to increase model accuracy. The refrigerant side pressure loss was modeled using the Tran et al. [54] boiling pressure loss correlation and Churchill [65] friction factor correlation for the single phase regions. The next step is to present the bar plate and plate frame heat exchanger results in the VCC.

5.2. Heat exchanger size optimization in VCC

It was theorized that an optimum pressure loss in the evaporator would lead to a minimum evaporator core volume. As mentioned in Chapter 2, Picon-Nunes [8] showed that increases in pressure drop through surface augmentations increased the heat transfer coefficient, reducing the required volume of a bar plate core. However the present study focuses on evaporators where the two phase refrigerant temperature is dependent on the pressure loss, opposed to the liquid to liquid heat exchangers in the Picon-Nunes study. This added relation is a key aspect in the optimization effort. The results of the modeling will be examined in the following sections for both plate frame and bar plate heat exchanger types.

5.2.1 Plate Frame Heat Exchanger Results

When the plate frame heat exchanger model was used to size a core for a fixed refrigerant outlet temperature over a range of low pressure drops, in both parallel and counter flow configurations, the core volume decreased with increasing pressure drop, as shown in Figure 5-10. This was caused by an increased mass flux as the number of channels was decreased to increase the pressure drop. The increased mass flux, lead to an increase in the heat transfer coefficient for

the water-glycol. Over the range of refrigerant mass fluxes used, the dominate mode of heat transfer on the refrigerant side was nucleate boiling, and therefore increase mass flux was negligible. As a competing effect, the entering temperature difference between the two fluids decreased as a function of increasing pressure drop. This required an increase in heat transfer area and the core volume. When the model was run over a range of higher pressure losses, this became more prevalent, shown in Figure 5-10.

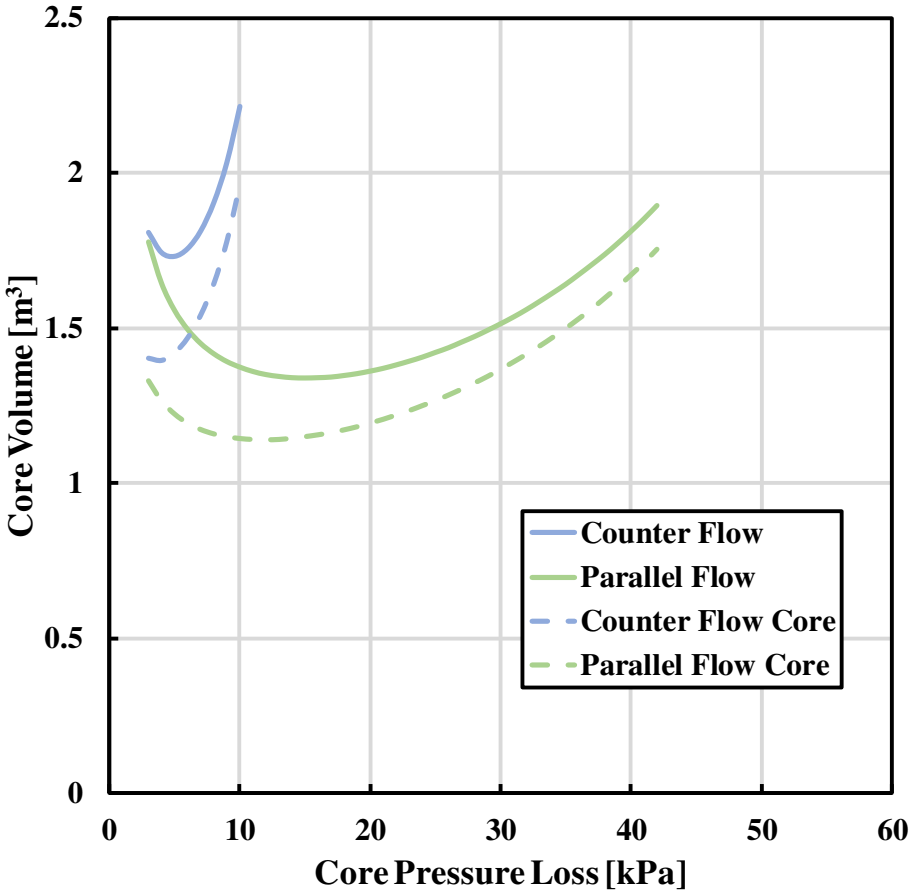

Figure 5-10. Demonstration of the relationship between volume and the pressure loss for the gasketed plate and frame heat exchanger. Both the core and manifold volume, as well core volume alone, are shown

At low pressure drops the effect of increasing heat transfer coefficient dominates over the effect of reduced thermal driving potential which led to an inverse relationship between volume and

pressure drop. At 5 kPa pressure drop in the counter flow configuration and 15 kPa pressure drop in the parallel flow configuration, the effect of the two trends were equally balanced, resulting in an inflection point. After this point the reduced thermal driving potential dominates, increasing volume with increasing pressure drop.

The plate frame heat exchanger model was optimized for both counter and parallel flow. The trends described above were observed in both cases. However, for the counter flow case, the volume was more sensitive to pressure drop via a change in number of plates. This was observed by the steeper slope seen in Figure 5-10. The counter flow arrangement was more sensitive, and had an overall optimum volume of 1.73 m^3, compared to the less sensitive 1.34 m^3 core volume for the parallel flow arrangement. The counter flow arrangement would be preferred for operation at or near a VCC design point with little fluctuation in operating conditions. However, the parallel flow core would be preferred for systems that perform over a range of conditions, because this configuration was less sensitive to pressure drop.

It is counter intuitive that the parallel flow configuration resulted in a smaller volume than the counter flow case when thinking about single phase heat exchangers. Figure 5-11 shows the temperature vs position for counter flow and parallel flow heat exchangers. Looking at the single phase graphs Figure 5-11 (a) and (b), the counter flow case has a larger temperature differential for the same inlet and out let temperatures. This is shown by the larger area between the temperature lines in the counter flow configuration. However in the evaporator case, the parallel flow configuration Figure 5-11 (d) had a temperature profile more similar to the counter flow profile for the single phase Figure 5-11 (a). Similarly, the temperature profile of the counter flow evaporator, Figure 5-11 (c), is more similar to the profile of the single phase parallel flow case, Figure 5-11 (b). The evaporator refrigerant temperature profiles are caused by the decrease in

saturation temperature of the refrigerant due to a large pressure loss through the core. Because of the saturation temperature decrease as the refrigerant evaporates, the parallel flow configuration will result in a smaller volume than the counter flow configuration.

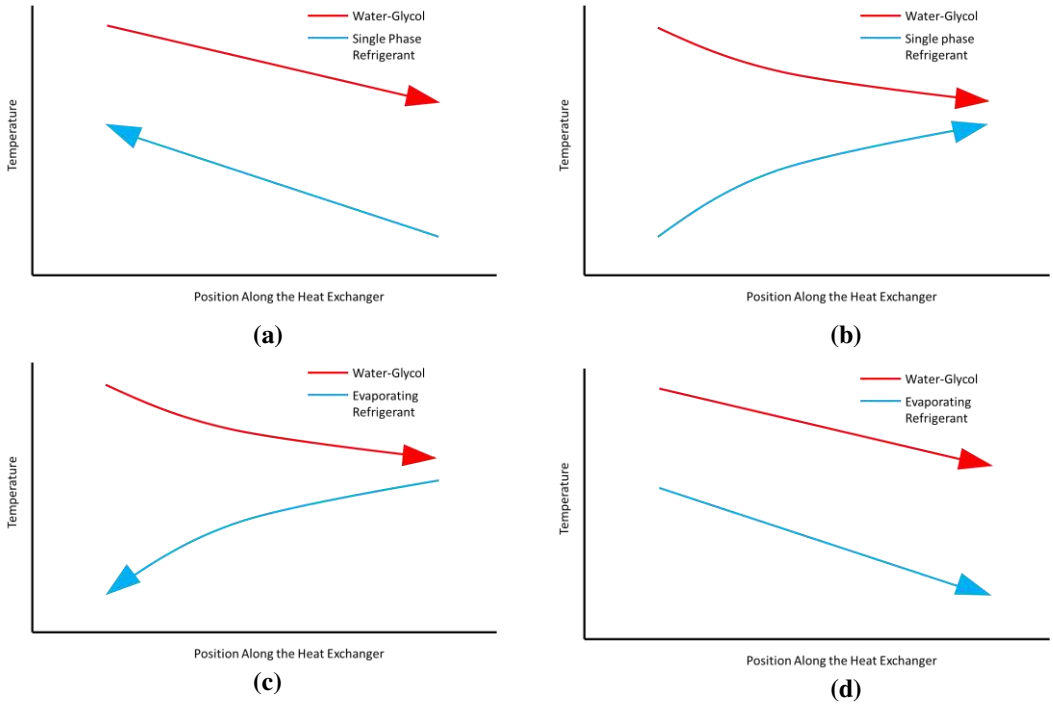

Figure 5-11. Temperature as a function of position in the core for (a) single phase counter flow heat exchanger, (b) single phase parallel flow heat exchanger, (c) counter flow evaporator, and (d) parallel flow evaporator.

The effects which caused the optimum trends were found to be independent of the refrigerant outlet temperature for the parallel flow configuration and predominantly independent for the counter flow configuration. Figure 5-12 shows the pressure vs volume relationship for the plate frame evaporator over a range of refrigerant outlet temperatures. The curves show the same optimum trend with the optimum points moving in the direction of smaller volume and larger pressure loss as the refrigerant outlet temperature reduces. For the parallel flow configuration, Figure 5-12 (a), all curves showed the trends. For the counter flow configuration, Figure 5-12 (b),

the 6 °C temperature line did not show an optimum because the temperature differential became so small than any change dominated over the change in heat transfer coefficient.

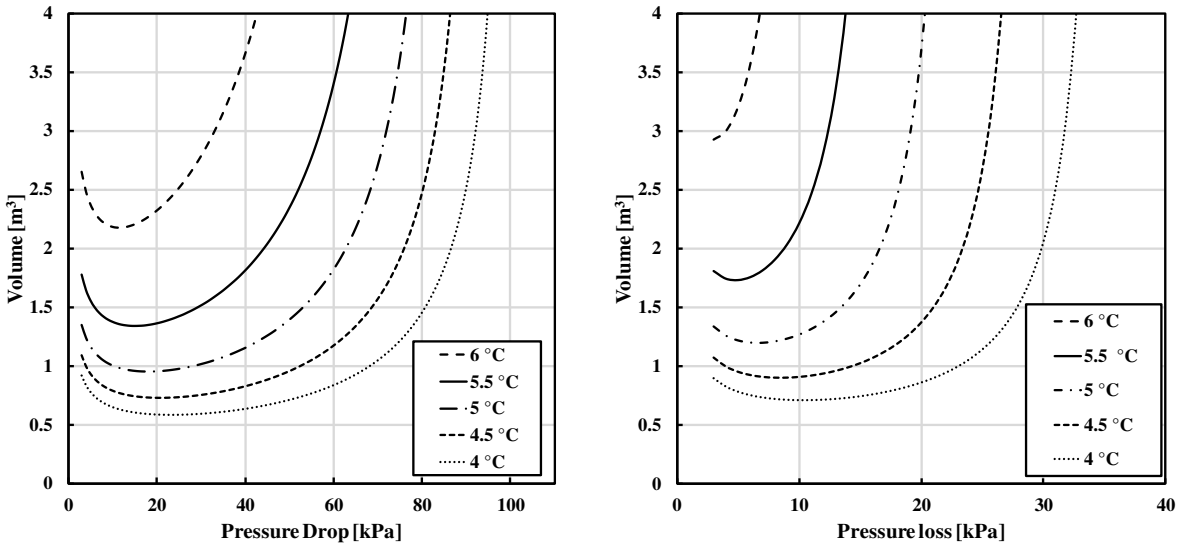

(a) **(b)**

Figure 5-12. Plate fame minimization sensitivity to refrigerant outlet temperature. (a) Parallel flow configuration (b) counter flow configuration.

It is important to note that through this optimization effort the heat exchanger model was not used far outside of the developed bounds, particularly mass flux. Figure 5-13 shows the volume of the plate frame heat exchanger as a function of mass flux, along with the associated bounds tested in the present investigation and bounds valid for the used two phase correlation.

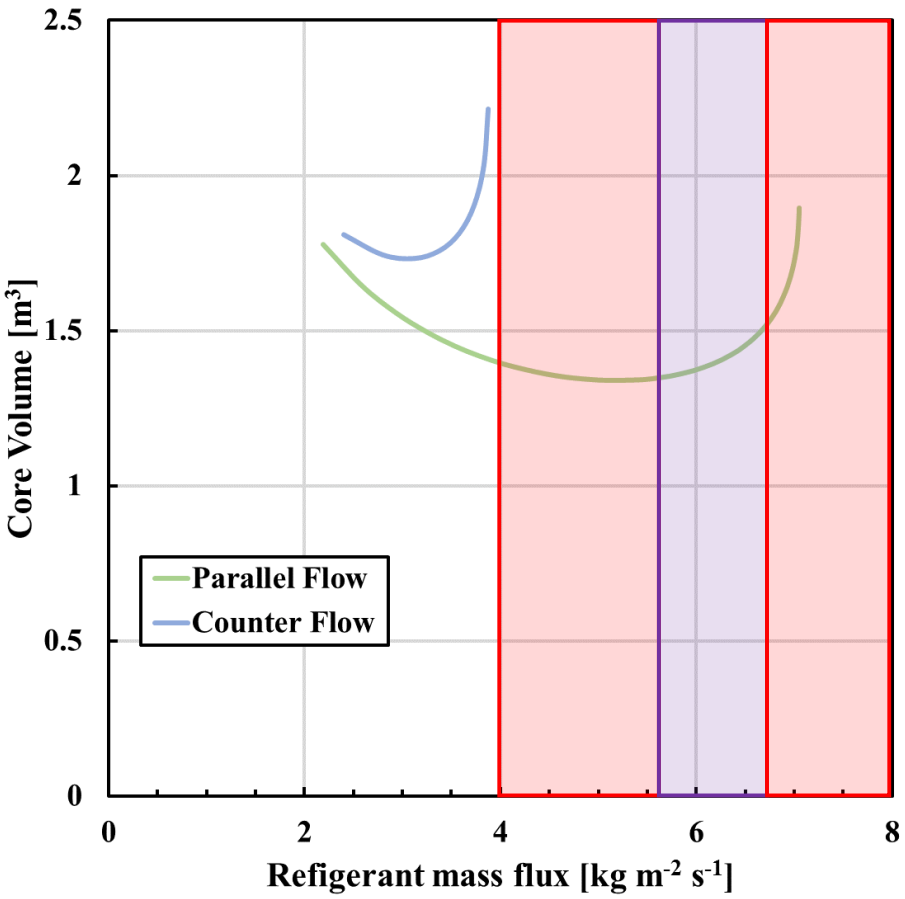

Figure 5-13. Volume of the plate frame heat exchanger as a function of refrigerant mass flux. The mass flux bounds tested in the present investigation are between the purple shading. The mass flux bounds for the heat transfer and pressure drop correlation used are between the red shading.

The bounds tested in the present investigation fail to cover much of the optimization range. However the Cooper [32] correlation, which covers everything between 4 kg m^{-2} s^{-1} and 50 kg m^{-2} s^{-1} within the presented results, does encompass the optimum value and the majority of the parallel flow configuration. Therefore the investigation is confident in the accuracy of the results for the parallel flow configuration. The counter flow configuration lies below the mass flux bounds of the correlation's developed range, and therefore the trend is extrapolated, losing some confidence in accuracy of the results.

It was also important to ensure that the uniform distribution assumption made in the modeling effort remained valid through the optimization effort. Large plate stacks are used to reduce the pressure drop through the evaporator, therefore at low pressure drop ranges, it is possible for the manifold pressure drop to dominate. However when looking at Figure 5-14 (a) and (b), the pressure drop through the manifolds remains to be a minimal portion of the total pressure drop for both configurations, affirming the uniform distribution assumption, even at the low pressure drop ranges.

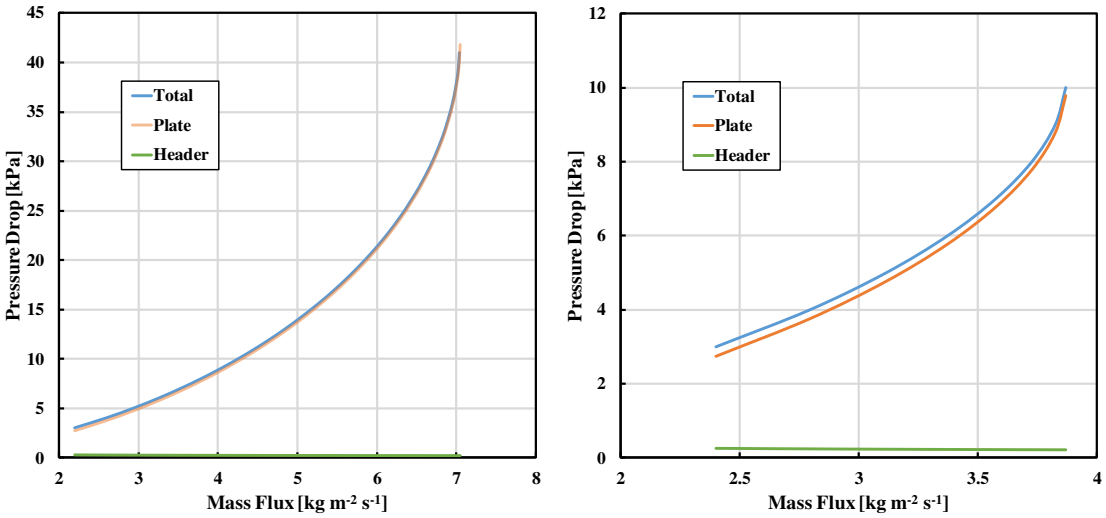

Figure 5-14. Pressure drop as a function of refrigerant mass flux for the plate frame heat exchanger. The total pressure loss is shown as well as the core and manifold contributions. (a) parallel flow heat exchanger, (b) counter flow heat exchanger.

5.2.2 Bar Plate Heat Exchanger Results

For the bar plate evaporator, the optimum relationship between pressure drop and volume was also observed as it was for the plate frame evaporator. In both arrangements, at low pressure drop ranges, as the pressure drop increased via channel number reduction, the core volume decreased. Then at larger pressure drop ranges, the volume increases with increasing pressure drop, all shown in Figure 5-15.

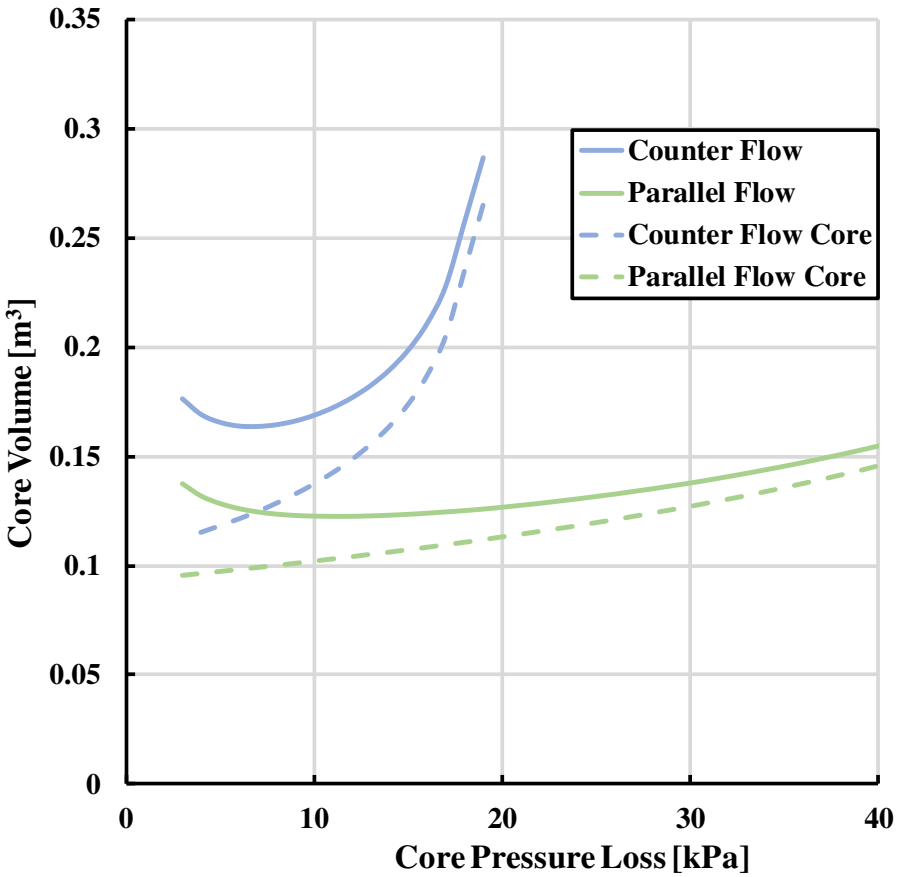

Figure 5-15. Demonstration of the relationship between volume and the pressure loss for the brazed bar plate heat exchanger. Both the core and manifold volume, as well core volume alone, are shown.

For the bar plate heat exchanger, there was another factor that contributed to the volume pressure drop relationship. The manifold size relative to the heat transfer core size was significant at smaller pressure drop ranges where the heat exchanger had many plates that were short. As channels were added to reduce the pressure drop, the manifolds became larger and the core shortened and reduced in volume. At lower pressure drop ranges, the change in manifold volume was greater than the change in core volume. At the minimum volume and greater pressure drop ranges, the core volume becomes significantly larger than the manifold volume, resulting in the change in manifold volume being less significant. Around the minimum this was the driving relationship for the bar plate evaporator, rather than the changing driving potential and heat transfer

coefficient. With the manifold volume removed, as the pressure drop increased via channel number reduction, the core volume always increased, Figure 5-15 shown with the dashed lines. This leads to the conclusion that the decrease in temperature driving potential always dominates over the increase in heat transfer coefficient, when the pressure loss is increased. At greater pressure drop ranges, the decreased temperature driving potential is the dominating factor, even when the manifold volume is included.

When comparing the parallel flow to counter flow cases at a refrigerant outlet temperature of 5.5°C, the minimum volume of the parallel flow arrangement, 0.123 m^3, was smaller than that of the counter flow arrangement, 0.164 m^3. In single phase flow, the counter flow heat exchanger will always have a smaller required heat transfer area due to a larger log mean temperature different compared to a parallel flow counterpart. However because of the saturated temperature decrease of the two phase refrigerant due to pressure drop, the parallel flow arrangement in this investigation will have a larger log mean temperature difference leading to a smaller required volume. In a similar manner as the plate frame heat exchanger, the parallel flow bar plate evaporator was less sensitive to an increase in pressure drop as shown by the flatter slope in Figure 5-15. Therefore, when considering which orientation should be used when designing an evaporator, the parallel flow case will likely be preferred to minimize volume. This is because the rate at which the volume increases with increasing pressure drop was less than that of the counter flow case for the same outlet refrigerant temperature.

The effects which caused the optimum trends were found to be independent of the refrigerant outlet temperature for the parallel flow and counter flow configurations. Figure 5-16 shows the pressure vs volume relationship for the bar plate evaporator over a range of refrigerant outlet temperatures. The curves show the same optimum trend with the optimum points moving in

the direction of smaller volume and larger pressure loss as the refrigerant outlet temperature reduces. For both flow configuration all curves showed the same trends.

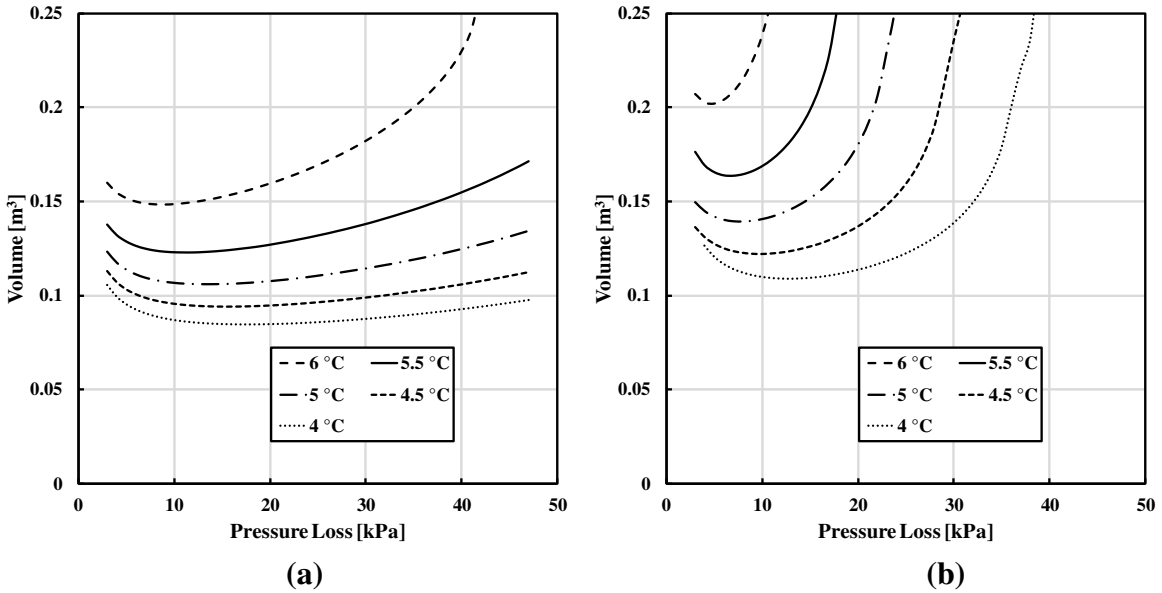

Figure 5-16. Bar plate minimization sensitivity to refrigerant outlet temperature. (a) Parallel flow configuration (b) counter flow configuration.

Like the plate frame heat exchanger, it was important to ensure that the optimization effort remained within the model developed bounds. The tested conditions for the present investigation, as well as the boiling heat transfer correlation used, covered a majority of the parallel flow trend, encompassing the minimum volume, see Figure 5-17.The counter flow trend was also mostly covered by both the experimentally tested and correlation tested bounds but the minimum value is near the lower end of both bounds.

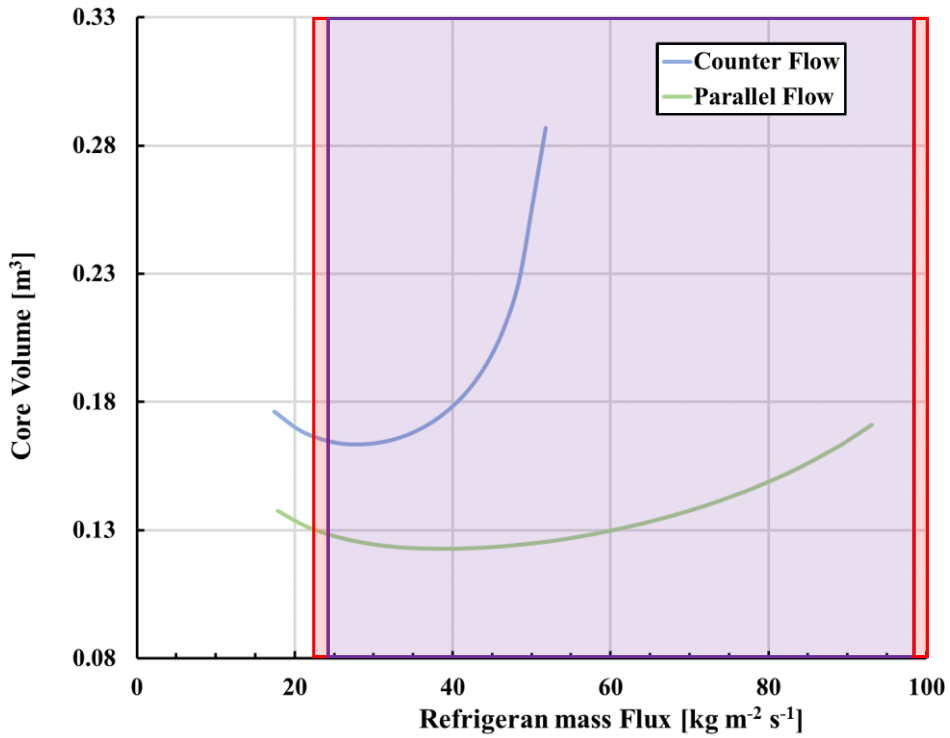

Figure 5-17. Volume of the bar plate heat exchanger as a function of refrigerant mass flux. The mass flux bounds tested in the present investigation are between the purple shading. The mass flux bounds for the heat transfer and pressure drop correlation used are between the red shading.

It was also important to ensure that the uniform distribution assumption made in the modeling effort remained valid through the optimization effort. Large plate stacks are used to reduce the pressure drop through the evaporator, therefore at low pressure drop ranges, it is possible for the manifold pressure drop to dominate. However when looking at Figure 5-18 (a) and (b), the pressure drop through the manifold remains to be a minimal portion of the total pressure drop for both configurations, affirming the uniform distribution assumption, even at the low pressure drop ranges.

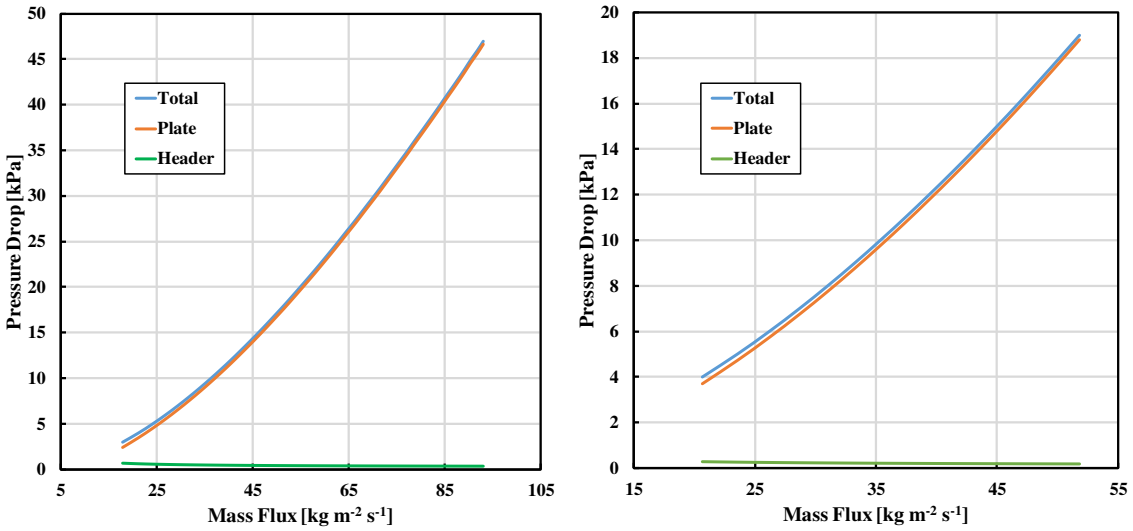

Figure 5-18. Pressure drop as a function of refrigerant mass flux for the bar plate heat exchanger. The total pressure loss is shown as well as the core and manifold contributions. (a) parallel flow heat exchanger, (b) counter flow heat exchanger.

This chapter presents the results for the correlations tested in the plate frame and bar plate models against experimentally collected data, and the results of the evaporator volume minimization effort for a standard vapor compression cycle. It was found that for the plate frame model the combination of Cooper [32] boiling heat transfer, Maslov and Kovalenko [35] refrigerant single phase heat transfer, and Muley [39] water-glycol heat transfer correlations, resulted in the most accurate model. For the bar plate model the combination of Kuznetsov et al. [49] boiling heat transfer, Tran et al. [54] boiling pressure loss, and Garimella [57] single phase refrigerant heat transfer and pressure drop, as well as Hartnett and Kostic [83] water-glycol heat transfer correlations, resulted in the lowest model error. When the models where used to size the evaporator in the standard vapor compression cycle, both the plate frame and bar plate heat exchangers had an optimum value. In both heat exchangers the parallel flow configuration resulted in a lower volume than the counter flow configuration and the bar plate always resulted in a smaller volume than the plate frame heat exchanger.

Chapter 6. Conclusions

The present investigation utilized two heat exchanger sizing models to determine the minimum volume required for a vapor compression evaporator. The models were developed to size the cores for an aluminum brazed bar plate evaporator and a gasketed plate and frame evaporator. A simple vapor compression cycle was modeled to determine the boundary conditions of the evaporator. All cycle state points remained constant except the evaporator inlet to allow for a constant compressor and condenser design.

The first step to completing the objective of the present study was to develop a validated heat exchanger model for a plate frame evaporator. An evaporator in a turbo-compression cooling system test facility with R134a working fluid and water-glycol coolant was used to collect data for model validation. The model used empirical correlations found in the literature to determine the required length of the heat exchanger core and the refrigerant side pressure drop. Wilson plot experiments were conducted to determine the water-glycol side heat transfer coefficients and the Muley [39] correlation was most accurate when compared to the other correlations tested, with a 22.8% MAE. Several boiling and single phase heat transfer correlations were tested in a matrix for the refrigerant side heat transfer, resulting with the most accurate combination being the Cooper [32] boiling heat transfer, Maslov and Kovalenko [35] single phase correlation. The final heat exchanger model predicted the heat exchanger length to a MAE of 7.9%. The model used the Huang et al. [19] correlation to determine the refrigerant side pressure drop, but was not validated due to high uncertainties in the pressure drop measurement.

The next step was to develop and validate a bar plate heat exchanger model. Wilson plot experiments were performed to determine an accurate water-glycol side heat transfer correlation.

However, the uncertainty of experiments were too large for accurate comparisons. Therefore the water-glycol heat transfer coefficient was assumed using the Hartnett and Kostic [83] correlation. The correlation was selected because of its development for similar geometric parameters and fluid properties. The Kuznetsov et. al. [49] correlation was used to predict the two-phase boiling heat transfer, while the Garimella et al. [57] correlation was used to predict the single phase refrigerant heat transfer. The model was then used to predict the heat exchanger width for a fixed heat transfer rate. The model consistently under predicted the width by 34%, implying that the model was over predicting the heat transfer coefficient. To bring the average predicted width equal to the actual heat exchanger width, a correction factor was applied to the refrigerant side heat transfer coefficient. The correction factor was 0.61 and the resulting MAE was 14.2% with 92% of the data within ±25% error. The refrigerant side pressure loss was modeled using the Tran et. al. [54] boiling pressure loss correlation. The model predicted pressure drop for the pressure side to a MAE of 14.0% with 85.7% of the data within ±25% error.

The bar plate evaporator resulted in a smaller optimum volume than the plate frame heat exchanger, 0.123 m^3 compared to 1.34 m^3, respectively. This was expected due to the higher surface area to volume ratio of the bar plate evaporator compared to the plate frame. The minimum volume occurred in the parallel flow arrangement for both the bar plate and plate frame designs, a counter intuitive result as compared to single phase flow experience. In single phase flow, the counter flow heat exchanger will always have a smaller required heat transfer area due to a larger log mean temperature different compared to a parallel flow counterpart. However because of the temperature decrease of the two phase refrigerant due to pressure drop, the parallel flow arrangement in this investigation will have a larger log mean temperature difference leading to a smaller required volume. For both heat exchangers the parallel flow arrangement was less sensitive

to pressure drop increases through the core, which could be important during off design operation. For systems that endure a varying heat load or operating conditions, the pressure loss through the evaporator may vary as well. In the counter flow arrangement of the evaporator, a slight deviation from the optimal pressure loss will result in a large change in required volume, and because these are fixed volume devices, the evaporator will not be able to transfer the required heat. In the parallel flow case this effect would be much smaller and will result in lower degradation.

Additional future work will consist of model validation with larger experimentation data sets. The current data set is small and future experiments may be required to reduce model error, incorporate a dimensionless parameter rather than the correction factor, or to test new correlations for single and boiling flow in the both heat exchangers. Future experiments should be conducted with a differential pressure transducer across the inlet and outlet of the refrigerant side of the plate frame heat exchanger, and a more reliable flow measurement device should be used on the water-glycol side of both heat exchangers. These changes would reduce the uncertainty in the refrigerant pressure drop and water-glycol mass flow rate calculations, leading to the ability to validate the plate frame pressure drop model and bar plate water-glycol heat transfer.

The present work can be used in future investigations or design situations to quickly determine the required size of evaporators. Both the plate frame and bar plate models allow for easy operation and parametric study, so investigations into performance and space tradeoffs of advanced chiller systems can be performed easily.

References

[1] Ding, G. liang, 2007, "Recent Developments in Simulation Techniques for Vapour-Compression Refrigeration Systems," Int. J. Refrig.

[2] O'grady, E., and Narsiour, S., 2018, "Cooling Is Warming the Planet, but Market Failures Are Preventing the AC Industry from Innovating," Glob. Cool. Prize.

[3] Borgnakke, C., and Sonntag, R. E., 2009, *Fundamentals of Thermodynamics, 7-Th Edition*.

[4] Shah, R. K., and Sekulić, D. P., 2003, *Fundamentals of Heat Exchanger Design*.

[5] Shah, R. K., 1994, "Heat Exchangers," *Encyclopedia of Energy Technology and the Eviroment*, A. Bisco, and S.G. Boots, eds., John Wiley & Sons, New York, pp. 1651–1670.

[6] Bansal, P. K., and Chin, T. C., 2003, "Modelling and Optimisation of Wire-and-Tube Condenser," Int. J. Refrig.

[7] Jokar, A., Hosni, M. H., and Eckels, S. J., 2006, "Dimensional Analysis on the Evaporation and Condensation of Refrigerant R-134a in Minichannel Plate Heat Exchangers," Appl. Therm. Eng.

[8] Picon-Nuñez, M., Polley, G. T., Torres-Reyes, E., and Gallegos-Muñoz, A., 1999, "Surface Selection and Design of Plate-Fin Heat Exchangers," Appl. Therm. Eng.

[9] Corberán, J. M., and Melón, M. G., 1998, "Modelling of Plate Finned Tube Evaporators and Condensers Working with R134A," Int. J. Refrig.

[10] Gray, D. L., and Webb, R. L., 1986, "{H}eat Transfer and Friction Correlations for Plate Finned-Tube Heat Exchangers Having Plain Fins," *Proceedings of the International Heat Transfer Conference*.

[11] Dittus, F. W., and Boelter, L. M. K., 1985, "Heat Transfer in Automobile Radiators of the Tubular Type," Int. Commun. Heat Mass Transf., **12**(1), pp. 3–22.

[12] Schlunder, E. U., 1990, *Heat Transfer Atlas: Calculation of Heat Transfer*, Woodhead Publishing, Germany.

[13] Martinelli, R. C., and Nelson, D. B., 1948, "Prediction of Pressure Drop during Forced-Circulation Boiling of Water," *Transactopns of the ASME*, pp. 695–702.

[14] Qiao, H., Aute, V., Lee, H., Saleh, K., and Radermacher, R., 2013, "A New Model for Plate Heat Exchangers with Generalized Flow Configurations and Phase Change," *International Journal of Refrigeration*.

[15] Yan, Y.-Y., and Lin, T.-F., 1999, “Evaporation Heat Transfer and Pressure Drop of Refrigerant R-134a in a Plate Heat Exchanger,” J. Heat Transfer.

[16] Hsieh, Y. Y., and Lin, T. F., 2002, “Saturated Flow Boiling Heat Transfer and Pressure Drop of Refrigerant R-410A in a Vertical Plate Heat Exchanger,” Int. J. Heat Mass Transf., **45**(5), pp. 1033–1044.

[17] Ayub, Z. H., 2003, “Plate Heat Exchanger Literature Survey and New Heat Transfer and Pressure Drop Correlations for Refrigerant Evaporators,” Heat Transf. Eng.

[18] Han, D. H., Lee, K. J., and Kim, Y. H., 2003, “Experiments on the Characteristics of Evaporation of R410A in Brazed Plate Heat Exchangers with Different Geometric Configurations,” Appl. Therm. Eng.

[19] Huang, J., Sheer, T. J., and Bailey-Mcewan, M., 2012, “Heat Transfer and Pressure Drop in Plate Heat Exchanger Refrigerant Evaporators,” *International Journal of Refrigeration*.

[20] Glazar, V., Frankovic, B., and Trp, A., 2015, “Experimental and Numerical Study of the Compact Heat Exchanger with Different Microchannel Shapes,” Int. J. Refrig.

[21] Gut, J. A. W., and Pinto, J. M., 2003, “Modeling of Plate Heat Exchangers with Generalized Configurations,” Int. J. Heat Mass Transf.

[22] R.K. Shah, E.C. Subbarao, R.A. MashelkarR.K. Shah, W. W. F., 1988, “Plate Heat Exchangers and Their Design Theory,” Heat Transf. Equip. Des. Hemisphere, New York.

[23] Saunders, E. A. D., 1988, *Heat Ecahngers: Selection, Design and Construction*, New York.

[24] Mehrabian, M. A., Poulter, R., and Quarini, G. L., 2000, “Hydrodynamic and Thermal Characteristics of Corrugated Channels: Experimental Approach,” Exp. Heat Transf.

[25] Lee, D. C., Kim, D., Park, S., Lim, J., and Kim, Y., 2018, “Evaporation Heat Transfer Coefficient and Pressure Drop of R-1233zd(E) in a Brazed Plate Heat Exchanger,” Appl. Therm. Eng.

[26] Hsieh, Y. Y., Chiang, L. J., and Lin, T. F., 2002, “Subcooled Flow Boiling Heat Transfer of R-134a and the Associated Bubble Characteristics in a Vertical Plate Heat Exchanger,” Int. J. Heat Mass Transf.

[27] Longo, G. A., and Gasparella, A., 2007, “Refrigerant R134a Vaporisation Heat Transfer and Pressure Drop inside a Small Brazed Plate Heat Exchanger,” Int. J. Refrig.

[28] Huang, H., and Thome, J. R., 2016, “Local Measurements and a New Flow Pattern Based Model for Subcooled and Saturated Flow Boiling Heat Transfer in Multi-Microchannel Evaporators,” Int. J. Heat Mass Transf.

[29] Amalfi, R. L., Vakili-Farahani, F., and Thome, J. R., 2016, “Flow Boiling and Frictional Pressure Gradients in Plate Heat Exchangers. Part 2: Comparison of Literature Methods to Database and New Prediction Methods,” Int. J. Refrig.

[30] Focke, W. W., Zachariades, J., and Olivier, I., 1985, "The Effect of the Corrugation Inclination Angle on the Thermohydraulic Performance of Plate Heat Exchangers," Int. J. Heat Mass Transf.

[31] Longo, G. A., and Gasparella, A., 2007, "Heat Transfer and Pressure Drop during HFC Refrigerant Vaporisation inside a Brazed Plate Heat Exchanger," Int. J. Heat Mass Transf.

[32] Cooper, M. G., 1984, "Heat Flow Rates in Saturated Nucleate Pool Boiling-A Wide-Ranging Examination Using Reduced Properties," Adv. Heat Transf.

[33] Gorenflo, D., Chandra, U., Kotthoff, S., and Luke, A., 2004, "Influence of Thermophysical Properties on Pool Boiling Heat Transfer of Refrigerants," Int. J. Refrig.

[34] Rosenblad, G., and Kullendorff, A., 1975, "Estimating Heat Transfer Rates from Mass Transfer Studies on Plate Heat Exchanger Surfaces," Wärme- und Stoffübertragung.

[35] Maslov, A., and Kovalenko, L., 1972, "Hydraulic Resistance and Heat Transfer in Plate Heat Exchangers," Molochnaya Promyshlenflost, **10**, pp. 20–22.

[36] Khan, T. S., Khan, M. S., Chyu, M. C., and Ayub, Z. H., 2010, "Experimental Investigation of Single Phase Convective Heat Transfer Coefficient in a Corrugated Plate Heat Exchanger for Multiple Plate Configurations," Appl. Therm. Eng.

[37] Pradhan, R. L., Ravikumar, D., and Pradhan, D. L., 2008, "Review of Nusselt Number Correlation for Single Phase Fluid Flow through a Plate Heat Exchanger to Develop C # Code Application Software," IOSR J. Mech. Civ. Eng.

[38] Muley, A., and Manglik, R. M., 1999, "Experimental Study of Turbulent Flow Heat Transfer and Pressure Drop in a Plate Heat Exchanger With Chevron Plates," J. Heat Transfer.

[39] Muley, A., 1997, "Heat Transfer and Pressure Drop in Plate Heat Exchangers," University of Cincinnati.

[40] Garcia-Cascales, J. R., Vera-Garcia, F., Corberan-Salvador, J. M., and Gonzalvez-Macia, J., 2007, "Assessment of Boiling and Condensation Heat Transfer Correlations in the Modelling of Plate Heat Exchangers," Int. J. Refrig. Int. Du Froid, **30**(6), pp. 1029–1041.

[41] Chisholm, D., and Wanniarachchi, A. S., 1990, "Plate Heat Exchangers: Plate Selection and Arrangement," *AIChE*, Orlando.

[42] Kim, Y. S., 1999, "An Experimental Study on Evaporation Heat Transfer Characteristics and Pressure Drop in Plate Heat Exchanger," Yonsei University.

[43] Bogaert, R., and Böles, A., 1995, "Global Performance of a Prototype Brazed Plate Heat Exchanger in a Large Reynolds Number Range," Exp. Heat Transf.

[44] Bertsch, S. S., Groll, E. A., and Garimella, S. V., 2009, "A Composite Heat Transfer Correlation for Saturated Flow Boiling in Small Channels," Int. J. Heat Mass Transf., **52**(7–8), pp. 2110–2118.

[45] Fernando, P., Palm, B., Ameel, T., Lundqvist, P., and Granryd, E., 2008, "A Minichannel Aluminium Tube Heat Exchanger - Part I: Evaluation of Single-Phase Heat Transfer Coefficients by the Wilson Plot Method," Int. J. Refrig.

[46] Thome, J. R., Dupont, V., and Jacobi, A. M., 2004, "Heat Transfer Model for Evaporation in Microchannels. Part I: Presentation of the Model," Int. J. Heat Mass Transf.

[47] Chen, J. C., 1966, "Correlation for Boiling Heat Transfer to Saturated Fluids in Convective Flow," Ind. Eng. Chem. Process Des. Dev.

[48] Hausen, H., 1943, "NDurch, Darstellung Des Wärmeüberganges in Rohren Potenzbeziehungen, Verallgemeinerteo Title," Z. VDI Beih. Verfahrenstechnik 4, pp. 91–102.

[49] Kuzentsov, V., Shamirzaev, A., Kozulin, I., and Kozlov, S., 2013, "Correlation of the Flow Pattern and Flow Boiling Heat Transfer in Microchannels," Heat Transf. Eng., **34**, pp. 235–245.

[50] Danilova, G. N., 1970, "Correlation of Boiling Heat Transfer Data for Freons," Heat Transf. Res., **2**(2), pp. 73–78.

[51] Kays, W. M., and Crawford, M. E., 1993, *Convection Heat and Mass Transfer*, McGraw-Hill, New York.

[52] Li, W., and Wu, Z., 2010, "A General Correlation for Evaporative Heat Transfer in Micro/Mini-Channels," Int. J. Heat Mass Transf.

[53] Warrier, G. R., Dhir, V. K., and Momoda, L. A., 2002, "Heat Transfer and Pressure Drop in Narrow Rectangular Channels," Exp. Therm. Fluid Sci., **26**(1), pp. 53–64.

[54] Tran, T. N., Chyu, M. C., Wambsganss, M. W., and France, D. M., 2000, "Two-Phase Pressure Drop of Refrigerants during Flow Boiling in Small Channels: An Experimental Investigation and Correlation Development," Int. J. Multiph. Flow, **26**(11), pp. 1739–1754.

[55] Wambsganss, M. W., France, D. M., Jendrzejczyk, J. A., and Tran, T. N., 2008, "Boiling Heat Transfer in a Horizontal Small-Diameter Tube," J. Heat Transfer.

[56] Chisholm, D., 1985, "Two-Phase Flow in Heat Exchangers and Pipelines," Heat Transf. Eng.

[57] Garimella, S., Dowling, W. J., Van Der Veen, M., and Killion, J. D., 2001, "The Effect of Simultaneously Developing Flow on Heat Transfer in Rectangular Tubes," Heat Transf. Eng.

[58] Sahar, A. M., Wissink, J., Mahmoud, M. M., Karayiannis, T. G., and Ashrul Ishak, M. S., 2017, "Effect of Hydraulic Diameter and Aspect Ratio on Single Phase Flow and Heat Transfer in a Rectangular Microchannel," Appl. Therm. Eng.

[59] Shah, R. K., and London, A. L., 1978, "Laminar Flow Forced Convection in Ducts: A

Source Book for Compact Heat Exchanger Analytical Data," Acad. Press.

[60] Bejan, A., 2004, *Convection Heat Transfer*, John Wiley & Sons, New Jersey.

[61] Peng, X. F., and Peterson, G. P., 1995, "Convective Heat Trnasfer and Flow Friction for Water Flow in Mirochannel Structures," Int. J. Heat Mass Transf., **39**(12), pp. 2599–2608.

[62] Choi, S. B., Barron, R. S., and Warrington, R. O., 1991, "Fluid Flow and Heat Trnasfer in Microtubes," micromechanical Sensors, Actuators, Syst., **32**, pp. 123–134.

[63] Tate, E. N. S. G. ., 1936, "Heat Transfer and Pressure Drop of Liquids in Tube," Ind. Eng. Chem.

[64] Gnielinski, V., 1989, "HEAT-TRANSFER ON LAMINAR-FLOW IN TUBES AND CONSTANT WALL TEMPERATURE," Chemie Ing. Tech., **61**(2), pp. 160–161.

[65] Churchill, S. W., 1977, "Comprehensive Correlating Equations for Heat, Mass and Momentum Transfer in Fully Developed Flow in Smooth Tubes," Ind. Eng. Chem. Fundam., **16**(1), pp. 109–116.

[66] Selbas, R., Kizilkan, O., and Sencan, A., 2006, "Thermeconomic Optimization of Subcooled and Superheated Vapor Compression Refigeration Cycle," Energy, **31**, pp. 2108–2128.

[67] Yee, R. P., and Hermes, C. J. L., 2019, "Thermodynamic Design of a Mesoscale Vapor Compression Cooling Device," Appl. Therm. Eng.

[68] Pak, T. C., and Ri, Y. C., 2019, "Optimum Designing of the Vapor Compression Heat Pump Using System Using Genetic Algorithm," Appl. Therm. Eng.

[69] Chen, L., Sun, F., and Wu, C., 2004, "Optimal Allocation of Heat-Exchanger Area for Refrigeration and Air-Conditioning Plants," Appl. Energy.

[70] Shiba, T., and Bejan, A., 2001, "Thermodynamic Optimization of Geometric Structure in the Counterflow Heat Exchanger for an Environmental Control System," Energy.

[71] Zhou, R., Catano, J., Zhang, T., Wen, J. T., Michna, G., Peles, Y., and Jensen, M. K., 2009, "The Steady-State Modeling and Static System Design of a Refrigeration System for High Heat Flux Removal," *ASME International Mechanical Engineering Congress and Exposition, Proceedings*.

[72] Kuo, W. S., Lie, Y. M., Hsieh, Y. Y., and Lin, T. F., 2005, "Condensation Heat Transfer and Pressure Drop of Refrigerant R-410A Flow in a Vertical Plate Heat Exchanger," Int. J. Heat Mass Transf., **48**(25–26), pp. 5205–5220.

[73] Wang, C. C., Chang, Y. J., Hsieh, Y. C., and Lin, Y. T., 1996, "Sensible Heat and Friction Characteristics of Plate Fin-and-Tube Heat Exchangers Having Plane Fins," Int. J. Refrig. Int. Du Froid, **19**(4), pp. 223–230.

[74] Sterner, D., and Sunden, B., 2006, "Performance of Plate Heat Exchangers for Evaporation of Ammonia," *Heat Transfer Engineering*.

[75] Ahmadi, P., Hajabdollahi, H., and Dincer, I., 2011, "Cost and Entropy Generation Minimization of a Cross-Flow Plate Fin Heat Exchanger Using Multi-Objective Genetic Algorithm," J. Heat Transf. Asme, **133**(2), p. 10.

[76] Klein, S. A., and Alvarado, F., 2002, "Engineering Equation Solver," F-Chart Softw.

[77] Kim, D., Lee, D. C., Jang, D. S., Jeon, Y., and Kim, Y., 2018, "Comparative Evaluation of Flow Boiling Heat Transfer Characteristics of R-1234ze(E) and R-134a in Plate Heat Exchangers with Different Chevron Angles," Appl. Therm. Eng., **132**, pp. 719–729.

[78] Talik, A. C., Fletcher, L. S., Anand, N. K., and Swanson, L. W., 1995, "Heat Transfer and Pressure Drop Characteristics of a Plate Heat Exchanger Using a Propylene Glycol–water Mixture as the Working Fluid," *Proceedings of HTD-ASME National Heat Transfer Conference*.

[79] Thonon, B., Vidil, R., and Marvillet, C., 1995, "Recent Research and Developments in Plate Heat Exchangers," J. Enhanc. Heat Transf., **2**(1–2), pp. 149–155.

[80] Emerson, W. H., 1995, "The Thermal and Hydrodynamic Performance of a Plateheat Exchanger: II A DeLaval Exchanger," Natl. Eng. Lab.

[81] Kumar, S., Heister, S. D., Xu, X. F., Salvador, J. R., and Meisner, G. P., 2013, "Thermoelectric Generators for Automotive Waste Heat Recovery Systems Part I: Numerical Modeling and Baseline Model Analysis," J. Electron. Mater., **42**(4), pp. 665–674.

[82] Incropera, F. P., DeWitt, D. P., Bergman, T. L., and Lavine, A. S., 2007, *Fundamentals of Heat and Mass Transfer*.

[83] Hartnett, J. P., and Kostic, M., 1989, "Heat Transfer to Newtonian and Non-Newtonian Fluids in Rectangular Ducts," Adv. Heat Transf.

[84] Schiffman, J., and Favrat, D., 2009, "Experimental Investigation of a Direct Driven Radial Compressor for Domestic Heat Pumps," Int. J. Refrig., **32**, pp. 1918–1928.

[85] 2016, "Series R® RTWD Helical Rotary Chiller," TraneIngersollrand.

[86] Garland, S. D., Noal, J., and Bandhauer, T. M., 2018, "Experimentally Validated Modeling of a Turbo-Compression Cooling System for Power Plant Waste Heat Recovery," Energy, **156**, pp. 32–44.

[87] Wilson, 1915, "A Basis of Rational Design of Heat Transfer Apparatus," J. Am. Soc. Mech. Eng., **37**(1), pp. 47–70.

[88] Fernandez-Seara, J., Diz, R., and Uhia, F. J., 2013, "Pressure Drop and Heat Transfer Characteristics of a Titanium Brazed Plate-Fin Heat Exchanger with Offset Strip Fins," Appl. Therm. Eng., **51**(1–2), pp. 502–511.

[89] Yanik, M. K., and Webb, R. L., 2004, "Prediction of Two-Phase Heat Transfer in a 4-Pass Evaporator Bundle Using Single Tube Experimental Data," Appl. Therm. Eng.

[90] Huang, H., and Thome, J. R., 2017, "An Experimental Study on Flow Boiling Pressure Drop in Multi-Microchannel Evaporators with Different Refrigerants," Exp. Therm. Fluid Sci., **80**.

[91] Hessami, M. A., 1998, "Laminar to Turbulent Flow Transition in Cross-Corrugated-Plate Cavities," *Proceedings of the 1998 Thirteenth Australasian Fluid Mechanics Conference, Melbourne, Australia, 13-18 December 1998 (Volume 2)*.

[92] Agostini, B., Thome, J. R., Fabbri, M., Michel, B., Calmi, D., and Kloter, U., 2008, "High Heat Flux Flow Boiling in Silicon Multi-Microchannels - Part I: Heat Transfer Characteristics of Refrigerant R236fa," Int. J. Heat Mass Transf.

[93] Agostini, B., Thome, J. R., Fabbri, M., Michel, B., Calmi, D., and Kloter, U., 2008, "High Heat Flux Flow Boiling in Silicon Multi-Microchannels – Part II: Heat Transfer Characteristics of Refrigerant R245fa," Int. J. Heat Mass Transf., **51**, pp. 5415–5425.

[94] Bertsch, S. S., Groll, E. A., and Garimella, S. V., 2008, "Refrigerant Flow Boiling Heat Transfer in Parallel Microchannels as a Function of Local Vapor Quality," Int. J. Heat Mass Transf.

[95] Hamdar, M., Zoughaib, A., and Clodic, D., 2010, "Flow Boiling Heat Transfer and Pressure Drop of Pure HFC-152a in a Horizontal Mini-Channel," Int. J. Refrig. Int. Du Froid, **33**(3), pp. 566–577.

[96] Kandlikar, S. G., 1990, "A General Correlation for Saturated Two-Phase Flow Boiling Heat Transfer Inside Horizontal and Vertical Tubes," J. Heat Transfer.

[97] Lazarek, G. M., and Black, S. H., 1982, "Evaporative Heat Transfer, Pressure Drop and Critical Heat Flux in a Small Vertical Tube with R-113," Int. J. Heat Mass Transf.

[98] Lee, H. J., and Lee, S. Y., 2001, "Heat Transfer Correlation for Boiling Flows in Small Rectangular Horizontal Channels with Low Aspect Ratios," Int. J. Multiph. Flow, **27**(12), pp. 2043–2062.

[99] Liu, Z., and Winterton, R. H. S., 1991, "A General Correlation for Saturated and Subcooled Flow Boiling in Tubes and Annuli, Based on a Nucleate Pool Boiling Equation," Int. J. Heat Mass Transf.

[100] Robertson, J. M., and Lovegrove, P. C., 1983, "Boiling Heat Transfer with Freon 11 (R11) in Brazed Aluminum, Plate-Fin Heat Exchangers," J. Heat Transfer, **105**(3), pp. 605–610.

[101] Amaranatha Raju, M., Ashok Babu, T. P., and Ranganayakulu, C., 2017, "Flow Boiling Heat Transfer and Pressure Drop Analysis of R134a in a Brazed Heat Exchanger with Offset Strip Fins," Heat Mass Transf. und Stoffuebertragung.

[102] Yun, R., Hyeok Heo, J., and Kim, Y., 2006, "Evaporative Heat Transfer and Pressure Drop of R410A in Microchannels," Int. J. Refrig.

[103] Stignor, C. H., Sunden, B., and Fahlen, P., 2009, "An Experimental Study of Liquid-Phase Heat Transfer in Multiport Minichannel Tubes," Heat Transf. Eng., **30**(12), pp. 941–951.

[104] “Sci-Tech.”

[105] “Danfoss.”

[106] 2017, “Every China.”

[107] 2019, “Alfa Laval.”

[108] 2019, “Alfa Laval.”

[109] Coffey, A., 2014, “Most Hydrolic Systems Generate Substantial Heat, so They Can Benefit Form Using a Heat Exchanger.”

[110] Churchill, S. W., and Chu, H. H. S., 1975, “Correlating Equations for Laminar and Turbulent Free Convection from a Horizontal Cylinder,” Int. J. Heat Mass Transf.

[111] Lloyd, J. R., and Moran, W. R., 1974, “Natural Convection Adjacent to Horizontal Surface of Various Planforms,” J. Heat Transfer.

Appendix

The following appendix provides a hand calculation to validate the heat exchanger models and vapor compression cycle, all calculated in EES.

A.1. Bar Plate Heat Exchanger Calculations

Table A-1. Input parameters use in bar plate heat exchanger hand calculation.

Refrigerant fluid parameters			
Parameter Name	**Parameter Symbol**	**Value**	**Units**
Change in Pressure	ΔP_r	9.96	kPa
Inlet enthalpy	$i_{r,in}$ i_r[1,1]	73.8	kJ kg^{-1}
Inlet Pressure	$P_{r,in}$ P_r[1,1]	528	kPa
Inlet Temp	$T_{r,in}$ T_r[1,1]	16.1	°C
Mass Flow Rate per channel	$\dot{M}_r$	0.00796	kg s^{-1}
Outlet Enthalpy	$i_{r,o}$ i_r[8,1]	261	kJ kg^{-1}
Outlet Temp	$T_{r,o}$	18.4	°C
Saturated Liquid Enthalpy	$i_{r,sl}$	75.5	kJ kg^{-1}
Saturated Vapor Enthalpy	$i_{r,sv}$	260	kJ kg^{-1}
Point Temp	T_r[3,2]	17.3	°C
Point Temp	T_r[3,3]	17.3	°C
Point Temp	T_r[4,4]	17.2	°C
Point Enthalpy	i_r[3,2]	96	kJ kg^{-1}
Point Enthalpy	i_r[3,3]	101	kJ kg^{-1}
Point Enthalpy	i_r[4,1]	135	kJ kg^{-1}
Point Pressure	P_r[3,2]	525.8	kPa
Point Pressure	P_r[3,3]	525.6	kPa
Point Pressure	P_r[4,2]	524.2	kPa
Point Quality	X_r[3,2]	0.111	-
Point Quality	X_r[3,3]	0.136	-
Point Heat Transfer	q[4,3]	0.0497	kW
Water-Glycol Fluid parameters			
Parameter Name	**Parameter Symbol**	**Value**	**Units**
Inlet Temp	$T_{g,in}$ T_g[8,4]	19.4	°C

Mass Flow Rate	$\dot{M}g$	0.132	kg s^{-1}
Outlet Temp	$T_{g,o}$ $T_g[1,4]$	18.7	°C
Specific Heat	Cp_g	3.85	kJ $kg^{-1}K^{-1}$
Point Temp	$T_g[2,1]$	18.7	°C
Point Temp	$T_g[3,1]$	18.9	°C
Point Temp	$T_g[4,1]$	19.0	°C
Point Temp	$T_g[5,3]$	19.0	°C
Heat Exchanger Geometric parameters			
Parameter Name	**Parameter Symbol**	**Value**	**Units**
Fin Height	Fh	0.003	m
Fin Pitch Refrigerant	Fp_r	941 X 10^{-6}	m
Fin Pitch Water-glycol	Fp_g	747 X 10^{-6}	m
Fin Thickness	Ft	1.5 X 10^{-3}	m
Horizontal saturated liquid coordinate	j_f	2	-
Horizontal saturated Vapor coordinate	j_g	4	-
Refrigerant Channel width,1,2,3	$W_{r,c}$	0.025, 0.050, 0.075	m
Total Horizontal coordinates	j_h	4	-
Total vertical coordinates	z_h	8	-
Vertical saturated liquid coordinate	z_f	1	-
Vertical saturated Vapor coordinate	z_g	7	-

Table A-2. Bar plate property distribution calculation.

Parameter	Equation	Evaluated	EES. Calc. Value	Hand Calc. Value	Units
Sub-cooled heat transfer rate	$q[z,j]=\frac{\dot{M}_{r}\cdot\left(i_{r,sl}-i_{r,in}\right)}{z_{sl}\cdot j_{sl}}$	$q[1,1]=\frac{0.00796\cdot\left(75.7-73.8\right)}{1\cdot 2}$	**7.45 X10^{-3}**	**7.56 X10^{-3}**	**kW**
Boiling heat transfer rate	$q[z,j]=\frac{\dot{M}_{r}\cdot\left(i_{sv}-i_{sl}\right)\cdot z}{j_{h}\cdot\sum_{z=z_f}^{z=z_g+1}\left(z\right)-j_{f}-j_{g}\cdot z_{h}}$	$q[3,1]=\frac{0.00796\cdot\left(260-75.7\right)\cdot 3}{4\cdot\sum_{z=z_f}^{z=z_g+1}\left(z\right)-7-3\cdot 8}$	**0.0373**	**0.0389**	**kW**
Superheated heat transfer rate	$q[z,j]=\frac{\dot{M}_{r}\cdot\left(i_{r}[z,j]-i_{r,sv}\right)}{\left(z_{h}-z_{sv}\right)\cdot j_{sv}}$	$q[8,1]=\frac{0.00796\cdot\left(261.3-260\right)}{\left(8-7\right)\cdot 3}$	**3.64 X10^{-3}**	**3.45 X10^{-3}**	**kW**
Refrigerant Enthalpy change, +j direction	$q[z,j]=\dot{m}_{r}\cdot\left(i_{r}[z,j]-[z,j+1]\right)$	$7.46\times10^{-3}=0.00796\cdot\left(73.8-i_{r}[1,2]\right)$	**74.8**	**74.7**	**kJ kg^{-1}**
Refrigerant Enthalpy change, -j direction	$q[z,j]=\dot{m}_{r}\cdot\left(i_{r}[z,j+1]-[z,j]\right)$	$49.7\times10^{-3}=0.00796\cdot\left(i_{r}[4,2]-123\right)$	**129**	**128**	**kJ kg^{-1}**
Water-glycol temperature change	$q[z,j]=\dot{m}_{g}\cdot Cp_{g}\cdot\left(T_{g}[z+1,j]-T_{g}[z,j]\right)$	$0.0373=0.123\cdot 3.85\cdot\left(T_{g}[1,4]-18.9\right)$	**18.8**	**19.0**	**ºC**

Control volume Effectiveness +j Direction	$q[z,j] = C_{\min} \cdot \varepsilon[z,j] \cdot \left(T_g[z+1,j] - T_r[z,j]\right)$	$7.46\times10^{-3} = 0.0111 \cdot \varepsilon[1,1] \cdot \left(18.7 - 16.1\right)$	**0.253**	**0.258**	**-**
Control volume Effectiveness -j Direction	$q[z,j] = C_{\min} \cdot \varepsilon[z,j] \cdot \left(T_g[z+1,j] - T_r[z,j+1]\right)$	$49.7\times10^{-3} = 0.472 \cdot \varepsilon[4,3] \cdot \left(19.0 - 17.2\right)$	**0.0602**	**0.0585**	**-**
Refrigerant Pressure Distribution +j Direction	$P_r[z,j+1] = P_r[z,j] - \Delta P_r[z,j]$	$P_r[3,3] = 525.8 - 0.244$	**525.6**	**225.6**	**kPa**
Pressure Distribution -j Direction	$P_r[z,j+1] = P_r[z,j] + \Delta P_r[z,j]$	$P_r[4,3] = 524.3 + 0.244$	**524.6**	**524.5**	**kPa**
C_{min} Single phase	$C_{\min}[z,j] = \min\left(\dot{M}_r[z,j] \cdot Cp_r[z,j], \dot{M}_g \cdot Cp_g\right)$	$C_{\min}[1,1] = \min\left(0.00796 \cdot 1.39, 0.123 \cdot 3.85\right)$	**0.0111**	**0.0111**	**kJ K^{-1}**
C_{min} Two phase	$C_{\min}[z,j] = \min\left(\dot{M}_r[z,j] \cdot Cp_r[z,j], \dot{M}_g \cdot Cp_g\right)$	$C_{\min}[3,2] = \min\left(0.00796 \cdot \infty, 0.123 \cdot 3.85\right)$	**0.472**	**0.474**	**kJ K^{-1}**
Average CV Temp	$T_{r,ave}[z,j] = \frac{T_r[z,j] + T_r[z,j+1]}{2}$	$T_{r,ave}[3,2] = \frac{17.3 + 17.3}{2}$	**17.3**	**17.3**	**ºC**
Average CV Pressure	$P_{r,ave}[z,j] = \frac{P_r[z,j] + P_r[z,j+1]}{2}$	$P_{r,ave}[3,2] = \frac{525.8 + 525.6}{2}$	**525.7**	**525.7**	**kPa**
Average CV Enthalpy	$i_{r,ave}[z,j] = \frac{i_r[z,j] + i_r[z,j+1]}{2}$	$i_{r,ave}[3,2] = \frac{96.0 + 101}{2}$	**98.4**	**98.5**	**kJ kg^{-1}**
Average CV Vapor Quality	$x_{r,ave}[z,j] = \frac{x_r[z,j] + x_r[z,j+1]}{2}$	$x_{r,ave}[3,2] = \frac{0.111 + 0.136}{2}$	**0.124**	**0.124**	**-**

Table A-3. Bar plate two phase refrigerant heat transfer coefficient calculations. The Kuznetsov et al. [49] correlation was used.

Parameter	Equation	Evaluated	EES. Calc. Value	Hand Calc. Value	Units
Refrigerant channel Cross sectional area	$A_{c,r} = W_{c,r} \cdot FH_r - \frac{W_{c,r}}{FP_r} \cdot FT_r \cdot FH_r$	$A_{c,r} = 0.075 \cdot 0.003 - \frac{0.075}{941 \times 10^{-6}} \cdot 150 \times 10^{-6} \cdot 0.003$	**1.89 X10^{-4}**	**1.89 X10^{-4}**	**m^2**
Refrigerant Channel Perimeter	$Per_r = 2 \cdot \left(W_{c,r} + FH_r\right) + 2 \cdot \frac{W_{c,r}}{FP_r} \cdot FH_r$	$Per_r = 2 \cdot \left(0.075 + 0.003\right) + 2 \cdot \frac{0.075}{941 \times 10^{-6}} \cdot 0.003$	**0.634**	**0.634**	**m**
Refrigerant channel hydraulic diameter	$Dh_r = \frac{4 \cdot A_{c,r}}{Per_r}$	$Dh_r = \frac{4 \cdot 1.89 \times 10^{-4}}{0.634}$	**1.19 X10^{-4}**	**1.19 X10^{-4}**	**m**
Refrigerant Reduced Pressure	$P_{red} = \frac{P_r[z, j]}{P_{crit}}$	$P_{red} = \frac{521}{4058}$	**0.128**	**0.128**	**-**

Refrigerant liquid Reynolds Number	$Re_{r,l} = \frac{4 \cdot \dot{M}_r}{Per \cdot \mu_{r,l}}$	$Re_{r,l} = \frac{4 \cdot 0.00796}{0.634 \cdot 215 \times 10^{-6}}$	**234**	**234**	**-**
Refrigerant vapor Reynolds Number	$Re_{r,v} = \frac{4 \cdot \dot{M}_r}{Per \cdot \mu_{r,v}}$	$Re_{r,v} = \frac{4 \cdot 0.00796}{0.634 \cdot 11.6 \times 10^{-6}}$	**4320**	**4330**	**-**
Refrigerant Weber Number	$We_r = \frac{4 \cdot \dot{M}}{Per_r \cdot \sigma_r}$	$We_r = \frac{4 \cdot 0.00796}{0.634 \cdot 0.00909}$	**5.52**	**5.52**	**-**
Two phase heat transfer coefficient	$h_{r,tp,convec} = \frac{4.4 \cdot k_{r,l}}{Dh_r}$	$h_{r,tp,convec} = \frac{4.4 \cdot 87.0 \times 10^{-6}}{1.19 \times 10^{-3}}$	**0.321**	**0.322**	**-**
Enhancement Factor	$F = \left[1 + X_{r,ave} \cdot Pr_{r,l} \cdot \left(\frac{\rho_{r,l}}{\rho_{r,v}} - 1\right)\right]^{0.35}$	$F = \left[1 + 0.95 \cdot 3.44 \cdot \left(\frac{1240}{25.3} - 1\right)\right]^{0.35}$	**5.87**	**5.88**	**-**

Suppression Factor	$S = \left(1 + 0.55 \cdot F^{0.1} \cdot Re_{\mathrm{r,l}}^{0.16}\right)^{-1}$	$S = \left(1 + 0.55 \cdot 5.87^{0.1} \cdot 234^{0.16}\right)^{-1}$	**0.389**	**0.389**	**-**
Secondary Suppression Factor	$A = 1 + \frac{1.2}{\exp\left(0.8 \cdot We_{\mathrm{r}}^{0.35}\right)}$	$A = 1 + \frac{1.2}{\exp\left(0.8 \cdot 5.52^{0.35}\right)}$	**1.28**	**1.28**	**-**
Nucleate boiling heat transfer coefficient	$h_{\mathrm{r,nb}} = \frac{0.55 \cdot P_{\mathrm{r,crit}}^{0.25}}{T_{\mathrm{r,crit}}^{0.875} \cdot Mw_{\mathrm{r}}^{0.125}} \cdot \left(q \cdot 1000\right)^{0.75} \cdot sr^{0.2} \cdot \left(0.14 + 2.2 \cdot P_{\mathrm{red}}\right)$	$h_{\mathrm{r,nb}} = \frac{0.55 \cdot 4058^{0.25}}{101^{0.875} \cdot 102^{0.125}} \cdot \left(0.0994 \cdot 1000\right)^{0.75} \cdot 0.8^{0.2} \cdot \left(0.14 + 2.2 \cdot 0.128\right)$	**0.551**	**0.551**	**-**
Refrigerate side heat transfer coefficient	$h_{\mathrm{r}} = Y \cdot \left(\left(A \cdot s \cdot h_{\mathrm{r,nb}}\right)^2 + \left(F \cdot h_{\mathrm{r,tp,convec}}\right)^2\right)^{0.5}$	$h_{\mathrm{r}} = 0.79 \cdot \left(\left(1.28 \cdot 0.389 \cdot 0.552\right)^2 + \left(5.87 \cdot 0.321\right)^2\right)^{0.5}$	**1.40**	**1.50**	**-**
Refrigerant Channel base area	$A_{\mathrm{r,b}} = 2 \cdot W_{\mathrm{r,c}} \cdot L_{\mathrm{r,c}} \left(1 - \frac{FT_r}{FP_r}\right)$	$A_{\mathrm{r,b}} = 2 \cdot 0.075 \cdot 0.0969 \left(1 - \frac{150 \times 10^{-6}}{941 \times 10^{-6}}\right)$	**0.0122**	**0.0122**	**m^2**

Refrigerant fin area	$A_{r,f} = 2 \cdot L_{r,c} \cdot FH_r$	$A_{r,f} = 2 \cdot 0.0969 \cdot 0.003$	**581 X10^{-6}**	**581 X10^{-6}**	**m^2**
Refrigerant Thermal resistance	$R_r = \left[h_r \cdot \left(A_{r,b} + \eta_{r,f} \cdot A_{r,f} \cdot \frac{W_{r,c}}{FP_r} \right) \right]^{-1}$	$R_r = \left[1.40 \cdot \left(0.0122 + 0.746 \cdot 581 \times 10^{-6} \cdot \frac{0.075}{941 \times 10^{-6}} \right) \right]^{-1}$	**15.3**	**15.3**	**KkW^{-1}**

Table A-4. Bar plate Refrigerant two phase pressure drop calculations. The Tran et al. [54] correlation was used.

Parameter	Equation	Evaluated	EES. Calc. Value	Hand Calc. Value	Units
Refrigerant liquid only friction factor	$f_{r,l} = \frac{64}{Re_{r,l}}$	$f_{r,l} = \frac{64}{234}$	**0.274**	**0.274**	**-**
Refrigerant vapor only friction factor	$f_{r,v} = \frac{0.316}{Re_{r,v}^{0.25}}$	$f_{r,v} = \frac{0.316}{4320^{0.25}}$	**0.0390**	**0.0390**	**-**
Change in liquid only pressure	$\Delta P_{r,l} = \frac{f_{r,l} \cdot L_{c,r} \cdot \dot{M}_r^2}{2 \cdot Dh_r \cdot A_{c,r}^2 \cdot \rho_{r,l} \cdot 1000}$	$\Delta P_{r,l} = \frac{0.274 \cdot 0.0969 \cdot 0.00796^2}{2 \cdot 0.00119 \cdot 0.000189^2 \cdot 1240 \cdot 1000}$	**0.0158**	**0.0159**	**kPa**
Change in vapor only pressure	$\Delta P_{r,v} = \frac{f_{r,v} \cdot L_{c,r} \cdot \dot{M}_r^2}{2 \cdot Dh_r \cdot A_{c,r}^2 \cdot \rho_{r,v} \cdot 1000}$	$\Delta P_{r,l} = \frac{0.039 \cdot 0.0969 \cdot 0.00796^2}{2 \cdot 0.00119 \cdot 0.000189^2 \cdot 25.3 \cdot 1000}$	**0.110**	**0.111**	**kPa**

Γ^2 value	$\Gamma^2 = \frac{f_{r,v} \cdot \rho_{r,l}}{f_{r,l} \cdot \rho_{r,v}}$	$\Gamma^2 = \frac{0.039 \cdot 1240}{0.274 \cdot 25.3}$	**6.96**	**6.98**	**-**
Confinement number	$Co = \frac{\left(\frac{\sigma}{g \cdot (\rho_{r,l} - \rho_{r,v})}\right)^{0.5}}{Dh_r}$	$Co = \frac{\left(\frac{0.009090}{9.8 \cdot (1240 - 25.3)}\right)^{0.5}}{0.00119}$	**0.734**	**0.734**	**-**
Two phase Frictional Pressure drop	$\Delta P_{r,tp,fric} = \Delta P_{r,l} \cdot \left(1 + \left(C \cdot \Gamma^2 - 1\right) \cdot \left(N_{conf} \cdot (1 - X)^{0.875} \cdot X^{0.875} + X^{1.75}\right)\right)$	$\Delta P_{r,tp,fric} = 0.0159 \cdot \left(1 + (4.3 \cdot 6.96 - 1) \cdot \left(0.734 \cdot (1 - 0.95)^{0.875} \cdot 0.95^{0.875} + 0.95^{1.75}\right)\right)$	**0.457**	**0.439**	**kPa**
B1 Parameter	$B1 = 1 + 0.12 \cdot (1 - X_{in}) \cdot \left(\frac{X_{in}}{\rho_{r,v}} + \frac{1 - X_{in}}{\rho_{r,l}}\right)$	$B1 = 1 + 0.12 \cdot (1 - 0.920) \cdot \left(\frac{0.920}{25.3} + \frac{1 - 0.920}{1240}\right)$	**1.00**	**1.00**	**$m^3 kg^{-1}$**
B2 Parameter	$B2 = \frac{1.18 \cdot (1 - X_{in}) \cdot \left(g \cdot \sigma \cdot (\rho_{r,l} - \rho_{r,v})\right)^{0.25}}{\dot{M}_r^2 \cdot \rho_{r,l}^{0.5}}$	$B2 = \frac{1.18 \cdot (1 - 0.920) \cdot \left(9.8 \cdot 0.00909 \cdot (1240 - 25.3)\right)^{0.25}}{0.00796^2 \cdot 1240^{0.5}}$	**136**	**136**	**$s^3 m^{1.5} kg^{-2}$**

Void fraction in	$\varepsilon_{\text{in}} = \frac{X_{\text{in}}}{\rho_{\text{r,v}} \cdot (B1 + B2)}$	$\varepsilon_{\text{in}} = \frac{0.92}{25.3 \cdot (1.00 + 136)}$	**266 X10^{-6}**	**265 X10^{-6}**	**-**
A1 Parameter	$A1 = \frac{(1 - X_{\text{in}})^2}{\rho_{\text{r,l}} \cdot (1 - \varepsilon_{\text{in}})}$	$A1 = \frac{(1 - 0.92)^2}{1240 \cdot (1 - 0.000266)}$	**5.13 X10^{-6}**	**5.16 X10^{-6}**	**m^{3}kg^{-1}**
A2 Parameter	$A2 = \frac{X_{\text{in}}^2}{\rho_{\text{r,v}} \cdot \varepsilon_{\text{in}}}$	$A2 = \frac{0.92^2}{25.3 \cdot 0.000266}$	**126**	**126**	**m^{3}kg^{-1}**
B3 Parameter	$B3 = 1 + 0.12 \cdot (1 - X_{\text{out}}) \cdot \left(\frac{X_{\text{out}}}{\rho_{\text{r,v}}} + \frac{1 - X_{\text{out}}}{\rho_{\text{r,l}}} \right)$	$B3 = 1 + 0.12 \cdot (1 - 0.977) \cdot \left(\frac{0.98}{25.3} + \frac{1 - 0.98}{1240} \right)$	**1.00**	**1.00**	**m^{3}kg^{-1}**
B4 Parameter	$B4 = \frac{1.18 \cdot (1 - X_{\text{out}}) \cdot \left(g \cdot \sigma \cdot (\rho_{\text{r,l}} - \rho_{\text{r,v}}) \right)^{0.25}}{\dot{M}_{\text{r}}^2 \cdot \rho_{\text{r,l}}^{0.5}}$	$B4 = \frac{1.18 \cdot (1 - 0.977) \cdot (9.8 \cdot 0.00909 \cdot (1240 - 25.3))^{0.25}}{0.00796^2 \cdot 1240^{0.5}}$	**34.9**	**39.1**	**s^3 m$^{1.5}$ kg^{-2}**

Void fraction in	$\varepsilon_{\text{out}} = \frac{X_{\text{out}}}{\rho_{\text{r,v}} \cdot (B3 + B4)}$	$\varepsilon_{\text{out}} = \frac{0.977}{25.3 \cdot (1.00 + 34.9)}$	**1.08 X10^{-3}**	**1.08 X10^{-3}**	**-**
A3 Parameter	$A3 = \frac{(1 - X_{\text{out}})^2}{\rho_{\text{r,l}} \cdot (1 - \varepsilon_{\text{out}})}$	$A3 = \frac{(1 - 0.980)^2}{1240 \cdot (1 - 0.00108)}$	**337 X10^{-9}**	**323 X10^{-9}**	**m^{3}kg^{-1}**
A4 Parameter	$A4 = \frac{X_{\text{out}}^2}{\rho_{\text{r,v}} \cdot \varepsilon_{\text{out}}}$	$A4 = \frac{0.98^2}{25.3 \cdot 0.00108}$	**35.1**	**35.1**	**m^{3}kg^{-1}**
Acceleration pressure loss	$\Delta P_{\text{accel,r}} = \dot{M}_{\text{r}}^2 \cdot 0.001 \cdot \left((A3 + A4) - (A1 + A2) \right)$	$\Delta P_{\text{accel,r}} = 0.00796^2 \cdot 0.001 \cdot \left(\left(337 \times 10^{-9} + 1.08 \times 10^{-3} \right) - \left(5.16 \times 10^{-6} + 126 \right) \right)$	**-5.76 X10^{-6}**	**-7.86 X10^{-6}**	**kPa**
Total Pressure loss	$\Delta P_{\text{r}} = \Delta P_{\text{r,fric}} + \Delta P_{\text{r,accel}}$	$\Delta P_{\text{r}} = 0.457 + -5.76 \times 10^{-6}$	**0.457**	**0.457**	**kPa**

Table A-5. Bar plate single phase refrigerant heat transfer and pressure drop calculations. The Garimella et al. [57] heat transfer correlation, and Churchill [65] friction factor correlation were used.

Parameter	Equation	Evaluated	EES. Calc. Value	Hand Calc. Value	Units
Refrigerant channel Cross sectional area	$A_{c,r} = W_{c,r} \cdot FH_r - \frac{W_{c,r}}{FP_r} \cdot FT_r \cdot FH_r$	$A_{c,r} = 0.075 \cdot 0.003 - \frac{0.075}{941 \times 10^{-6}} \cdot 150 \times 10^{-6} \cdot 0.003$	**1.89 X10^{-4}**	**1.89 X10^{-4}**	**m^2**
Refrigerant Channel Perimeter	$Per_r = 2 \cdot \left(W_{c,r} + FH_r\right) + 2 \cdot \frac{W_{c,r}}{FP_r} \cdot FH_r$	$Per_r = 2 \cdot \left(0.075 + 0.003\right) + 2 \cdot \frac{0.075}{941 \times 10^{-6}} \cdot 0.003$	**0.634**	**0.634**	**m**
Refrigerant channel hydraulic diameter	$Dh_r = \frac{4 \cdot A_{c,r}}{Per_r}$	$Dh_r = \frac{4 \cdot 1.89 \times 10^{-4}}{0.634}$	**1.19 X10^{-4}**	**1.19 X10^{-4}**	**m**
Refrigerant Reynolds Number	$Re_r = \frac{4 \cdot \dot{M}_r}{Per \cdot \mu_r}$	$Re_{r,l} = \frac{4 \cdot 0.00796}{0.634 \cdot 11.6 \times 10^{-6}}$	**4320**	**4320**	**-**

A parameter in Churchill	$A=\left(2.2088+2.457\cdot\ln\left(\frac{42.683}{Re_{\mathrm{r}}^{0.9}}\right)\right)^{16}$	$A=\left(2.2088+2.457\cdot\ln\left(\frac{42.683}{4320^{0.9}}\right)\right)^{16}$	**3.96 X10^{13}**	**3.95 X10^{13}**	**-**
B parameter in Churchill	$B=\left(\frac{37530}{Re_{\mathrm{r}}}\right)^{16}$	$B=\left(\frac{37530}{4320}\right)^{16}$	**1.07 X10^{15}**	**1.05 X10^{15}**	**-**
Friction Factor	$F_{\mathrm{r}}=8\cdot\left(\left(\frac{8}{Re_{\mathrm{r}}}\right)^{12}+\frac{1}{(A+B)^{1.5}}\right)^{1/12}$	$F_{\mathrm{r}}=8\cdot\left(\left(\frac{8}{4320}\right)^{12}+\frac{1}{\left(3.96\times10^{13}+1.07\times10^{15}\right)^{1.5}}\right)^{1/12}$	**0.105**	**0.105**	**-**
Nussel fd	$Nu_{\mathrm{FD}}=8.235\cdot(1-2.0421\cdot Z+3.0853\cdot Z^2$ $-2.4753\cdot Z^3+1.0578\cdot Z^4-0.1861\cdot Z^5$	$Nu_{\mathrm{FD}}=8.235\cdot(1-2.0421\cdot0.04+3.0853\cdot0.04^2$ $-2.4753\cdot0.04^3+1.0578\cdot0.04^4-0.1861\cdot0.04^5$	**7.60**	**7.60**	**-**
Nussel l	$Nu_{\mathrm{l}}=\left[Nu_{\mathrm{FD}}^3+\left(\frac{0.468\cdot\frac{Dh}{W}\cdot Re_{\mathrm{r}}\cdot Pr_{\mathrm{r}}}{\left(\frac{Dh}{W}\cdot Re_{\mathrm{r}}\cdot Pr_{\mathrm{r}}\right)^{2/3}\cdot0.165+1}\right)^3\right]^{1/3}$	$Nu_{\mathrm{l}}=\left[7.60^3+\left(\frac{0.468\cdot\frac{0.00119}{0.963}\cdot4320\cdot0.828}{\left(\frac{0.00119}{0.963}\cdot4320\cdot0.828\right)^{2/3}\cdot0.165+1}\right)^3\right]^{1/3}$	**9.08**	**9.07**	**-**

Nussel T	$Nu_T = 0.012 \cdot Re_{\mathrm{r}}^{0.85} \cdot Pr_{\mathrm{r}}^{0.4} \cdot \left(1+\left(\frac{Dh}{W}\right)^{2/3}\right)$	$Nu_T = 0.012 \cdot 4320^{0.85} \cdot 0.828^{0.4} \cdot \left(1+\left(\frac{0.00119}{0.0963}\right)^{2/3}\right)$	**14.42**	**14.4**	**-**
Nusselt Number	$Nu_{\mathrm{r}} = \left\{ Nu_{\mathrm{l}}^{10} + \left[\frac{\exp\left(\frac{360 - Re_{\mathrm{r}}}{925}\right)}{Nu_{\mathrm{l}}^{2}} + Nu_{\mathrm{T}}^{-2} \right]^{-5} \right\}^{0.1}$	$Nu_{\mathrm{r}} = \left\{ 9.08^{10} + \left[\frac{\exp\left(\frac{360-4320}{925}\right)}{9.08^{2}} + 14.4^{-2} \right]^{-5} \right\}^{0.1}$	**14.19**	**14.19**	**-**
Heat transfer Coefficient	$h_{\mathrm{r}} = \frac{Nu_{\mathrm{r}} \cdot K_{\mathrm{r}}}{Dh_{\mathrm{r}}}$	$h_{\mathrm{r}} = \frac{14.4 \cdot 13.8 \times 10^{-6}}{1190 \times 10^{-6}}$	**0.164**	**0.167**	**$kWm^{-2}K^{-1}$**
Refrigerant Channel base area	$A_{\mathrm{r,b}} = 2 \cdot W_{\mathrm{r,c}} \cdot L_{\mathrm{r,c}} \left(1 - \frac{FT_r}{FP_r}\right)$	$A_{\mathrm{r,b}} = 2 \cdot 0.075 \cdot 0.0168 \left(1 - \frac{150 \times 10^{-6}}{941 \times 10^{-6}}\right)$	**2.12 X10^{-3}**	**2.12 X10^{-3}**	**m^2**
Refrigerant fin area	$A_{\mathrm{r,f}} = 2 \cdot L_{\mathrm{r,c}} \cdot FH_{\mathrm{r}}$	$A_{\mathrm{r,f}} = 2 \cdot 0.0168 \cdot 0.003$	**101 X10^{-6}**	**101 X10^{-6}**	**m^2**

Refrigerant Thermal resistance	$R_{\mathrm{r}} = \left[h_{\mathrm{r}} \cdot \left(A_{\mathrm{r,b}} + \eta_{\mathrm{r,f}} \cdot A_{\mathrm{r,f}} \cdot \frac{W_{\mathrm{r,c}}}{FP_r} \right) \right]^{-1}$	$R_{\mathrm{r}} = \left[0.164 \cdot \left(0.00218 + 0.999 \cdot 101 \times 10^{-6} \cdot \frac{0.075}{941 \times 10^{-6}} \right) \right]^{-1}$	**601**	**602**	**KkW^{-1}**
Refrigerant Pressure Changer	$\Delta P_r = \frac{F \cdot L_{\mathrm{c,r}} \cdot \dot{M}_{\mathrm{r}}^2}{2 \cdot Ac_{\mathrm{r}}^2 \cdot \rho_{\mathrm{r}} \cdot Dh_{\mathrm{r}} \cdot 1000}$	$\Delta P_r = \frac{0.105 \cdot 0.0168 \cdot 0.00796^2}{2 \cdot 0.000189^2 \cdot 25.0 \cdot 0.00119 \cdot 1000}$	**52.1 X10^{-3}**	**52.1 X10^{-3}**	**kPa**

Table A-6. Bar plate water glycol heat transfer calculations. The Hartnett and Kostic [83] correlation was used.

Parameter	Equation	Evaluated	EES. Calc. Value	Hand Calc. Value	Units
Water-glycol channel Cross sectional area	$A_{c,g} = L_{c,g} \cdot FH_g - \frac{L_{c,g}}{FP_g} \cdot FT_g \cdot FH_g$	$A_{c,r} = 0.0963 \cdot 0.003 - \frac{0.0963}{747 \times 10^{-6}} \cdot 150 \times 10^{-6} \cdot 0.003$	**2.31 X10^{-4}**	**2.31 X10^{-4}**	**m^2**
Water-glycol Channel Perimeter	$Per_g = 2 \cdot \left(L_{c,g} + FH_g\right) + 2 \cdot \frac{L_{c,g}}{FP_g} \cdot FH_g$	$Per_r = 2 \cdot \left(0.0963 + 0.003\right) + 2 \cdot \frac{0.0963}{747 \times 10^{-6}} \cdot 0.003$	**0.972**	**0.972**	**m**
Water-glycol channel hydraulic diameter	$Dh_g = \frac{4 \cdot A_{c,g}}{Per_g}$	$Dh_r = \frac{4 \cdot 2.31 \times 10^{-4}}{0.972}$	**9.50 X10^{-4}**	**9.51 X10^{-4}**	**m**
Water-glycol vapor Reynolds Number	$Re_g = \frac{4 \cdot \dot{M}_g}{Per \cdot \mu_g}$	$Re_{r,v} = \frac{4 \cdot 0.123}{0.972 \cdot 3.21 \times 10^{-3}}$	**158**	**158**	**-**

Friction Factor	$F_g = 64 / Re$	$F_g = 64/158$	**0.406**	**0405**	**-**
Nusselt Number	$Nu_g = 8.235 \cdot (1 - 2.0421 \cdot Z + 3.0853 \cdot Z^2 - 2.4753 \cdot Z^3 + 1.0578 \cdot Z^4 - 0.1861 \cdot Z^5$	$Nu_g = 8.235 \cdot (1 - 2.0421 \cdot 2 + 3.0853 \cdot 2^2 - 2.4753 \cdot 2^3 + 1.0578 \cdot 2^4 - 0.1861 \cdot 2^5$	**5.74**	**5.74**	**-**
Heat transfer Coefficient	$h_g = \frac{Nu_g \cdot K_g}{Dh_g}$	$h_g = \frac{5.74 \cdot 440 \times 10^{-6}}{950 \times 10^{-6}}$	**2.66**	**2.66**	**$kWm^{-2}K^{-1}$**
Water-glycol base area	$A_{b,g} = 2 \cdot \left(W_{c,g} \cdot L_{c,g} - \frac{L_{c,g}}{Fp_g} \cdot FT_g \cdot W_{c,g} \right)$	$A_{b,g} = 2 \cdot \left(0.025 \cdot 0.0963 - \frac{0.0963}{747 \times 10^{-6}} \cdot 150 \times 10^{-6} \cdot 0.025 \right)$	**3.85 X10^{-3}**	**3.83 X10^{-3}**	**m^2**
Water-glycol fin area	$A_{f,g} = 2 \cdot W_{c,g} \cdot FH_r$	$A_{f,g} = 2 \cdot 0.025 \cdot 0.003$	**150 X10^{-6}**	**150 X10^{-6}**	**m^2**

Water-glycol thermal resistance	$R_{\mathrm{g}} = \left[h_g \cdot \left(A_{\mathrm{g,b}} + \eta_{\mathrm{g,f}} \cdot A_{\mathrm{g,f}} \cdot \frac{L_{\mathrm{g,c}}}{FP_g} \right) \right]^{-1}$	$R_{\mathrm{g}} = \left[2.66 \cdot \left(3.83 \times 10^{-3} + 0.99 \cdot 150 \times 10^{-6} \cdot \frac{0.0963}{747 \times 10^{-6}} \right) \right]^{-1}$	**24.1**	**24.1**	**KkW^{-1}**

Table A-7. Bar plate thermal resistance network calculations**.**

Parameter	Equation	Evaluated	EES. Calc. Value	Hand Calc. Value	Units
Single Phase wall resistance	$R_{\text{wall}}[z,j]=\frac{\delta_{\text{wall}}}{k_{\text{wall}}\cdot L_{\text{c}}[z,j]\cdot W_{\text{c}}}$	$R_{\text{wall}}[1,1]=\frac{150\times10^{-6}}{0.159\cdot0.144\cdot0.025}$	**0.263**	**0.262**	**KkW^{-1}**
Single Phase UA	$UA[z,j]=\frac{1}{R_{\text{r}}[z,j]+R_{\text{wall}}[z,j]+R_{\text{g}}[z,j]}$	$UA[1,1]=\frac{1}{277+0.0657+31.1}$	**3.25 X10^{-3}**	**3.25 X10^{-3}**	**kWK^{-1}**
Single Phase NTU	$NTU[z,j]=\frac{UA[z,j]}{C_{\min}[z,j]}$	$NTU[z,j]=\frac{3.25\times10^{-3}}{11.1\times10^{-3}}$	**0.293**	**0.293**	**-**
Single Phase Effectiveness	$\varepsilon[z,j]=1-\exp\left(\frac{1}{Cr}\cdot NTU[z,j]^{0.22}\cdot\left(\exp\left(-Cr\cdot NTU[z,j]^{0.78}\right)-1\right)\right)$	$\varepsilon[1,1]=1-\exp\left(\frac{1}{0.0234}\cdot0.293^{0.22}\cdot\left(\exp\left(-0.0234\cdot0.293^{0.78}\right)-1\right)\right)$	**0.253**	**0.253**	**-**

Two Phase wall resistance	$R_{\text{wall}}[z,j]=\frac{\delta_{\text{wall}}}{k_{\text{wall}}\cdot L_{\text{c}}[z,j]\cdot W_{\text{c}}}$	$R_{\text{wall}}[3,2]=\frac{150\times10^{-6}}{0.159\cdot0.159\cdot0.050}$	**0.119**	**0.119**	**KkW^{-1}**
Two Phase UA	$UA[z,j]=\frac{1}{R_{\text{r}}[z,j]+R_{\text{wall}}[z,j]+R_{\text{g}}[z,j]}$	$UA[3,2]=\frac{1}{25.0+0.119+15.6}$	**24.6 X10^{-3}**	**24.6 X10^{-3}**	**kWK^{-1}**
Two Phase NTU	$NTU[z,j]=\frac{UA[z,j]}{C_{\min}[z,j]}$	$NTU[3,2]=\frac{24.6\times10^{-3}}{422\times10^{-3}}$	**51.5 X10^{-3}**	**58.2 X10^{-3}**	**-**
Two Phase Effectiveness	$\varepsilon[z,j]=1-\exp\left(-NTU[z,j]\right)$	$\varepsilon[3,2]=1-\exp\left(-51.5\times10^{-3}\right)$	**50.0 X10^{-3}**	**56.6 X10^{-3}**	**-**

Table A-8. Bar plate results calculations.

Parameter	Equation	Evaluated	EES. Calc. Value	Hand Calc. Value	Units
Weighted Average Width	$W_{ave} = \frac{\sum_{j=1}^{j=4} L_c[1,j] \cdot W_{c1} + \sum_{z=2}^{z=3}\sum_{j=1}^{j=4} L_c[1,j] \cdot W_{c2} + \sum_{z=4}^{z=8}\sum_{j=1}^{j=4} L_c[1,j] \cdot W_{c3}}{1 \cdot W_{c1} + 2 \cdot W_{c1} + 5 \cdot W_{c3}}$	$W_{ave} = \frac{0.796 \cdot 0.025 + 1.15 \cdot 0.05 + 1.74 \cdot 0.075}{1 \cdot 0.025 + 2 \cdot 0.050 + 5 \cdot 0.075}$	**0.415**	**0.416**	**m**
Core Pressure drop	$\Delta P_{core} = \Delta P_{fric} + \Delta P_{accel} + \Delta P_{grav}$	$\Delta P_{core} = 5.72 + 0.61 + 3.63$	**9.96**	**9.96**	**kPa**

A.2. Plate Frame heat exchanger model hand calculations

Table A-9. Input parameters used in plate frame heat exchanger hand calculation**.**

Refrigerant fluid parameters			
Parameter Name	**Parameter Symbol**	**Value**	**Units**
Change in Pressure	ΔP_r	2.15	kPa
Inlet enthalpy	$i_{r,in}$ i_r[21]	71.4	kJ kg^{-1}
Inlet Pressure	$P_{r,in}$ P_r[21]	485	kPa
Inlet Temp	$T_{r,in}$ T_r[21]	14.2	°C
Mass Flow Rate per channel	$\dot{M}_r$	0.00114	kg s^{-1}
Outlet Enthalpy	$i_{r,o}$ i_r[1]	259	kJ kg^{-1}
Outlet Temp	$T_{r,o}$ T_r[1]	14.75	°C
Saturated Liquid Enthalpy	$i_{r,sl}$	71.9	kJ kg^{-1}
Saturated Vapor Enthalpy	$i_{r,sv}$	259	kJ kg^{-1}
Water-Glycol Fluid parameters			
Parameter Name	**Parameter Symbol**	**Value**	**Units**
Inlet Temp	$T_{g,in}$ T_g[1]	15.9	°C
Mass Flow Rate	$\dot{M}$g	0.293	kg s^{-1}
Outlet Temp	$T_{g,o}$ T_g[21]	15.75	°C
Specific Heat	Cp_g	3.84	kJ $kg^{-1}K^{-1}$
Heat Exchanger Geometric parameters			
Parameter Name	**Parameter Symbol**	**Value**	**Units**
Plate Spacing	Ps	2.57 X 10^{-3}	m
Chevron Angle	β	$\pi/3$	Rad
Saturated liquid coordinate	j_{sl}	5	-
Saturated Vapor coordinate	j_{sv}	3	-
Plate width	W	0.43	m
Total Coordinates	j_h	20	-

Table A-10. Plate frame property distribution.

Parameter	Equation	Evaluated	EES. Calc. Value	Hand Calc. Value	Units
Sub-cooled heat transfer rate	$q[j]=\frac{\dot{M}_{\mathrm{r}}\cdot\left(i_{\mathrm{r,sl}}-i_{\mathrm{r}}[21]\right)}{j_{\mathrm{h}}-j_{\mathrm{sl}}}$	$q[20]=\frac{0.00114\cdot(71.9-71.23)}{20-15}$	**154 X10^{-6}**	**154 X10^{-6}**	**kW**
Boiling heat transfer rate	$q[j]=\frac{\dot{M}_{\mathrm{r}}\cdot\left(i_{\mathrm{sv}}-i_{\mathrm{sl}}\right)}{j_{\mathrm{sl}}-j_{\mathrm{sv}}}$	$q[15]=\frac{0.00114\cdot(259-71.9)}{15-3}$	**0.0177**	**0.0178**	**kW**
Superheated heat transfer rate	$q[j]=\frac{\dot{M}_{\mathrm{r}}\cdot\left(i_{\mathrm{r}}[1]-i_{\mathrm{r,sv}}\right)}{j_{sv}}$	$q[1]=\frac{0.00114\cdot(258.9-258.6)}{3}$	**119 X10^{-6}**	**119 X10^{-6}**	**kW**
effectiveness	$\varepsilon[j]=\frac{q[j]}{C_{\min}\cdot\left(T_g[j]-T_r[j+1]\right)}$	$\varepsilon[15]=\frac{0.0177}{1.12\cdot(15.8-14.7)}$	**0.0146**	**0.0144**	**-**
Refrigerant Enthalpy Change	$i_{\mathrm{r}}[j+1]=i_{\mathrm{r}}[j]-\frac{q[j]}{\dot{m}_{\mathrm{r}}}$	$i_{\mathrm{r}}[5]=259-\frac{0.0178}{0.00114}$	**243**	**243**	**kJ kg^{-1}**
Water-glycol temperature Change	$T_{\mathrm{g}}[j+1]=T_{\mathrm{g}}[j]+\frac{q[j]}{\dot{M}_{\mathrm{g}}\cdot Cp_{\mathrm{g}}}$	$T_{\mathrm{g}}[5]=15.9+\frac{0.0178}{0.293\cdot3.84}$	**15.9**	**15.9**	**°C**

Table A-11. Plate frame refrigerant two phase heat transfer coefficient calculation. The Cooper [32] correlation was used.

Parameter	Equation	Evaluated	EES. Calc. Value	Hand Calc. Value	Units
Cross Sectional Area	$A_{c,r} = W \cdot PS$	$A_{c,r} = 0.43 \cdot 0.00257$	**1.11 X10^{-3}**	**1.11 X10^{-3}**	**m^2**
Wetted Perimeter	$Per = 2 \cdot (W + PS)$	$Per_{c,r} = 2 \cdot (0.43 + 0.00257)$	**0.865**	**0.865**	**m**
Hydraulic Diameter	$DH_r = \frac{4 \cdot A_{c,r}}{Per_{c,r}}$	$DH_r = \frac{4 \cdot 1.11 \times 10^{-3}}{0.865}$	**5.12 X10^{-3}**	**5.12 X10^{-3}**	**m**
Heat Transfer Coefficient	$h_r = 0.0055 \cdot Pr_{r,sl}^{0.12} \cdot \left(-\log\left(Pr_{r,sl}\right)\right)^{-0.55} \cdot MW_r^{-0.5} \cdot q''^{0.67}$	$h_r = 0.0055 \cdot 0.109^{0.12} \cdot \left(-\log\left(0.109\right)\right)^{-0.55} \cdot 102^{-0.5} \cdot 1640^{0.67}$	**0.607**	**0.607**	**kW m^{-2}K^{-1}**
Refrigerant Thermal Resistance	$R_r = \frac{1}{h_r \cdot L_c \cdot W}$	$R_r = \frac{1}{0.607 \cdot 0.144 \cdot 0.43}$	**13.27**	**13.3**	**KkW^{-1}**

Table A-12. Plate frame refrigerant two phase pressure drop calculation. The Huang et al. [19] correlation was used.

Parameter	Equation	Evaluated	EES. Calc. Value	Hand Calc. Value	Units
Two phase viscosity	$\mu_{tp}=\frac{X\cdot\frac{\mu_{r,sv}}{\rho_{r,sv}}+(1-X)\cdot\frac{\mu_{r,sl}}{\rho_{r,sl}}}{X\cdot\left(\frac{1}{\rho_{r,sv}}-\frac{1}{\rho_{r,sl}}\right)+\frac{1}{\rho_{r,sl}}}$	$\mu_{tp}=\frac{0.0834\cdot\frac{11.4\times10^{-6}}{21.6}+(1-0.0834)\cdot\frac{2.29\times10^{-3}}{1250}}{0.0834\cdot\left(\frac{1}{21.6}-\frac{1}{1250}\right)+\frac{1}{1250}}$	**459 X10^{-6}**	**459 X10^{-6}**	
Refrigerant Mass Flux	$G_r=\frac{\dot{M}_r}{A_{c,r}}$	$G_r=\frac{0.00646}{0.00111}$	**5.84**	**5.82**	**kgm^{-2}s^{-1}**
Equivalent Reynolds Number	$Re_{eq,r}=\frac{G_r\cdot Dh_r}{\mu_{r,TP}}$	$Re_{eq,r}=\frac{5.84\cdot5.12\times10^{-3}}{459\times10^{-6}}$	**651**	**651**	**-**
FR Constant	$FR=0.183\cdot\left(\frac{\beta}{30}\right)^2-0.275\cdot\left(\frac{\beta}{30}\right)+1.1$	$FR=0.183\cdot\left(\frac{60}{30}\right)^2-0.275\cdot\left(\frac{60}{30}\right)+1.1$	**1.28**	**1.28**	**-**
Two Phase Friction Factor	$f=\frac{38100\cdot FR}{Re_{eq,r}^{0.9}\cdot\left(\frac{\rho_{r,sl}}{\rho_{r,sv}}\right)^{0.16}}$	$f=\frac{38100\cdot1.28}{651^{0.9}\cdot\left(\frac{1254}{21.6}\right)^{0.16}}$	**74.9**	**74.8**	**-**

Two Phase Specific Volume	$V_{r,tp} = X \cdot \left(\rho_{r,sv}^{-1} - \rho_{r,sl}^{-1}\right) + \rho_{r,s1}^{-1}$	$V_{r,tp} = 0.834 \cdot \left(21.6^{-1} - 1250^{-1}\right) + 1250^{-1}$	**4.60 X10^{-3}**	**4.60 X10^{-3}**	**m^{3}kg^{-1}**
Frictional Pressure Drop	$\Delta P_{r,fric} = \frac{2 \cdot f \cdot L_c \cdot G_r^2 \cdot V_{r,tp}}{Dh_r \cdot 1000}$	$\Delta P_{r,fric} = \frac{2 \cdot 74.9 \cdot 0.132 \cdot 5.84^2 \cdot 4.6 \times 10^{-3}}{5.12 \times 10^{-3} \cdot 1000}$	**606 X10^{-3}**	**606 X10^{-3}**	**kPa**
Acceleration Pressure loss	$\Delta P_{accel,r} = G_r^2 \cdot \frac{1}{13} \cdot \left(\frac{1}{\rho_{r,sv}} - \frac{1}{\rho_{r,sl}}\right) \cdot 0.001$	$\Delta P_{accel,r} = 5.84 \cdot \frac{1}{13} \cdot \left(\frac{1}{21.6} - \frac{1}{1250}\right) \cdot 0.001$	**119 X10^{-6}**	**119 X10^{-6}**	**kPa**
Gravitational Pressure loss	$\Delta P_{r,grav} = \frac{g \cdot L_c}{V_{r,tp} \cdot 1000}$	$\Delta P_{r,grav} = \frac{9.8 \cdot 0.132}{4.6 \times 10^{-3} \cdot 1000}$	**0.281**	**0.281**	**kPa**

Table A-13. Plate frame refrigerant single phase heat transfer coefficient and pressure drop calculations. The Maslov and Kovalencko [35] correlation was used.

Parameter	Equation	Evaluated	EES. Calc. Value	Hand Calc. Value	Units
Cross Sectional Area	$A_{c,r} = W \cdot PS$	$A_{c,r} = 0.43 \cdot 0.00257$	**1.11 X10^{-3}**	**1.11 X10^{-3}**	**m^2**
Wetted Perimeter	$Per = 2 \cdot (W + PS)$	$Per_{c,r} = 2 \cdot (0.43 + 0.00257)$	**0.865**	**0.865**	**m**
Hydraulic Diameter	$DH_r = \frac{4 \cdot A_{c,r}}{Per_{c,r}}$	$DH_r = \frac{4 \cdot 1.11 \times 10^{-3}}{0.865}$	**5.12 X10^{-3}**	**5.12 X10^{-3}**	**m**
Refrigerant Mass Flux	$G_r = \frac{\dot{M}_r}{A_{c,r}}$	$G_r = \frac{0.00114}{0.00111}$	**1.03**	**1.02**	**kgm^{-2}s^{-1}**
Refrigerant Reynolds Number	$Re_r = \frac{4 \cdot \dot{M}_r}{Per_r \cdot \mu_r}$	$Re_r = \frac{4 \cdot 1.14 \times 10^{-3}}{0.865 \cdot 222 \times 10^{-6}}$	**23.7**	**23.7**	**-**

Refrigerant Nusselt Number	$Nu_r = 0.78 \cdot Re_r^{0.5} \cdot Pr_r^{1/3}$	$Nu_r = 0.78 \cdot 23.7^{0.5} \cdot 3.48^{1/3}$	**5.75**	**5.75**	**-**
Heat Transfer Coefficient	$h_r = \frac{Nu_r \cdot K_r}{Dh_r}$	$h_r = \frac{5.75 \cdot 88.3 \times 10^{-6}}{5.12 \times 10^{-3}}$	**0.0992**	**0.0992**	**$kWm^{-2}K^{-1}$**
Thermal Resistance	$R_r = \frac{1}{h_r \cdot L_c \cdot W \cdot 2}$	$R_r = \frac{1}{0.0992 \cdot 0.00348 \cdot 0.43 \cdot 2}$	**3390**	**3390**	**KkW^{-1}**
Single Phase Friction Factor	$f = 0.6857 \cdot Re_r^{-0.172}$	$f = 0.6857 \cdot 23.7^{-0.172}$	**0.398**	**0.398**	**-**
Frictional Pressure Drop	$\Delta P_{r,fric} = \frac{2 \cdot f \cdot L_c \cdot G_r^2}{\rho_r \cdot Dh_r \cdot 1000}$	$\Delta P_{r,fric} = \frac{2 \cdot 0.398 \cdot 0.00348 \cdot 1.027}{1250 \cdot 5.12 \times 10^{-3} \cdot 1000}$	**4.57 $X10^{-7}$**	**445 $X10^{-9}$**	**kPa**
Gravitational Pressure loss	$\Delta P_{r,grav} = \frac{\rho_r \cdot g \cdot L_c}{1000}$	$\Delta P_{r,grav} = \frac{1250 \cdot 9.8 \cdot 0.00348}{1000}$	**0.0424**	**0.0426**	**kPa**

Table A-14. Plate frame water-glycol heat transfer coefficient calculations. The Muley [39] correlation was used.

Parameter	Equation	Evaluated	EES. Calc. Value	Hand Calc. Value	Units
Cross Sectional Area	$A_{c,r} = W \cdot PS$	$A_{c,r} = 0.43 \cdot 0.00257$	**1.11 X10^{-3}**	**1.11 X10^{-3}**	**m^2**
Wetted Perimeter	$Per = 2 \cdot (W + PS)$	$Per_{c,r} = 2 \cdot (0.43 + 0.00257)$	**0.865**	**0.865**	**m**
Hydraulic Diameter	$DH_r = \frac{4 \cdot A_{c,r}}{Per_{c,r}}$	$DH_r = \frac{4 \cdot 1.11 \times 10^{-3}}{0.865}$	**5.12 X10^{-3}**	**5.12 X10^{-3}**	**m**
Water-glycol Reynolds Number	$Re_g = \frac{4 \cdot \dot{M}_g}{Per_g \cdot \mu_g}$	$Re_r = \frac{4 \cdot 0.293}{0.865 \cdot 3.61 \times 10^{-3}}$	**375**	**375**	**-**
Nuselet Number	$Nu_g = 0.44 \cdot \left(\frac{6\beta}{\pi}\right)^{0.38} \cdot Re_g^{0.5} \cdot Pr_g^{1/3}$	$Nu_g = 0.44 \cdot \left(\frac{6 \cdot 1.05}{\pi}\right)^{0.38} \cdot 375^{0.5} \cdot 31.6^{1/3}$	**35.1**	**35.1**	**-**

Heat Transfer Coefficient	$h_g = \frac{Nu_g \cdot K_g}{Dh_g}$	$h_r = \frac{35.1 \cdot 437 \times 10^{-6}}{5.12 \times 10^{-3}}$	**3.00**	**3.00**	**$kWm^{-2}K^{-1}$**
Thermal Resistance	$R_g = \frac{1}{h_g \cdot L_c \cdot W \cdot 2}$	$R_r = \frac{1}{3.00 \cdot 0.00348 \cdot 0.43 \cdot 2}$	**112**	**112**	**KkW^{-1}**

Table A-15. Plate frame thermal resistance network calculation.

Parameter	Equation	Evaluated	EES. Calc. Value	Hand Calc. Value	Units
Single Phase wall resistance	$R_{\text{wall}}[j]=\frac{\delta_{\text{wall}}}{k_{\text{wall}}\cdot L_{\text{c}}[j]\cdot W}$	$R_{\text{wall}}[20]=\frac{4\times10^{-4}}{0.0151\cdot0.00348\cdot0.43}$	**17.7**	**17.7**	**KkW^{-1}**
Single Phase UA	$UA[j]=\frac{1}{R_{\text{r}}[j]+R_{\text{wall}}[j]+R_{\text{g}}[j]}$	$UA[20]=\frac{1}{9485+17.7+223}$	**103 X10^{-6}**	**103 X10^{-6}**	**kWK^{-1}**
Single Phase NTU	$NTU[j]=\frac{UA[j]}{C_{\min}[j]}$	$NTU[j]=\frac{103\times10^{-6}}{1.57\times10^{-3}}$	**65.4 X10^{-3}**	**65.6 X10^{-3}**	**-**
Single Phase Effectiveness	$\varepsilon[j]=\frac{1-\exp\left(-NTU[j]\cdot(1-Cr)\right)}{1-Cr\cdot\exp\left(-NTU[j]\cdot(1-Cr)\right)}$	$\varepsilon[20]=\frac{1-\exp\left(-65.4\times10^{-3}\cdot\left(1-1.40\times10^{-3}\right)\right)}{1-1.40\times10^{-3}\cdot\exp\left(-65.4\times10^{-3}\cdot\left(1-1.40\times10^{-3}\right)\right)}$	**63.3 X10^{-3}**	**63.3 X10^{-3}**	**-**

Two Phase wall resistance	$R_{\text{wall}}[j] = \frac{\delta_{\text{wall}}}{k_{\text{wall}} \cdot L_{\text{c}}[j] \cdot W}$	$R_{\text{wall}}[15] = \frac{4 \times 10^{-4}}{0.0151 \cdot 0.0755 \cdot 0.43}$	**0.815**	**0.816**	**KkW^{-1}**
Two Phase UA	$UA[j] = \frac{1}{R_{\text{r}}[j] + R_{\text{wall}}[j] + R_{\text{g}}[j]}$	$UA[15] = \frac{1}{48.9 + 0.815 + 10.3}$	**16.7 X10^{-3}**	**16.7 X10^{-3}**	**kWK^{-1}**
Two Phase NTU	$NTU[j] = \frac{UA[j]}{C_{\min}[j]}$	$NTU[2] = \frac{16.7 \times 10^{-3}}{1.12}$	**14.9 X10^{-3}**	**14.9 X10^{-3}**	**-**
Two Phase Effectiveness	$\varepsilon[j] = 1 - \exp\left(-NTU[j]\right)$	$\varepsilon[15] = 1 - \exp\left(-14.9 \times 10^{-3}\right)$	**14.6 X10^{-3}**	**14.8 X10^{-3}**	**-**

Table A-16. Plate frame results calculation.

Parameter	Equation	Evaluated	EES. Calc. Value	Hand Calc. Value	Units
Predicted length	$L_{hx} = \sum_{j=1}^{j=j_n} L[j]$	$L_{hx} = (4.29 + 3.98 + 0 + 51.9 + 54.2 + 56.0 + 57.8 + 59.6 + 61.5 + 63.5 + 65.5 + 67.7 + 70.0 + 72.5 + 75.5 + 4.70 + 4.32 + 4.00 + 3.72 + 3.48) \times 10^{-3}$	**7.84**	**7.81**	**m**
Core Pressure drop	$\Delta P_{core} = \Delta P_{fric} + \Delta P_{accel} + \Delta P_{grav}$	$\Delta P_{core} = 0.481 + 0.0001 + 1.67$	**2.15**	**2.15**	**kPa**

A.3. Vapor compression cycle hand calculation for the bar plate evaporator in counter flow at 3 kpa pressure drop

Table A-17. Input parameters use in the vapor compression cycle hand calculation.

Refrigerant fluid parameters			
Parameter Name	**Parameter Symbol**	**Value**	**Units**
Evaporator Water-Glycol mass flow	$\dot{M}_{g,evap}$	16.0	kg s^{-1}
Condenser Water-Glycol mass flow	$\dot{M}_{g,cond}$	11.9	kg s^{-1}
Water-Glycol Specific heat	Cp_g	3.82	kJ $kg^{-1}K^{-1}$
Compressor Efficiency	η_{com}	0.675	-
Compressor Outlet Refrigerant Enthalpy	$i_r[1]$	284	kJ kg^{-1}
Condenser Refrigerant Saturation Enthalpy	$i_{r,sv}$	270	kJ kg^{-1}
Condenser Outlet Refrigerant Enthalpy	$i_r[2]$	104	kJ kg^{-1}
Evaporator Inlet Refrigerant Enthalpy	$i_r[3]$	104	kJ kg^{-1}
Evaporator outlet Refrigerant Enthalpy	$i_r[4]$	254	kJ kg^{-1}
Isentropic Compressor Outlet Enthalpy	$i_{r,s}[1]$	275	kJ kg^{-1}
Evaporator Inlet Water-glycol Temp	$T_g[4]$	12	**°C**
Evaporator Outlet Water-glycol Temp	$T_g[3]$	7	**°C**
Condenser Inlet Water-Glycol Temp	$T_{g,in}$	29	**°C**
Evaporator Effectiveness	ε_{evap}	0.800	**-**
Refrigerant Specific heat, Superheated Condenser	Cp_r	1.06	kJ $kg^{-1}K^{-1}$

Table A-18. Thermodynamic standard vapor compression cycle.

Parameter	Equation	Evaluated	EES. Calc. Value	Hand Calc. Value	Units
Evaporator Heat duty	$q_{\text{evap}} = \dot{M}_{\text{g}} \cdot Cp_{\text{g,evap}} \cdot \left(T_{\text{g}}[4] - T_{\text{g}}[3]\right)$	$q_{\text{evap}} = 16 \cdot 3.82 \cdot \left(12 - 7\right)$	**306**	**306**	**kW**
Inlet refrigerant temperature	$T_{\text{r}}[3] = T_{\text{g}}[4] - \frac{q_{\text{evap}}}{\dot{M}_{\text{g,evap}} \cdot Cp_{\text{g}} \cdot \varepsilon_{\text{evap}}}$	$T_{\text{r}}[3] = 12 - \frac{306}{16 \cdot 3.82 \cdot 0.800}$	**5.74**	**5.74**	**ºC**
Refrigerator mass flow rate	$\dot{M}_{r} = \frac{q_{\text{evap}}}{i_{\text{r}}[4] - i_{\text{r}}[3]}$	$\dot{M}_{r} = \frac{306}{254 - 104}$	**2.05**	**2.04**	**Kgs^{-1}**
Compressor Outlet Enthalpy	$i_{\text{r}}[1] = \frac{i_{\text{r,s}}[1] - i_{\text{r}}[4]}{\eta_{\text{com}}} + i_{\text{r}}[4]$	$i_{\text{r}}[1] = \frac{272 - 254}{0.675} + 254$	**284**	**284**	**kJkg^{-1}**
Compressor work	$\dot{W}_{\text{com}} = \dot{M}_{\text{r}} \cdot \left(i_{\text{r}}[1] - i_{\text{r}}[4]\right)$	$\dot{W}_{\text{comp}} = 2.05 \cdot \left(284 - 254\right)$	**61.2**	**61.5**	**kW**

Superheated Condenser duty	$q_{\text{cond,sh}} = \dot{M}_{\text{r}} \cdot \left(i_{\text{r}}[1] - i_{\text{r,sv}}\right)$	$q_{\text{cond,sh}} = 2.05 \cdot \left(284 - 270\right)$	**27.7**	**27.9**	**kW**
Superheated Condenser Effectiveness	$\varepsilon_{\text{cond,sh}} = \frac{q_{\text{cond,sh}}}{\dot{M}_{\text{r}} \cdot Cp_{\text{r}} \cdot \left(T_{\text{r}}[1] - T_{\text{g,in}}\right)}$	$\varepsilon_{\text{cond,sh}} = \frac{27.7}{1.99 \cdot 1.06 \cdot \left(49.6 - 29\right)}$	**0.619**	**0.637**	**-**
Mid condenser water-glycol temp	$T_{\text{g,m}} = T_{\text{g,i}} + \frac{q_{\text{cond,sh}}}{Cp_{\text{g}} \cdot \dot{M}_{\text{g,con}}}$	$T_{\text{g,m}} = 29 + \frac{27.7}{3.82 \cdot 11.9}$	**29.6**	**29.6**	**ºC**
Two Phase condenser duty	$q_{\text{cond,tp}} = \dot{M}_{\text{r}} \cdot \left(i_{\text{r,sv}} - i_{\text{r}}[2]\right)$	$q_{\text{cond,tp}} = 2.05 \cdot \left(270 - 104\right)$	**339**	**340**	**kW**
Two Phase Condenser Effectiveness	$\varepsilon_{\text{cond,tp}} = \frac{q_{\text{cond,tp}}}{\dot{M}_{g} \cdot Cp_{g} \cdot \left(T_{\text{r,sv}} - T_{\text{g,m}}\right)}$	$\varepsilon_{\text{cond,tp}} = \frac{339}{11.9 \cdot 3.82 \cdot \left(37.2 - 29.6\right)}$	**0.980**	**0.981**	**-**
Coefficient of Performance	$COP = \frac{q_{\text{evap}}}{\dot{W}_{\text{Comp}}}$	$COP = \frac{306}{61.2}$	**5**	**5**	**-**